

Diss. ETH No. 26068

**The Capillary Gap Sampler: A Microfluidic Platform Directly  
Coupled to ESI-MS for Rapid Analysis of Small Sample Amounts**

A thesis submitted to attain the degree of

**DOCTOR OF SCIENCES of ETH ZURICH**

(Dr. sc. ETH Zurich)

presented by

**SAHAR GHIASIKHOU**

MSc in Material Science and Engineering, EPFL Lausanne, Switzerland

born on 23.06.1989

citizen of Iran

accepted on the recommendation of

Prof. Dr. Renato Zenobi, examiner  
Prof. Dr. Andrew de Mello, co-examiner

2019

This page intentionally left blank.

---

## **I. Declaration of Originality**

I hereby declare that this dissertation is the result of my own original work during my PhD studies in ETH, and it has not been submitted, in whole or in part, to any other university. I also declare that no material written by another person without proper citation in the text.

*Zurich, May 10, 2019*

---

*Sahar Ghiasikhou*

*Dedicated to my beloved family.*

---

## II. Acknowledgements

My doctoral studies were accomplished between the first of September, 2014 and the thirty-first of March, 2019 in the group of Professor Renato Zenobi at Eidgenössische Technische Hochschule (ETH) Zürich.

First and foremost, I am thankful to my family: my parents Homeira and Hassan and my brother Ali for being extremely kind and supportive throughout every stage of my life, for providing me whatever I needed to grow and learn, and for teaching me the most precious value of my life. Words cannot express how much I love you and how much this world needs people like you to spread love and peace. I dedicate this thesis to you to thank you for your love and unconditional support.

I want to express my sincere gratitude to my advisor Professor Renato Zenobi for accepting me in his group and for his continuous support of my PhD studies. Besides my advisor, I would like to thank my co-examiner Prof. Andrew de Mella. My sincere thanks also go to Brigitte Bräm for being helpful and kind and for taking care of all the administrative work. Furthermore, in 2016, I had the pleasure of supervising Marcos Fabrício da Silva Masters project. He improved our system performance significantly. Thank you for your hard work! In particular, I am grateful to all our group members for making this journey more joyful: for the pleasant memories during all our group activities, our daily lunch conversations and friendly interactions, the birthday cakes and the watermelon team. Christian Marro and Christoph Bärtschi from the mechanical workshop performed most of the design work on the new compartments for my instrument. Thank you for your precise work and the permanent smiles on your faces.

Thanks to my collaboration partners at Roche, Basel: Christof Fattinger, Roger Steiner, Stephan Muller and others. It was a tremendously constructive collaboration! Also, special thanks to the other collaboration team on my last PhD project, Samuele Cazzamalli, Jorge Scheuermann and Prof. Dario Neri, for providing me with samples and taking part in useful discussions. I also want to thank Falk Lucas from the ScopeM team for taking scanning electron microscope images of my specimens. Moreover, thanks to Samuele Tosatti and Stefan Zürcher for providing me with coating solutions. Without their support it would not have been possible to conduct this research.

---

I must thank my lovely relatives, especially my grandmother and cousins, for all the positive energy they send me. Also, I appreciate my friends because of whom this period was more colorful: Golnoosh and Payam for all our long conversations and endless laughs, Linda for our German-Farsi learning sessions, activities and short trips, Parisa, Samira and Adrina for being awesome friends and for the beautiful memories we built together. Special thanks to Jonas for being a very supportive friend.

Finally, I want to thank the Swiss National Science Foundation (SNSF) for funding this project (Grant numbers 200020-159929 and 200020-178765), as well as the Swiss public transport system (ZVV), since I frequently wrote and read in the trams and buses while commuting from my home to ETH Honggerberg.

---

## III. Table of Contents

<b>Chapter 1</b>	<b>Introduction</b>	<b>1</b>
<b>1.1</b>	<b>High-Throughput Screening</b>	<b>2</b>
1.1.1	Mechanical Valve Systems	3
1.1.2	Chip-based Systems	3
1.1.3	Non-chip-based Systems	4
<b>1.2</b>	<b>Capillary Gap Sampler</b>	<b>5</b>
1.2.1	CGS Design	5
1.2.2	Characteristics of the Liquid Bridge	7
1.2.3	Operation Cycle of a Sample Injection	8
<b>1.3</b>	<b>High-Throughput Sample Extraction</b>	<b>9</b>
1.3.1	Solid-Phase Microextraction	9
1.3.2	Small Molecule-Drug Conjugates	10
<b>1.4</b>	<b>Outline of the Thesis</b>	<b>11</b>
<b>Chapter 2</b>	<b>Methodology</b>	<b>13</b>
<b>2.1</b>	<b>Principles of Mass Spectrometry</b>	<b>14</b>
2.1.1	Mass Spectrum	14
2.1.2	Ion Chromatogram	14
<b>2.2</b>	<b>Performance of Mass Spectrometry</b>	<b>15</b>
2.2.1	Sensitivity	15
2.2.2	Limit of Detection	15
2.2.3	Signal-to-Noise Ratio	15
2.2.4	Resolution	15
<b>2.3</b>	<b>Ionization Techniques</b>	<b>16</b>
<b>2.4</b>	<b>Electrospray Ionization</b>	<b>16</b>
2.4.1	Ion Formation in ESI	17
2.4.2	Applications of ESI	18
<b>2.5</b>	<b>Time-of-Flight Mass Spectrometry</b>	<b>18</b>
2.5.1	Ion Velocity	18
<b>2.6</b>	<b>Synapt G2-S</b>	<b>20</b>
<b>Chapter 3</b>	<b>A Comparative Study Between a Miniaturized Liquid Junction Built in a Capillary Gap versus Semi-open Capillaries for nL Sample Infusion to Mass Spectrometry</b>	<b>23</b>
<b>3.1</b>	<b>Abstract</b>	<b>24</b>
<b>3.2</b>	<b>Introduction</b>	<b>25</b>
<b>3.3</b>	<b>Experimental Section</b>	<b>27</b>
3.3.1	Chemicals and Materials	27
3.3.2	Equipment for Detection, Software, Buffer Delivery	27
3.3.3	Preparation of Semi-open Capillaries	28
<b>3.4</b>	<b>Results and Discussion</b>	<b>28</b>
3.4.1	Design of the Semi-open Capillary	28

3.4.2	Capillary Coating .....	30
3.4.3	Increased Liquid Junction Robustness with the Semi-open Capillaries.....	30
3.4.4	Repeatability of Sample Infusion Using Semi-open Capillary.....	34
3.4.5	Less Sample Dilution and Dead Volume.....	35
3.4.6	System Sensitivity.....	37
3.4.7	Injection Cycle.....	39
<b>3.5</b>	<b>Conclusion .....</b>	<b>39</b>
<b>Chapter 4</b>	<b>The capillary gap sampler, a new microfluidic platform for direct coupling of automated solid-phase micro extraction to ESI-MS.....</b>	<b>41</b>
<b>4.1</b>	<b>Abstract .....</b>	<b>42</b>
<b>4.2</b>	<b>Introduction .....</b>	<b>43</b>
<b>4.3</b>	<b>Experimental Section .....</b>	<b>44</b>
4.3.1	Chemicals and Materials .....	44
4.3.2	Preparation of Biocompatible C <sub>18</sub> -PAN SPME Coatings.....	45
4.3.3	Mass Spectrometry Conditions .....	45
4.3.4	Operation with a Miniaturized SPME Tool.....	45
<b>4.4</b>	<b>Automation and User Interface .....</b>	<b>47</b>
<b>4.5</b>	<b>Results and Discussion .....</b>	<b>47</b>
4.5.1	Optimization of Coating Preparation .....	47
4.5.2	Kinetics .....	51
4.5.3	Effect of Desorption Solution Flow Rate and Position of the Pin Within the Gap on Desorption Profile	53
4.5.4	Influence of the Pin Position Inside the Gap on the Extraction Profile .....	55
4.5.5	Evaluation of Time Profile of the Extraction .....	56
4.5.6	Reproducibility of Extractions of Benzodiazepines from PBS and Dynamic Linear Range .....	58
4.5.7	Evaluation of the Method for Extraction of Benzodiazepines from Human Plasma.....	59
4.5.8	Extracted Ion Chromatogram.....	61
<b>4.6</b>	<b>Conclusions .....</b>	<b>63</b>
<b>Chapter 5</b>	<b>Automated and Enhanced Extraction of a Small Molecule-drug Conjugate Using an Enzyme-inhibitor Interaction Based SPME Tool Followed by Direct Analysis by ESI-MS.....</b>	<b>65</b>
<b>5.1</b>	<b>Abstract .....</b>	<b>66</b>
<b>5.2</b>	<b>Introduction .....</b>	<b>67</b>
<b>5.3</b>	<b>Material and Methods.....</b>	<b>68</b>
5.3.1	Chemical and Materials.....	68
5.3.2	Equipment for detection, Software, Buffer Delivery.....	69
<b>5.1</b>	<b>Preparation of the SPME tool .....</b>	<b>69</b>
5.1.1	Workflow for Sample Extraction and Elution .....	70
<b>5.2</b>	<b>Results and Discussion .....</b>	<b>71</b>
5.2.1	Proof of CAII Immobilization .....	71
<b>5.3</b>	<b>Carbonic Anhydrase II and Acetazolamide Binding .....</b>	<b>73</b>
5.3.1	Influence of the Desorption Solution on the Acetazolamide Signal.....	74



---

5.3.2	Extraction of AAZ-VC-MMAE from Human Plasma by the CGS.....	77
5.3.3	Specificity of the Extraction .....	80
5.3.4	Time Profile of the Extraction .....	82
5.3.5	AAZ Extraction Linearity, Sensitivity, Limit of Detection, and Recovery .....	83
5.3.6	Repeatability .....	85
<b>5.4</b>	<b>Conclusion .....</b>	<b>85</b>
<b>Chapter 6</b>	<b>Outlook.....</b>	<b>86</b>
<b>6.1</b>	<b>Technical Improvements .....</b>	<b>88</b>
6.1.1	Sensitivity .....	88
6.1.2	Robustness .....	88
<b>6.2</b>	<b>Applications .....</b>	<b>90</b>
6.2.1	Kinetic Studies .....	90
6.2.2	Studying Non-covalent Interactions.....	91
6.2.3	Ligand Ranking .....	92
6.2.4	Bioimaging.....	94
<b>References</b>	<b>.....</b>	<b>95</b>
<b>Appendix A</b>	<b>.....</b>	<b>108</b>
<b>A.1</b>	<b>Introduction and Content.....</b>	<b>109</b>
<b>A.2</b>	<b>Materials.....</b>	<b>109</b>
<b>A.3</b>	<b>Connection of Components and System Preparation .....</b>	<b>112</b>
<b>A.4</b>	<b>Overview of Electric and Gas Connections .....</b>	<b>112</b>
<b>A.5</b>	<b>Preparation of Gas Lines.....</b>	<b>114</b>
<b>A.6</b>	<b>Installation of Mechanical Pressure Regulators .....</b>	<b>115</b>
A.6.1	Station 1 .....	115
A.6.2	Station 2 .....	116
<b>A.7</b>	<b>Installation of Pressurized Bottles and Valve Connectors.....</b>	<b>118</b>
A.7.1	Station 2 .....	118
<b>A.8</b>	<b>Zoomed Pictures of the System Setup .....</b>	<b>122</b>
A.8.1	Connections of Mechanical and Electrical Pressure Regulators.....	122
A.8.2	Connections to the Wash Solvent Valves and the Wash Port.....	124
A.8.3	Connections to the Pressure Chamber .....	125
<b>A.9</b>	<b>Establishing Electrical Connections and Location of Control LEDs .....</b>	<b>126</b>
A.9.1	Removable Connections on the Upper Level of the Sampler Setup .....	126
<b>A.10</b>	<b>Connections on the Middle level of the Sampler Setup.....</b>	<b>128</b>
<b>A.11</b>	<b>Purging of the Buffer line Using neMESYS Syringe Pump .....</b>	<b>129</b>
<b>A.12</b>	<b>Adjustment of the Pin Tool.....</b>	<b>133</b>
<b>A.13</b>	<b>Gap Formation .....</b>	<b>137</b>
<b>A.14</b>	<b>Teaching the Microrobot.....</b>	<b>140</b>
A.14.1	Robot Positions .....	140
A.14.2	Sample Plate Configuration.....	144

---

<b>A.15</b>	<b>Defining and Testing a Custom Automated Process .....</b>	<b>145</b>
A.15.1	Additional Robot Positions.....	145
A.15.2	Method.....	146
A.15.3	Method Steps.....	146
A.15.4	Process .....	148
A.15.5	Sample Sequence .....	149
A.15.6	Process Testing.....	149
<b>A.16</b>	<b>Operation of New Process Automation Software .....</b>	<b>150</b>
A.16.1	Calibration Procedure .....	152
A.16.2	Solid-phase Microextraction .....	155
A.16.3	Infusion .....	157
A.16.4	Important Considerations .....	158
<b>A.17</b>	<b>Sampler Connection to the Mass Spectrometer.....</b>	<b>160</b>
<b>A.18</b>	<b>Sampler Operation .....</b>	<b>163</b>
A.18.1	Establishing a Stable Liquid Bride and ESI Plume .....	163
A.18.2	Analysis .....	165
<b>A.19</b>	<b>Troubleshooting.....</b>	<b>166</b>
<b>A.20</b>	<b>Coating Single Layer Beads on the Tip of Pin Tool for SPME.....</b>	<b>167</b>
<b>Appendix B Curriculum Vitae .....</b>		<b>171</b>

---

## IV. List of Figures

- Figure 1. Components of the capillary gap sampler: (a) overall design of the capillary gap sampler, which consists of different components including: (1) extraction tool and pin sleeve, held by delta robot arms, (2) microwell plate, (3) camera for online monitoring of the gap, (4) pressure chamber ( $V=0.65$  ml) held under a controlled overpressure, (5) solid stainless-steel pin ( $229\ \mu\text{m}$  diameter) used as an SPME tool, (6) liquid bridge for sample desorption, (7) stainless-steel capillary with a tapered tip, which sprays the desorption solution into the orifice of the MS by applying a high voltage to the spray.4 ..... 6
- Figure 2. Major steps of the operation cycle of sample injection. .... 9
- Figure 3. Three main ion formation mechanisms in the gas-phase, (a) the ion evaporation model (IEM), (b) the charge residual model (CRM) and (c) the chain ejection model (CEM). .... 17
- Figure 4. Principle of operation of a reflectron TOF mass analyzer. .... 20
- Figure 5. Synapt G2-S ion optics overview, including ion source, StepWave, TriWave and TOF mass analyzer. .... 21
- Figure 6. Different liquid connector configurations. .... 24
- Figure 7. Key parts of the Capillary Gap Sampler: sampling tool held by the robot arm (1), liquid bridge (2), ESI spray tip (3), capillary gap so-called “Gap 1” (4), semi-open capillary (fabricated by laser ablation) called “Gap 2” (5), semi-open capillary (fabricated by EDM) introduced as “Gap 3” (6) sample receptors. .... 27
- Figure 8. SEM images of the different holes in the stainless-steel capillary made by (a) laser ablation ( $300\ \mu\text{m} \times 200\ \mu\text{m}$ ) and (b) a combination of wire and sinker EDM method.  $115\ \mu\text{m}$  of the thickness is removed by wire EDM and a hole ( $r=115\ \mu\text{m}$ ) is made inside. .... 29
- Figure 9. XPS survey spectra on the stainless-steel capillary before (upper curve) and after (lower curve) coating. .... 30
- Figure 10. TIC of the spray stability tests which was evaluated as a function of the flow rate and chamber pressure for high surface tension liquid (MeOH/Water 1:1 ( $V/V$ )). .... 31
- Figure 11. Results of the spray stability as a function of the flow rate and chamber pressure for low surface tension liquid (Pure ACN). .... 32
- Figure 12. Pressure dependence experiment for Gap 1 and Gap 3, (a) Gap 1 (low surface tension solution), (b) Gap 3 (high surface tension solution), (c) Gap 3 (low surface tension solution). Different colors correspond to the liquid connector stability (Green=stable, yellow=short term stability, red= not possible to make liquid connector). .... 33
- Figure 13. Representative injection sequence of Rhodamine B [ $1.5\ \mu\text{M}$ ], used for determining the repeatability of injections in different experimental conditions. (CV=capillary voltage, F=Flow rate, P=chamber overpressure, S.I=signal intensity, RSD=relative standard deviation). \*A data point was excluded in RSD and mean value calculation in part a (due to instrumental error). Considering the excluded point RSD and the average are 9.9% and 9055738 respectively. ... 34
- Figure 14. Comparison of different sample peak widths for three gap configurations. .... 35
- Figure 15. (a) Flow COMSOL simulation for Gap 1, 2 and 3 at different times. Color code is from dark red to blue, with dark red for the highest and blue for the lowest sample concentration and is identical for all three gaps. (b) Normalized extracted ion current for small molecules. .... 37

---

Figure 16. Corrected signal intensity (a.u) versus concentration (nM) of diazepam, rhodamine B, acetazolamide using (a) Gap 3 and (b) Gap 1.....	38
Figure 17. Injection cycle into semi-open capillary which takes 2 seconds (from step 1 to step 4).....	39
Figure 18. The CGS as an automated SPME-MS interface.....	42
Figure 19. SEM imaging of bead coatings using two different procedures. (a) result of immobilizing C18 using a mixture of glue and particles. This SEM image clearly shows that C18 particles are covered by glue. (b) using discrete steps, beads are free of glue on the surface. ....	48
Figure 20. EIC for diazepam ( $m/z=285.1$ ) using a pin coated with free beads (left), and a pin coated by a mixture of PAN glue and C18 beads 20% (w/w) (right). ....	49
Figure 21. Average diazepam signal intensity ( $n=5$ ) extracted by pins covered by single, triple and multiple layers of C18 which were fabricated by using one, three, and seven coating cycles. ....	50
Figure 22. Extraction kinetics of 500 ng/ml of, (a) nordiazepam, (b) diazepam, (c) oxazepam from PBS. Each drug was extracted with and without stirring. Then the extracted analyte was eluted with acetonitrile/water (80:20 $V/V$ ) + 0.1% formic acid as the desorption solution, using a 0.6 $\mu\text{L}/\text{min}$ flow rate .....	52
Figure 23. COMSOL Multiphysics simulation of the flow profile in a liquid bridge.....	54
Figure 24. Different pin positions inside the liquid bridge, (a) Top (gap distance=290 $\mu\text{m}$ ), (b) Gap (gap distance=290 $\mu\text{m}$ ), (c) Gap (gap distance= 560 $\mu\text{m}$ ). ....	55
Figure 25. Benzodiazepines peak intensities extracted from different pin positions inside the gap. Solid fill) Top (gap distance= 290 $\mu\text{m}$ , dotted) Gap (gap distance= 290 $\mu\text{m}$ , hatching) Gap (gap distance= 560 $\mu\text{m}$ )......	56
Figure 26. Time profiles of extraction of benzodiazepines, (a) nordiazepam, (b) diazepam, (c) oxazepam. Corrected analyte intensity is plotted against the loading time. In all experiments, no significant increase was observed after 30 minutes of loading time. The extracted analyte was eluted with acetonitrile/water (80:20 $V/V$ ) + 0.1% formic acid as the desorption solution with a 1 $\mu\text{L}/\text{min}$ flow rate. ....	57
Figure 27. Peak intensity was obtained for twenty extractions of nordiazepam, diazepam, oxazepam (500 ng/ml from PBS). Loading time was kept constant ( $t=5$ minutes) for all experiments. The lines show the mean value for each analyte. Confidence intervals are shown as colored bands. The extracted analyte was eluted with acetonitrile/water (80:20 $V/V$ ) + 0.1% formic acid as the desorption solution, using a 1 $\mu\text{L}/\text{min}$ flow rate. ....	59
Figure 28. Shows the extraction of benzodiazepines from, human plasma 600 ng/ml. Peaks observed at $m/z=271.1$ , 285.1, 287.1 corresponds to nordiazepam (blue), diazepam (green), and oxazepam (red) respectively. The spectrum was acquired from $m/z=250$ . The extracted analyte was eluted with acetonitrile/water (80:20 $V/V$ ) + 0.1% formic acid as the desorption solution with a 1 $\mu\text{L}/\text{min}$ flow rate. ....	60
Figure 29. Extraction from human plasma (blank sample). The extracted analyte was eluted with acetonitrile/water (80:20 $V/V$ ) + 0.1 % formic acid as the desorption solution with a 1 $\mu\text{L}/\text{min}$ flow rate. ....	61
Figure 30. EICs from extraction of 600 ng/ml benzodiazepines from human plasma.....	61

---

Figure 31. Signal intensities obtained for thirteen extractions of nordiazepam, diazepam, oxazepam (700 ng/ml) from human plasma. Loading time was kept constant ( $t=5$ minutes) for all experiments. The lines show the mean value for each analyte. Confidence intervals are shown as shaded bands. The extracted analyte was eluted with acetonitrile:water 80:20 ( $V/V$ ) + 0.1% formic acid as the desorption solution with a 1 $\mu\text{L}/\text{min}$ flow rate. ....	62
Figure 32. CAII-based extraction tool to evaluate MMAE targeted delivery to kidney cancer cells. ....	66
Figure 33. Extraction tool preparation steps, (a) gluing epoxy-modified beads onto the solid pin and curing at $180^{\circ}\text{C}$ , (b) incubation with CAII and amine-epoxy reaction, (c) incubation in Tris buffer, (d) SEM image of the CAII-modified beads after immobilization on the extraction tool, confirming that beads are not covered with PAN glue. ....	70
Figure 34. In this figure extraction workflow including loading, washing, elution, conditioning is shown. The elution step happens in the liquid bridge formed in between two capillaries. ....	71
Figure 35. Bright field and blue channel images from the epoxy-modified beads (incubated (a) with, (b) without CAII) after reacting with ANS. ....	72
Figure 36. Showing the 1:1 ratio of the CAII and AAZ complex ESI-MS spectrum. ....	73
Figure 37. The pH profile of AAZ-CAII binding. ....	74
Figure 38. Average amount of eluted acetazolamide ( $n=10$ ) using acetonitrile, methanol, ethanol and acetone 50% mixed with water (plus 0.1% of formic acid) as the desorption solution. The results are normalized to methazolamide (1 $\mu\text{M}$ ). ....	75
Figure 39. EIC ( $m/z=223.25 \pm 5\text{ppm}$ ) of acetazolamide (20 $\mu\text{M}$ ) after extraction from PBS. ....	76
Figure 40. The nano-ESI spectrum of CAII 20 $\mu\text{m}$ incubated in 50% ACN: H <sub>2</sub> O for 2 minutes. ....	77
Figure 41. Spectrum of AAZ-VC-MMAE, (a) direct infusion by nanospray, (b) extraction from human plasma. The following peaks were observed in both spectra: ( $\diamond$ ) MMAE+ H <sup>+</sup> =718.51 $m/z$ , ( $\circ$ ) AAZ-VC-MMAE+ 2H <sup>+</sup> =1113.03 $m/z$ , ( $\circ$ ) AAZ-VC-MMAE+H <sup>++</sup> Na <sup>+</sup> =1123.53 $m/z$ , ( $\square$ ) AAZ-VC-MMAE – MMAE – CO <sub>2</sub> =1461 $m/z$ , ( $\Delta$ ) AAZ-VC-MMAE+=2224.05 $m/z$ . Part (c) shows the chemical structure of AAZ-VC-MMAE. ....	78
Figure 42. The AAZ-VC-MMAE 2.5 $\mu\text{g}/\text{ml}$ extraction spectrum from PBS using, (a) bare beads (control), (b) CAII beads. The following peaks were observed in both spectra: ( $\diamond$ ) MMAE+ H <sup>+</sup> =718.51 $m/z$ , ( $\circ$ ) AAZ-VC-MMAE+ 2H <sup>+</sup> =1113.03 $m/z$ , ( $\circ$ ) AAZ-VC-MMAE+H <sup>++</sup> Na <sup>+</sup> =1123.53 $m/z$ , ( $\square$ ) AAZ-VC-MMAE – MMAE – CO <sub>2</sub> =1461 $m/z$ , ( $\Delta$ ) AAZ-VC-MMAE+=2224.05 $m/z$ . Part c shows the chemical structure of AAZ-VC-MMAE. ....	79
Figure 43. Extraction of acetazolamide using three different proteins (bovine serum albumin, myoglobin and carbonic anhydrase II) immobilized on the pins, plus a control experiment (bare beads). The acetazolamide signal intensities are normalized to methazolamide 2 $\mu\text{M}$ . ( $n=7$ ) ....	80
Figure 44. Comparison of the extraction of three different analytes, (a) acetazolamide, (b) diazepam, (c) MMAE, using CAII and epoxy-modified beads. ( $n=5$ ) ....	81
Figure 45. The time profile of the extraction acetazolamide (20 $\mu\text{M}$ ) from PBS ( $n=3$ ). The results are normalized to methazolamide (2 $\mu\text{M}$ ). "Loading time" (x axis) is equal to "Extraction time".	83
Figure 46. Linear range of AAZ extraction ( $n=3$ ). Results are normalized to methazolamide 1 $\mu\text{M}$ . ....	84
Figure 47. Repeatability test. RSD for forty extractions of 500 nM acetazolamide from PBS was found to be 13.5%. The solid blue line represents the mean value. The data were normalized to methazolamide (200 nM). ....	85

---

Figure 48. The comparison between (a) slotted hollow pins and (b) solid sampling pins.....	89
Figure 49. Different proposals for the system configuration, (a) the current setup where the chamber pressure $P_2$ is higher than the ambient pressure $P_1$ , (b) the entire system is kept under overpressure $P_2$ , and the spray tip operates at $P_1$ , (c) the entire system is kept at $P_1$ and the spray tip pressure is reduced. (the idea and Figure 49 are reproduced with a few modifications from Jérôme Kaeslin).....	90
Figure 50. EIC of the lysozyme NAG <sub>3</sub> and the complex for different ligand concentrations and corresponding mass spectra. ....	91
Figure 51. The KD measurement plot for lysozyme – NAG <sub>3</sub> (Assumption: $[L] \sim [L_0] = \text{total ligand concentration}$ ).....	92
Figure 52. Diagram of the catalyst screening concept. Reagents A and B are mixed and form the liquid connector. A library of potential catalysts can be added via the sampling pin. The resulting product (P) will be screened by the mass spectrometer. ....	93

---

## List of Appendix Figures

Figure A 1. Overview of electric connections. ....	113
Figure A 2. Overview of gas connections.....	113
Figure A 3. Line type (I): 2 lines needed.....	114
Figure A 4. Line type (II): 1 line needed.....	114
Figure A 5. Line type (III): 2 lines needed.....	114
Figure A 6. Line type (IV): 2 lines needed.....	114
Figure A 7. IR2000-F02 mechanical pressure regulators. ....	115
Figure A 8. IR2000-F02 connected to polyurethane lines. ....	115
Figure A 9. IR2000-F02 connected to the gas exit line. ....	115
Figure A 10. Gas flow meter. ....	116
Figure A 11. Gas flow meter connected to the main gas supply.....	116
Figure A 12. Pressure regulator (step 1). ....	117
Figure A 13. Connected pressure regulator (front). ....	117
Figure A 14. Connected pressure regulator (back). ....	117
Figure A 15. AW20-F02BM pressure regulator (step 1). ....	118
Figure A 16. AW20-F02BM pressure regulator (step 2). ....	118
Figure A 17. AW20-F02BM pressure regulator (step 3). ....	118
Figure A 18. The buffer bottle cap.....	119
Figure A 19. The buffer bottle cap.....	119
Figure A 20. The buffer bottle cap connections (line type 3). ....	120
Figure A 21. The buffer bottle connection to the pressure line.....	120
Figure A 22. Vacuum generator. ....	121
Figure A 23. Vacuum generator connected to a long polyurethane line.....	121
Figure A 24. A Y-PEEK union with two short lines of line type IV. ....	121
Figure A 25. Connection of mechanical pressure station 2 to the bottle for wash solvents. ....	123
Figure A 26. Connection of mechanical pressure station 2 to the vacuum generator to the waste bottle. ....	123
Figure A 27. Connection of mechanical.....	123
Figure A 28. Connection of buffer dampening bottle to the outlet of the Bronkhorst IQ flow gas regulator.....	123
Figure A 29. Connections of washing solvent bottles to the wash solvent valves.....	124

---

Figure A 30. Connections to the wash/dry station; (a) gas for pin drying, (b) solvent for pin washing, (c) solvent to the waste bottle. ....	124
Figure A 31. Connection of pressure dampening .....	125
Figure A 32. Electrical Connections.....	126
Figure A 33. Electrical connections and location of control LED. ....	127
Figure A 34. Connection of power supply to the red-Y gas flow meter. ....	128
Figure A 35. Connection to electrical pressure regulator. ....	128
Figure A 36. Connection to solenoid valve at the.....	128
Figure A 37. Overview of the three levels of the sampler setup. ....	128
Figure A 38. The neMESYS user interface, gap scanner and gap controller software. ....	129
Figure A 39. Syringe pump setting on the gap controller software. ....	130
Figure A 40. Components for syringe fixation. ....	130
Figure A 41. A hexagon-headed PEEK finger tight, double grip ferrule and a green sleeve.....	131
Figure A 42. Syringe fixation in the syringe holder (step 1). ....	132
Figure A 43. Syringe fixation in the syringe holder (step 2). ....	132
Figure A 44. Metal pin tools.....	133
Figure A 45. Pin tool diameter fixation. ....	134
Figure A 46. Pin tool fixation components.....	135
Figure A 47. Pin tool fixation (step 1).....	135
Figure A 48. Pin tool fixation (step 2).....	136
Figure A 49. Pin tool fixation (step 3).....	136
Figure A 50. Fixed pin tool.....	137
Figure A 51. Original gap controller software, (a) chamber pressure, (b) injection port, (c) online monitoring, and (d) robot control.....	138
Figure A 52. Capillary adjustment (step 1).....	139
Figure A 53. Capillary adjustment (step 2).....	139
Figure A 54. Capillary adjustment inside the chamber (step 3).....	140
Figure A 55. Robot position training .....	140
Figure A 56. Gap position. ....	141
Figure A 57. Above gap position.....	142
Figure A 58. Washing position.....	142
Figure A 59. Drying position.....	143
Figure A 60. Sample plate configuration.....	144



---

Figure A 61. Defining method steps (step 1).....	147
Figure A 62. Defining method steps (step 2).....	147
Figure A 63. Defining sampling sequence.....	149
Figure A 64. Robot control GUI.....	151
Figure A 65. Process Selection Interface.....	152
Figure A 66. Delta Robot Break Message.....	154
Figure A 67. Reference Point Placement.....	154
Figure A 68. Final Calibration Message.....	155
Figure A 69. SPME control panel.....	156
Figure A 70. SPME position input.....	157
Figure A 71. Infusion Control Panel.....	158
Figure A 72. Tools for fixing the sampler at the ESI source basis plate.....	160
Figure A 73. Fixation screws for Synapt G2-S source.....	161
Figure A 74. X, Y and Z fixation platform (left), (right), dongle connection to the blue frame at the electrical connection plug.....	161
Figure A 75. CGS fixation to the MS. (a) screw the X, Y and Z stand, (b) socket screw, (c) pin for electrical contact closure.....	162
Figure A 76. The plate fixation screw.....	163
Figure A 77. Connection of the Voltmeter in three steps.....	163
Figure A 78. Optimized spray position.....	164
Figure A 79. A stable liquid bridges.....	165
Figure A 80. Contactless injection into the liquid bridge.....	165
Figure A 81. Preparation of a thin layer of beads for SPME extraction tool.....	168
Figure A 82. Fresh coated metal pin.....	169
Figure A 83. Microscope (left) and SEM (right) images of a single layer coated C18 beads.....	169

This page intentionally left blank.

---

## V. List of Tables

Table 1. Comparison of the effect of desorption solution flow rate on the desorption profile.....	53
---	----

## List of Appendix Tables

Table A 1. List of required tubing and spare parts.....	109
Table A 2. Lis of required instruments. ....	111
Table A 3. List of required tools. ....	112
Table A 4. Troubleshooting of common errors.....	166

This page intentionally left blank.

---

## VI. Abstract

This thesis introduces the “Capillary Gap Sampler” (CGS), an automated electrospray ionization (ESI) source interfacing mass spectrometry (MS) for high-throughput screening (HTS) applications. HTS methods allow large libraries of compounds to be analyzed in a short amount of time. HTS methods are of significant use to the modern pharmaceutical industry, in particular drug discovery. Among existing HTS methods, mass spectrometry is the dominant technology in the first stage of drug discovery research. Mass spectrometry is an analytical technique that enables fast and comprehensive analysis of chemical compounds and yields qualitative and quantitative information. Manual sample loading on a commercial MS source is a slow process and thus is not applicable for large sample archives. Hence, the development of a sampling source capable of rapidly analyzing a high number of samples has attracted considerable attention.

Groundbreaking technologies such as chip-based and non-chip-based autosamplers fulfill the initial need for HTS applications. However, several drawbacks, such as high sample volume requirements and analyte adhesion to the sample introduction lines leave room for further improvements. The CGS has been developed to address the demand to interface a fast (< 20 seconds) and fully automated low volume (< 100 nL) sampling process to the MS, while minimizing the surface area exposed to the sample.

The original design of the sample receptor in the CGS consists of a liquid bridge formed by a micrometer gap between two capillaries. The liquid bridge downstream is ionized and analyzed by the MS. The advancement achieved and reported initially in this project is the replacement of the liquid bridge with a single pierced capillary termed a “semi-open capillary,” in order to enhance the robustness and sensitivity of the sampler. To optimize the structure for the opening on the capillary body, two different micromachining methods were examined, laser ablation and electro-discharge micromachining (EDM). According to COMSOL simulation and experimental results, the recent design achieved by the EDM method was found to have less sample dilution and reduced dead volume. Thus, this improvement leads to a nearly two-fold lower limit of detection (LOD) in comparison to the CGS. Moreover, the robustness of the system is significantly increased.

This CGS application can be further expanded to sample up-concentration prior to MS analysis. In this case, the sampling tool role changes to an extraction tool and the sample receptor platform acts as a sample dilution station. Thus, the CGS is capable of directly coupling the solid-phase microextraction (SPME) to the MS. Diazepam, oxazepam and nordiazepam were utilized as test compounds to be extracted by a C<sub>18</sub> bead extraction phase. High stability and reusability of the coating were achieved through systematic optimization. The limit of benzodiazepine detection in human plasma is 0.3 µg/ml, which covers 80% of the therapeutic range. A linear dynamic range of 1 to 1000 ng/ml for all three analytes ensures the reliability of the quantitative analysis. The relative standard deviation of twenty extractions was found to be less than 18%, indicating an acceptable repeatability for the method.

The CGS was later used to implement a more specific extraction of an anti-cancer drug from human plasma. This extraction was performed on the basis of a noncovalent and reversible interaction between carbonic anhydrase II (CAII) and acetazolamide (AAZ). CAII was immobilized on the extraction tool to filter out the AAZ, which is used as the targeting head of a recently synthesized anti-cancer drug. The specificity of the AAZ extraction was systematically optimized. It was demonstrated that CAII increases AAZ extraction by a factor of 3.3 in comparison to the use of a bare extraction tool. The LOD of AAZ from phosphate-buffered saline (PBS) and human plasma are 0.4 and 1.2 µg/ml, respectively, which covers the entire therapeutic range. In addition, the relative standard deviation of less than 14% (*n*=40) proves the repeatability of the method.

---

## VI. Zusammenfassung

In dieser Arbeit wird der "Capillary Gap Sampler" (CGS) vorgestellt, eine automatisierte Elektrospray-Ionisierung (ESI)-Quelle an der Schnittstelle zur Massenspektrometrie (MS) für Hochdurchsatz-Screening (HTS)-Anwendungen. Mit HTS-Methoden können grosse Sammlungen von chemischen Verbindungen in kurzer Zeit analysiert werden. HTS-Methoden sind für die moderne pharmazeutische Industrie von erheblichem Nutzen, insbesondere für die Wirkstoffentdeckung. Unter den bestehenden HTS-Methoden ist die Massenspektrometrie die vorherrschende Technologie in der ersten Phase der Arzneimittelforschung. Die Massenspektrometrie ist eine Analysetechnik, die eine schnelle und umfassende Analyse chemischer Verbindungen ermöglicht und qualitative wie auch quantitative Informationen liefert. Das manuelle Laden von Proben auf eine kommerzielle MS-Quelle ist ein langsamer Prozess und daher nicht für grosse Probensammlungen geeignet. Daher hat die Entwicklung einer Quelle zur Probennahme, die in der Lage ist, eine hohe Anzahl von Proben schnell zu analysieren, beträchtliche Aufmerksamkeit auf sich gezogen.

Bahnbrechende Technologien wie chipbasierte und nicht-chipbasierte Autosampler erfüllen den anfänglichen Bedarf an HTS-Anwendungen. Einige Nachteile, wie die Erfordernis eines grossen Probenvolumens und die Haftung des Analyten an den Probeneinführungsleitungen, lassen jedoch Raum für weitere Verbesserungen. Der CGS wurde entwickelt, um dem Bedarf nach einem an die MS angeschlossenen Vorgangs zur Probennahme gerecht zu werden, welcher schnell ( $< 20$  Sekunden) und vollautomatisch ist, mit geringen Volumina ( $< 100$  nL) arbeiten kann, und gleichzeitig auch die Oberfläche minimiert, welche der Probe ausgesetzt ist.

Das ursprüngliche Design des Probenrezeptors im CGS besteht aus einer Flüssigkeitsbrücke, die im Mikrometerabstand zwischen zwei Kapillaren gebildet wird. Die Flüssigkeitsbrücke stromabwärts wird ionisiert und von der MS analysiert. Die Fortschritte, die im Rahmen dieses Projekts erzielt wurden, sind der Ersatz der Flüssigkeitsbrücke durch eine einzelne durchstochene Kapillare ("halboffene Kapillare") um die Robustheit und Empfindlichkeit des Probenehmers zu verbessern. Zwei verschiedene Mikrobearbeitungsmethoden wurden untersucht, um die Struktur für die Öffnung am Kapillarkörper zu optimieren: die Laserablation und die Elektroentladungs-Mikrobearbeitung (EDM). Gemäss der COMSOL-Simulation und experimentellen Ergebnissen wurde festgestellt, dass das durch die EDM-Methode erzielte neue Design eine geringere Probenverdünnung und ein verringertes Totvolumen aufweist. Somit führt diese Verbesserung zu nahezu einer Halbierung der unteren Nachweisgrenze (engl. lower limit of detection, LOD) im Vergleich zum konventionellen CGS. Darüber hinaus wird die Robustheit des Systems deutlich erhöht.

Diese CGS-Anwendung kann vor der MS-Analyse auf die Probenaufkonzentrierung erweitert werden. In diesem Fall wird die Rolle des Probennahmegeräts zu einem Extraktionswerkzeug, und die Probenaufnahmeplattform fungiert als Probenverdünnungsstation. Somit ist das CGS in der Lage, die Festphasen-Mikroextraktion (SPME) direkt an die MS zu koppeln. Diazepam, Oxazepam und Nordiazepam wurden als Testverbindungen verwendet, die durch eine  $C_{18}$  Extraktionsphase aus Kügelchen extrahiert wurden. Durch systematische Optimierung wurde eine hohe Stabilität und Wiederverwendbarkeit der Beschichtung erreicht. Die Nachweisgrenze für Benzodiazepine im menschlichen Plasma liegt bei  $0.3 \mu\text{g/ml}$ , was 80% des therapeutischen Bereichs abdeckt. Ein linearer dynamischer Bereich von 1 bis  $1000 \text{ ng/ml}$  für alle drei Analyten gewährleistet die Zuverlässigkeit der quantitativen Analyse. Die relative Standardabweichung von 20 Extraktionen betrug weniger als 18%, was auf eine akzeptable Wiederholbarkeit der Methode hinweist.

---

Der CGS wurde später verwendet, um eine spezifischere Extraktion eines Krebsmedikaments aus menschlichem Plasma durchzuführen. Diese Extraktion wurde auf der Basis einer nichtkovalenten und reversiblen Wechselwirkung zwischen Carboanhydrase II (CAII) und Acetazolamid (AAZ) durchgeführt. CAII wurde auf dem Extraktionswerkzeug immobilisiert, um AAZ herauszufiltern, welches als Zielkopf eines kürzlich synthetisierten Krebsmedikaments verwendet wird. Die Spezifität der AAZ-Extraktion wurde systematisch optimiert. Es wurde gezeigt, dass CAII die AAZ-Extraktion im Vergleich zur Verwendung eines blossen Extraktionswerkzeugs um den Faktor 3.3 erhöht. Die LOD von AAZ aus phosphatgepufferter Kochsalzlösung (PBS) und menschlichem Plasma beträgt 0.4 bzw. 1.2 µg/ml, was den gesamten therapeutischen Bereich abdeckt. Darüber hinaus belegt die relative Standardabweichung von weniger als 14% ( $n=40$ ) die Wiederholbarkeit der Methode.

This page intentionally left blank.



---

## VII. Acronyms and Abbreviations

ALIS	Automated Ligand Identification System
AMS	Ambient Mass Spectrometry
ANS	8-AnilinoNaphthalene-1-Sulfonic Acid
APCI	Atmospheric Pressure Chemical Ionization
API	Atmospheric-Pressure Ionization
APPI	Atmospheric Pressure Photo Ionization
CCD	Charge Coupled Device
CE	Capillary Electrophoresis
CEM	Chain Ejection Model
CGS	Capillary Gap Sampler
CI	Chemical Ionization
CRM	Charge Residue Model
DBDI	Dielectric Barrier Discharge Ionization
DMF	DiMethyl Formamide
EDM	Electro-Discharge Micromachining
EI	Electron Ionization
ESI	Electrospray Ionization
ETHZ	Eidgenössische Technische Hochschule Zürich
FAB	Fast Atom Bombardment
GC	Gas Chromatography
HTS	High-Throughput Screening
ICP	Inductively Coupled Plasma
ID	Inner Diameter
IEM	Ion Evaporation Model
ITC	Isothermal Titration Calorimetry
LASs	Linear Alkylbenzene Sulfonates
LC	Liquid Chromatography
LDI	Laser Desorption Ionization
LOD	Limit Of Detection

---

LOQ	Limit Of Quantification
MALDI	Matrix Assisted Laser Desorption Ionization
MS	Mass Spectrometry
NAG <sub>3</sub>	N, N', N''-triacetylchitotriose
NMR	Nuclear Magnetic Resonance
OD	Outer Diameter
PAN	Poly Acrylo Nitrile
PBS	Phosphate Buffered Saline
PDMS	Poly DiMethyl Siloxane
PEEK	Poly Ether Ketone
PFAND	PerFluoro Alkyl Nitro Dopamine
PMMA	Poly Methyl Methacrylate
RSD	Relative Standard Deviation
SCS	Semi-open Capillary Sampler
SEM	Scanning Electron Microscopy
SIL	Stable Isotope Labeling
SIMS	Secondary Ion Mass Spectrometry
SPE	Solid-Phase Extraction
SPME	Solid-Phase Microextraction
SPR	Surface Plasmon Resonance
SMDC	Small Molecule-Drug Conjugate
TI	Thermal Ionization
TIC	Total Ion Current
XIC/EIC	Extracted Ion Current

# Chapter 1

## Introduction

This Chapter provides a general overview of the necessity of high-throughput screening (HTS) techniques. Moreover, the different categories of miniaturized microfluidic platforms interfacing mass spectrometry are illustrated. Then major focus of this chapter is the introduction of the capillary gap sampler as a solution to overcome the drawbacks of the existing high-throughput sampling devices for mass spectrometry.

## 1.1 High-Throughput Screening

The path from studying and understanding a disease to introducing a potent treatment on the market is long, complicated, expensive and high-risk. Drug discovery and preclinical stages consume a significant amount of time during this process. It takes years of research to study vast libraries of chemical compounds. High-throughput screening (HTS) allows researchers to quickly conduct millions of chemical, genetic or pharmacological tests within a short time. Therefore, HTS is a crucial step in drug discovery due to the immense savings in time and costs.<sup>1-4</sup>

There are various screening methods that provide qualitative information, quantitative information or both types of information. Well-known examples include X-ray spectroscopy,<sup>5</sup> surface plasmon resonance (SPR),<sup>6</sup> isothermal titration calorimetry (ITC),<sup>7</sup> nuclear magnetic resonance (NMR),<sup>8</sup> automated ligand identification system (ALIS)<sup>9</sup> and mass spectrometry (MS).<sup>10</sup> In order to describe and evaluate a screening method, various figures of merit are used, such as screening speed, sensitivity, sample preparation and consumption, robustness and cost. A fast screening method utilizing low sample amounts can be referred to as a HTS method. Among the aforementioned screening methods, MS is a powerful tool for sample analysis. The sample introduction process for electrospray (ESI)-MS includes manually loading a few microliters of a sample into a capillary and spraying it into the MS orifice. The time-consuming process of manual capillary loading limits the throughput of ESI-MS analysis. As a result, development of a high-throughput sampling source for ESI-MS has attracted a lot of attention in the last decade. The majority of HTS sources are based on microfluidic technology, where the flow is controllable.<sup>11-13</sup> Using microfluidics not only decreases sample consumption, but also allows for sample introduction to be parallelized. This parallelization ultimately increases the throughput of the screening. Therefore, merging microfluidics to MS is interesting due to the increased speed of analysis and also because they can handle small sample amounts, in particular biological samples which are only available in very tiny amounts. Critical points for miniaturized sampling systems include: (1) controllable and robust sample uptake, and (2) continuous sample transfer and delivery to the MS. In the following section, three groundbreaking techniques for coupling microfluidics to MS, including mechanical valves, chip-based systems and non-chip-based systems are introduced.<sup>14</sup>

### **1.1.1 Mechanical Valve Systems**

Mechanical valve sample injectors consist of an internal rotor bore, which replaces the traditional sample loop. However, while mechanical valves offer high robustness and repeatability of injection, they have some restrictions for low sample amounts. A few nanoliter (nL) sample is exposed to a large area during injection, causing non-specific sample adsorption on the walls of the injection path. Furthermore, the existence of dead volumes, like connection points, traps the sample. This is very critical for integration into lab-on-chip (LOC) platforms. Despite these limitations, mechanical valves have been used for HTS<sup>15</sup> and flow injection analysis, where the sample is injected into a flow stream and is transferred through a modulator into a detector.<sup>16, 14</sup>

### **1.1.2 Chip-based Systems**

Due to developments in chip fabrication technology, chip-based sample analysis by MS is growing extensively.<sup>17- 19</sup> Improvements in chip micromachining techniques such as X-ray photolithography, HF etching, UV exposure, laser ablation, plasma etching and injection molding allow for advances in chip design. The initial fabrication process was optimized for silicon but has been expanded to include a broad range of materials including glass/Pyrex, quartz, PDMS, PMMA, polycarbonate, polyimide, polyester, etc.<sup>20</sup> Microfluidic chips are coupled to the mass spectrometer using the electrospray ionization (ESI) technique. This can be applied in three approaches. In the first approach, the sample was transferred through microfluidics channels and was directly sprayed into the MS from the edge of the chip.<sup>20</sup> However, the precise positioning of the electrospray at the chip edge is not easy to control and the liquid leaving the microfluidic channel tends to spread along the edge of the chip. One of the solutions to this problem is applying a coating to the channel and the chip edge, which is not stable in the long-term, and is not applicable in cases of on-chip separations, where a gradient of different solution polarities is required. The second and the third approach were devised to overcome this issue. The solution involved using a spray tip at the end of the channel, either by inserting a fused-silica capillary into the channel<sup>21</sup> or by integrating a monolithic emitter during the fabrication process. Integrated emitters became popular due the ease of mass fabrication, since the fabrication of the channels and emitter is performed in one step, and due to the elimination of dead volumes.<sup>22</sup> In addition, chips were used for separation by filling selected channels with adsorption material. A major drawback of using classical mechanical valve

and chip-based miniaturized sampling systems is that sample is adsorbed on the walls while passing through the platform to reach the detector. Using inert coatings such as Teflon or inert system liquids such as oils and surfactants were attempts to minimize sample adsorption. Still, direct sample uptake and delivery remain challenging.<sup>14</sup>

### 1.1.3 Non-chip-based Systems

Alternatively, several non-chip-based platforms that can be coupled to ESI-MS are available. The Swan-probe sampler, comprised of a U-shaped micro-channel with a horizontal emitter tip, is one high-throughput sampler example. The channel is vertically grounded at the bottom of the U-shaped section to create a 100  $\mu\text{m}$  hole for sample reception.<sup>23</sup>

Rapidfire from Agilent and Nanomate from Advion are the well-known established examples of non-chip-based systems.<sup>15, 24</sup> Using an automated pressure-assisted sample uptake system, the Rapidfire reduces the injection cycle to 6-13 seconds per sample. A robot scans and moves the microwell plates automatically, so that a high number of samples can be analyzed without human supervision. Additionally, it provides an automated online solid-phase extraction (SPE) by injecting sample volumes of  $> 10 \mu\text{L}$  into an extraction cartridge. Furthermore, the Nanomate<sup>25</sup> enables the analysis of a sample without cross-contamination, by applying an automated pipette to deliver a few microliters into the mass spectrometer. The pneumatically assisted spraying through nano-electrospray nozzles can last up to several minutes. Four hundred independent nozzles are fabricated on one chip. Both systems require vacuum for sample uptake and transfer, and gas or liquid flow driven overpressure for sample infusion.

Although HTS methods with a high level of maturity exist, there is room for improvement in terms of sample consumption, screening speed and system functionality. One of the drawbacks of conventional systems is analyte adsorption on the exposed surface area of the sample introduction line and challenges in direct uptake and introduction of a few nL sample. This thesis focuses on a high-throughput sampler coupled to the MS that not only overcomes these drawbacks, but also provides further functionalities such as sample up-concentration and online reaction monitoring.

## **1.2 Capillary Gap Sampler**

In 2008, Hoffmann-La Roche developed an autosampler called the “Capillary Gap Sampler” (CGS).<sup>26</sup> The CGS (shown in Figure 1) is a miniaturized sampling device that combines the sampling of low sample volumes (> 4 nL) with direct ESI-MS analysis. The basic idea consists of the delivery of a small sample droplet to a liquid bridge to be analyzed by the MS. The liquid bridge is formed in a gap between two capillaries, where the second capillary sprays the sample into the MS inlet. The continuous flow through the liquid bridge provides a continuous fresh surface to receive new samples. This device enables fast (9–11 seconds), automated and comprehensive analysis of various samples. Therefore, its main application is direct online high-throughput screening. The advantage of the CGS over other HTS technologies is its sample uptake mechanism, which decreases the sample volume drastically and does not require valves or additional lines. Another unique feature of the CGS is the possibility of site-specific sample pickup, hence increasing its usefulness for imaging applications.

However, the formation and maintenance of the liquid bridge depend on different factors such as the surface tension of the flowing solution, the flow rate, the spray voltage, the gap distance between the capillaries, the pressure inside the chamber, the surface composition and the geometries of the capillaries.<sup>14</sup> Optimization of these parameters can be difficult and time consuming. In Chapter 3, improvements in stability and sensitivity of the microfluidic platform are described.<sup>27</sup>

### **1.2.1 CGS Design**

The main components of the CGS are shown in Figure 1, including a sampling tool and a microfluidic platform as the sample receptor. Using an x, y and z positioning stand, the setup (< 5 kg) is fixed to the front section of the ESI-MS.

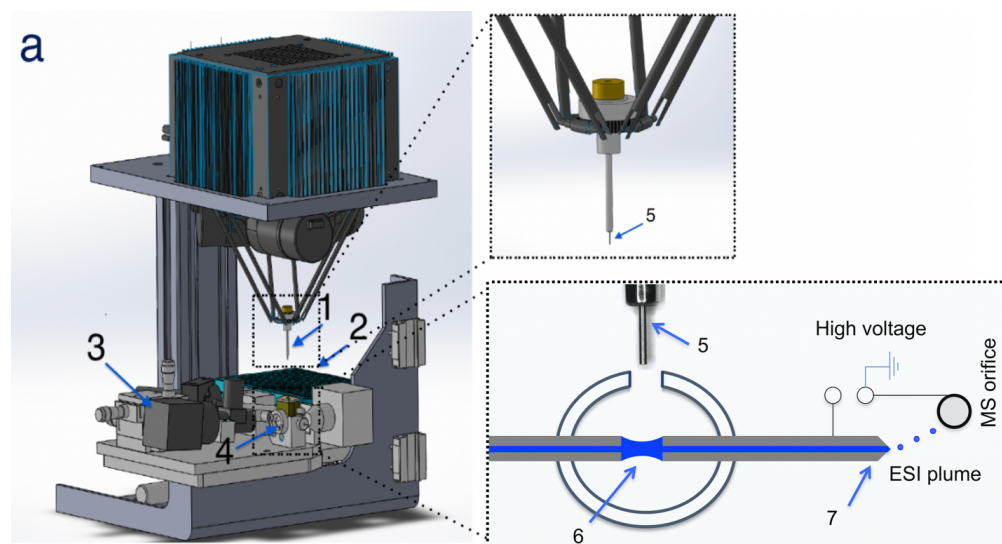


**Figure 1.** Components of the capillary gap sampler: (a) overall design of the capillary gap sampler, which consists of different components including: (1) extraction tool and pin sleeve, held by delta robot arms, (2) microwell plate, (3) camera for online monitoring of the gap, (4) pressure chamber ( $V=0.65$  ml) held under a controlled overpressure, (5) solid stainless-steel pin (229  $\mu\text{m}$  diameter) used as an SPME tool, (6) liquid bridge for sample desorption, (7) stainless-steel capillary with a tapered tip, which sprays the desorption solution into the orifice of the MS by applying a high voltage to the spray.<sup>4</sup>

The sampling tool is responsible for sample uptake, extraction and delivery into a liquid connector. The sampling tool is a solid stainless-steel pin (356  $\mu\text{m}$  in diameter, V&P Scientific, San Diego, CA, USA), which picks up a small droplet of the sample by dipping into a microwell. A metal sleeve surrounds the pin and allows entrance to the injection port with a tolerance of a few micrometers and seals the chamber when it becomes open for injection. Thanks to the sealing of the chamber and precise injection port manufacturing, the pressure drop monitored by the online pressure regulator is  $< 1$  mbar.<sup>26</sup> This sampling tool is held and moved by a light microrobot (model PocketDelta, Asyril, Villaz-St-Pierre, Switzerland) with fast, pulsation-free and precise movement (3  $\mu\text{m}$ ). The volume of the sample depends on the pin diameter and sample solvent. The sample delivery occurs in the pressure chamber, where two capillaries face each other with a gap of about 200-300  $\mu\text{m}$ . This chamber ( $V= 0.65$  ml) is made of PEEK and is held under a controlled overpressure of several mbars. A liquid bridge is formed when a solution is delivered by a syringe and flows through the fused silica capillary (360  $\mu\text{m}$  O.D., 50  $\mu\text{m}$  I.D., Polymicro, Phoenix, AZ,



USA) and then fills the gap between the two capillaries and enters the second stainless-steel capillary (320  $\mu\text{m}$  O.D., 50  $\mu\text{m}$  I.D., 50 mm length, New Objective, Woburn, MA, USA). In order to spray the solution, a high voltage is applied between the MS orifice and the second capillary using a conductive ferrule and a nut holding the spray capillary. The second capillary sprays the sample directly into the MS inlet. With a buffer flow of 1  $\mu\text{L}/\text{min}$  and a voltage of 2.8–3.5 kV, a liquid bridge of 10–40 nL is formed. Alternatively, a single capillary with a hole can be used as the sample receptor. This yields higher sensitivity, robustness and ability to function when using high surface tension solutions.<sup>27</sup> The sample delivery step is monitored by a CCD camera (model  $\mu$ -eye, VS Technology Cooperation, Tokyo, Japan) and Telocentric optics (VS Technology Cooperation). More information and details can be found in the Appendix and in a previous publication by Neu *et al.*, 2013.<sup>26</sup>

### 1.2.2 Characteristics of the Liquid Bridge

Liquid bridge formation is initiated when a solution is pumped through a capillary which faces another capillary with a micrometer-sized distance between the two; the solution then enters the inlet of the second capillary while filling the gap between them. Several significant factors influence the formation of the liquid bridge. The flow rate of the liquid inside the capillary defines the probability and ease of the formation of the liquid bridge as well as its stability. High flow rates ( $> 1.5 \mu\text{L}/\text{min}$ ) will cause the solution to flood, and low flow rates ( $< 0.5 \mu\text{L}/\text{min}$ ) are not sufficient to build a constant flow from the outlet of the first capillary to the inlet of the second capillary. Changing the overpressure inside the sealed chamber controls the bridge shape whenever it shrinks or expands. The difference between the chamber pressure (that surrounds the second capillary inlet) and the ambient pressure (which surrounds the outlet) causes a pressure gradient along the capillary. This pressure gradient, the applied voltage to the spray tip, the backpressure generated at the capillary outlet tip, the flow rate and the gap distance are all factors that can be adjusted when building and maintaining the liquid bridge.

On the other hand, the formation, stability and shape of the bridge are strongly dependent on the surface tension of the solution. High surface tension solutions ( $> 60 \text{ mN m}^{-1}$ ) are very difficult to control. The main explanation for this observation is their long response time to changes in flow

rate or pressure. This long response time causes failure in the formation of the bridge. The gap distance, capillary dimensions and capillaries' inner and outer coating are the main factors that can be controlled prior to the test but cannot be modified during the experiment. Based on the results of a study by Volker Neu *et al.*,<sup>26</sup> this microfluidic element was found to have intrinsic self-stabilization fluctuations. However, if these fluctuations exceed a certain range of values, they cause flooding or break the bridge.

### 1.2.3 Operation Cycle of a Sample Injection

Sample injection consists of several automatic steps: (1) the pin moves with a defined speed from the home position to the selected microwell and dips into a certain depth of the well, (2) the hanging sample droplet is then transferred to the injection port, (3) the pin enters the injection port and stops before the rotating bore, which acts as a valve for pressure sealing, (4) the bore rotates 90 degrees and opens, (5) the pin enters the chamber and stops a few micrometers above the liquid bridge, (6) contactless sample injection is performed, (7) it leaves the chamber, (8) the bore rotates 90 degrees to the closed position, (9) the pin moves to the washing and drying station, and is dabbed on a blotting paper, (10) later it returns to the home position and is ready for the next injection. The entire cycle takes approximately 9–20 seconds, depending on the length of the washing and drying process. Figure 2 illustrates the main steps of the sample infusion cycle.

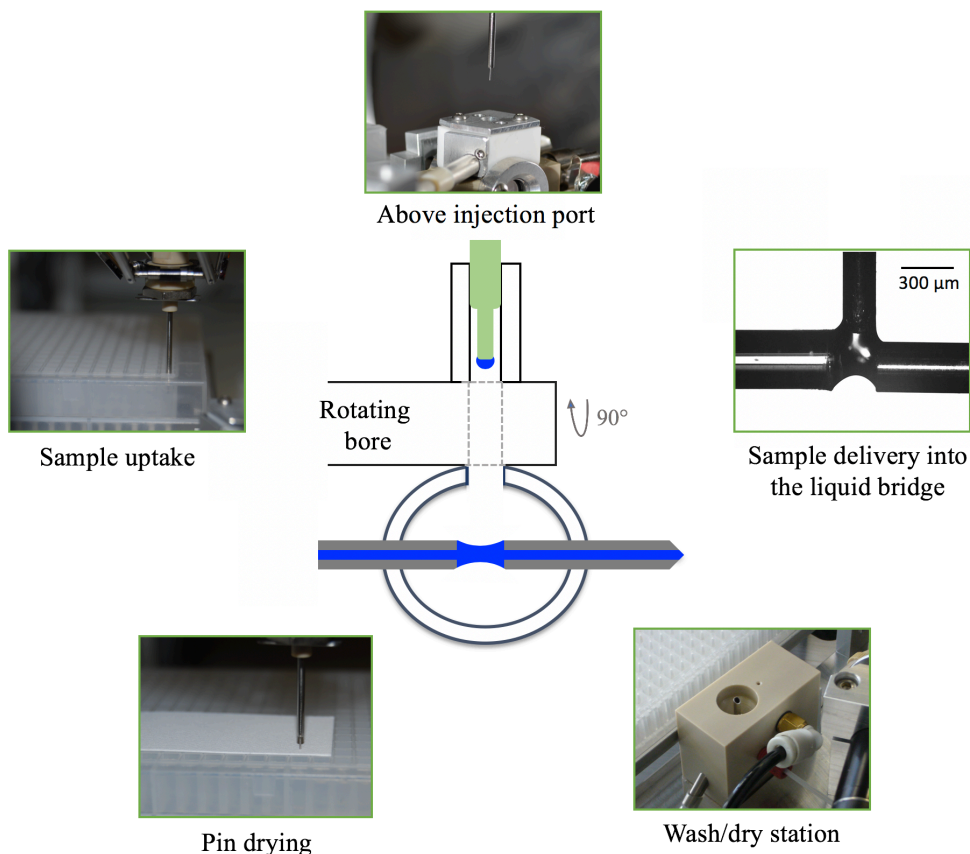


**Figure 2.** Major steps of the operation cycle of sample injection.

### 1.3 High-Throughput Sample Extraction

Complex samples often require preparation such as extraction before being analyzed, because they are not useable by most of the analytical instruments that cannot handle matrices. Accordingly, there is a great need for a method which can isolate the component of interest from the sample matrix in a high-throughput fashion. The solid-phase microextraction (SPME) technique is an established example of a clean-up method which can be coupled to the CGS for fast sample up-concentration prior to MS analysis. In the next section, the importance of SPME and a case study are discussed.

#### 1.3.1 Solid-Phase Microextraction

SPME is an innovative, solvent-free sample preparation technique in which an extractive phase is deposited on the outer surface of a carrier. This method is applicable to complex matrices

containing particulate matter, as well as unprocessed samples without any need for sample pretreatment. Therefore, since its introduction in 1990 by the Pawliszyn group,<sup>28, 24</sup> it has been an alternative sample clean-up method and has undergone extensive development. Performing SPME addresses several drawbacks of conventional extraction methods such as SPE. It reduces the solvent use, the amount of extraction material required, the extraction tool size and the impact on the sampled system, especially for on-site applications. Depending on the experimental conditions and goals, three significant methods for performing SPME exist: a direct extraction, a headspace extraction and a membrane-protection extraction. In direct extraction, the coated fiber is directly inserted inside the sample, and the analyte of interest moves from the bulk of the solution to the extraction phase. If the analyte of interest is a volatile compound with high-molecular-weight interferences, headspace sampling is recommended as the method of choice. Here, the fiber is placed on top of the solution in a closed vial, and the volatile compounds are extracted from the gas-phase. If extraction is focused on a non-volatile compound in the presence of a high-molecular-weight interference, membrane-protected SPME is performed. It decreases non-specific adsorption and results in better accuracy and reproducibility. Once the method is selected, there are two possible approaches to implement it. In the first approach, a partitioning equilibrium between the extraction phase and the sample is reached, which is known as equilibrium-based SPME. The maximum extraction occurs at the equilibrium stage, and therefore, convection does not affect the extraction amount. Another way of performing SPME is pre-equilibrium extraction. In this case, extraction time and convection influence the accumulation of the analyte in the extraction phase.<sup>29</sup>

Drug extraction from human plasma or whole blood is one of the major focuses of SPME. Extraction of small molecule-drug conjugate (SMDC) compounds from human plasma was chosen as a case study to be performed by the CGS. Chapter 5 covers the SMDC extraction study in detail.

### **1.3.2 Small Molecule-Drug Conjugates**

The majority of anti-cancer drugs are designed to interfere with cell proliferation or survival events. However, chemotherapeutic agents often do not selectively accumulate in tumor tissue after systemic administration. The unspecific biodistribution of the anti-cancer drugs causes

undesired toxicities in healthy organs and limits their therapeutic effectiveness. The targeted delivery of potent cytotoxic agents to tumors represents a promising strategy to improve the therapeutic index and to limit undesired systemic toxicities.<sup>30- 33</sup> In an attempt to improve drug efficacy, tumor-specific antibodies and small molecules have been proposed as selective delivery vehicles of toxic payloads to malignant cells. This approach led to the generation of new classes of drugs called Antibody-Drug Conjugates (ADCs) and Small Molecule-Drug Conjugates (SMDCs). The general structure of ADC and SMDC products includes a therapeutic payload attached to a ligand specific to a marker of the disease, through a spacer that often contains a cleavable bond.<sup>31</sup> In this way, the drug will accumulate and act at the intended site of action, therefore increasing the efficiency of the applied dose, while side effects for the healthy cells decrease.

#### **1.4 Outline of the Thesis**

In this work, the development of an autosampler called the “semi-open capillary sampler” is reported, which is capable of automatic and direct low-volume (> 4 nL) sample introduction into electrospray mass spectrometry (ESI-MS), as well as automatic solid-phase microextraction. The first chapter has summarized high-throughput screening methods and the necessity of developing the semi-open capillary sampler. The second chapter focuses on mass spectrometry principles, figures of merit and the necessary instrumentations.

Chapter 3 discusses an advancement to the system that increases the sensitivity and robustness of the original system (CGS). This improvement was achieved by replacing the liquid bridge with a monolithic pierced capillary as the sample receptor, which allows for a wider range of applications, in particular those that require an aqueous solution.

Chapter 4 describes how this sampler was directly coupled to ESI-MS as a solid-phase microextraction (SPME) tool by extracting several benzodiazepine compounds from phosphate-buffered saline (PBS) and human plasma as a case study. The successful extraction of benzodiazepine from human plasma within the therapeutic range confirms that the device can be used as a sample clean-up method.

Chapter 5 demonstrates the preparation and use of a specific SPME tool to extract a recently designed anti-cancer drug from human plasma. This extraction is based on a protein-inhibitor high-affinity interaction. The ultimate goal of this chapter is to show the future potential of the sampler for the evaluation of targeted drug delivery performance by investigating the biodistribution of the drug in cancer cells versus in healthy cells.

The conclusion of each chapter, future potential applications and possible advancements are discussed in Chapter 6. The last chapters combine the experiments that support the claims made in Chapters 3, 4 and 5. Finally, the appendix includes the standard operating procedure (SOP) of the instrument, where the instrumentation is discussed in detail.

# Chapter 2

## Methodology

This thesis is a product of experiments conducted by coupling the CGS to a Synapt G2-S, a high-definition time-of-flight (TOF) mass spectrometer. The main focus of this chapter is the description of the ESI-TOF MS. It starts with the principles of MS and continues with the description of figures of merit representing the performance of MS. Various ionization techniques are described, including detailed discussions of ESI mechanisms and applications. Moreover, the theoretical basis of the reflectron time-of-flight mass analyzer, as well as the Synapt G2-S, are explained.

## 2.1 Principles of Mass Spectrometry

MS is a technique that measures the mass-to-charge ratio of ions and thus provides both qualitative and quantitative (molecular mass or concentration) information about certain analytes. It consists of three main parts: an ion source, a mass analyzer and a detector. It has many applications and is in widespread use due to its high sensitivity, selectivity and accuracy. The foundation of this significant analytical tool was laid by Joseph John Thomson and led to his Nobel prize at the end of the nineteenth century, and later Francis William Aston invented the MS.<sup>34</sup> It has applications in biomedical science, pharmaceutical science, food authentication, forensic science and sports doping research.<sup>35-41</sup>

### 2.1.1 Mass Spectrum

Mass spectrum is composed of two-dimensional data and represents ion intensity against mass-to-charge ( $m/z$ ) ratio. The intensity of the ion species is normalized to the most intense peak, called the base peak. The peak at the highest  $m/z$  is called the molecular ion, and other peaks mostly represent fragmented and multiply charged molecular ions. These data yield molecular structure determination.<sup>42</sup>

The type of information mass spectrum can provide for a particular analyte differs depending on the type of mass spectrometer and the instrumental tuning parameters. For example, molecules can be ionized to single or multiply charged species, and can stay intact or become fragmented. Therefore, in cases of fragmentation, mass spectra provide more detailed structural information.

### 2.1.2 Ion Chromatogram

Ion chromatogram refers to the intensity of ions versus time or scan number. The total ion current (TIC) refers to a chromatogram presenting the total ion current detected during the analysis period versus time. The term “reconstructed ion chromatogram” (RIC) or “extracted ion chromatogram” (EIC, XIC) is used to describe a chromatogram obtained by recording the intensity of a certain  $m/z$  ratio.<sup>42</sup>



## **2.2 Performance of Mass Spectrometry**

The performance of a mass spectrometer can be defined in different ways. Sensitivity, detection limit, signal-to-noise ratio and resolution are among the most important evaluation factors, which are briefly introduced in the following section.

### **2.2.1 Sensitivity**

Sensitivity is the slope of the calibration curve and defines the instrument's response to a particular amount of a substance: the higher the response, the more sensitive the technique. The sensitivity of a mass spectrometer depends on the ionization method, the ionization efficiency, the mass analyzer and other instrumental tuning parameters.

### **2.2.2 Limit of Detection**

Limit of Detection (LOD) defines the smallest quantity of a substance that is detectable when it is compared to the corresponding blank solution.<sup>43</sup> In this thesis, LOD was calculated for a signal-to-noise (S/N) ratio of 3:1 by using the EIC extracted at a certain mass range. Although the sensitivity of an instrument affects the detection limit, LOD yields entirely different information.

### **2.2.3 Signal-to-Noise Ratio**

The S/N ratio describes the accuracy of an intensity measurement. The level of accuracy depends on the noise value. Usually, noise results from electronics, matrix effects, etc. Noises appear not only between the signals, but also on the signals. Consequently, they affect intensity measurements.<sup>42</sup> The S/N ratio can be used to compare the performance of different MS systems because it provides a quantitative measure of a signal's quality.

### **2.2.4 Resolution**

The resolving power of a MS defines its ability to distinguish between two peaks with slightly different  $m/z$  in a mass spectrum. A high-resolution MS allows the detection of an analyte to almost 0.001 mass units, hence it is considered a very selective analytical instrument.<sup>44</sup>

### 2.3 Ionization Techniques

Depending on the analyte, different ionization methods can be used. Ionization occurs in the ion source. There are different types of ion sources available, each providing advantages and disadvantages for a particular application. The large variety of ionization techniques can be classified by their relative softness or hardness. Hard ionization techniques cause a high degree of fragmentation, thus yielding very detailed mass spectra. Electron ionization (EI) is one of the hard ionization examples.<sup>45, 46</sup> These techniques provide detailed information on the structural elucidation of an unknown compound and therefore facilitate its identification. Soft ionization methods expose little residual energy to the molecules, thus causing less fragmentation. These methods are especially useful when considering biological substances of large molecular mass. Examples of soft ionization techniques include fast atom bombardment (FAB),<sup>47</sup> chemical ionization (CI),<sup>48</sup> electrospray ionization (ESI),<sup>49, 50</sup> matrix-assisted laser desorption/ionization (MALDI),<sup>51, 53</sup> atmospheric pressure chemical ionization (APCI)<sup>54, 55</sup> and atmospheric pressure photo ionization (APPI).<sup>56</sup> ESI and MALDI-MS were introduced in the 1980s by Fenn Yamashita and by Tanaka and Hillenkamp, respectively.<sup>57, 59</sup> ESI and MALDI are the most prominent among these techniques, and both have expanded the application of MS in the fields of biology and biomedical science.<sup>42, 62</sup>

### 2.4 Electrospray Ionization

ESI is a soft ionization technique that provides a sensitive, robust tool for sample ionization. A dilute (less than mM) analyte is injected through a capillary. A high voltage (2–6 kV) is applied to the capillary metal or metal-covered tip. The strong electric field causes the formation of an aerosol. The molecules are ionized into multiply charged ions. One of the advantages of ESI is that solution-phase information can be retained in the gas-phase.<sup>63</sup> The other advantage is that the molecular ion is mostly observable due to the minimal ion fragmentation. However, only less-structured information can be gained. Coupling ESI with tandem MS (ESI-MS/MS) overcomes this disadvantage.

### 2.4.1 Ion Formation in ESI

The ionization mechanism involves three main stages: (1) dispersion of the liquid containing the analytes into a fine aerosol, (2) solvent evaporation, and (3) ion ejection from the highly charged droplets. Large-flow or high surface tension liquids can benefit from a heated inert gas (e.g. N<sub>2</sub>), which flows around the eluted sample solution and enhances the desolvation speed. There are three main mechanisms suggested for gas-phase ion formation as shown in Figure 3, including the ion evaporation model (IEM), the charge residue model (CRM) and the chain ejection model (CEM).<sup>64, 67</sup> The IEM model is generally used to describe the gas-phase ion formation of low-molecular-weight analytes. This model suggests that when the droplet reaches a certain radius and the field on its surface becomes strong enough to overcome solvation forces, a solute ion leaves the droplet surface. The CEM model applies to large species such as folded proteins. This model suggests that Coulomb explosions and solvent evaporation to dryness will ultimately liberate large molecule ions. The CRM has been proposed by Konermann *et al.*<sup>67</sup> for i) partially hydrophobic polymers and ii) unfolded proteins. This model suggests that the unfolded chains of a protein or a polymer migrate to the surface of the droplet, followed by a stepwise ejection and a complete separation from the droplet.<sup>67</sup>

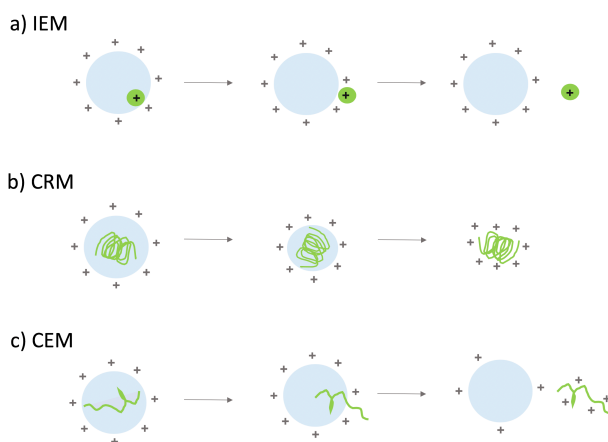


**Figure 3.** Three main ion formation mechanisms in the gas-phase, (a) the ion evaporation model (IEM), (b) the charge residual model (CRM) and (c) the chain ejection model (CEM).

### 2.4.2 Applications of ESI

ESI is a gentle method of ionization in which electrical voltage is used for the ionization and transformation of ions from the solution into the gas-phase at atmospheric pressure. Therefore, large nonvolatile, chargeable compounds can be studied by ESI-MS.

ESI is the interface of choice for coupling liquid or gas chromatography (LC/GC) and capillary electrophoresis (CE) to the MS. This facilitates the analysis of very small biological and chemical compounds, metal complexes, oligonucleotides, DNA, RNA, high mass proteins, protein complexes, protein-protein interactions, protein folding, non-covalent gas-phase interactions, screening for human metabolic disorders, high-throughput analysis, solid-phase extractions, etc.

## 2.5 Time-of-Flight Mass Spectrometry

The time-of-flight (TOF) mass analyzer was developed in the late 1940s by W. E. Stephens.<sup>68</sup> This method determines the ion's mass-to-charge ratio based on the time it takes for an ion to reach the detector. All ions become accelerated by an electric field to the same potential energy. The ions move towards the detector through a flight tube. Their velocity depends on their mass-to-charge ratio. Ions with the same charge have the same potential energy. Considering the conversion of potential energy into kinetic energy, lighter ions have a higher speed. The time that it subsequently takes for the ions to fly a known distance and hit the detector is determined (as shown in 2.5.1). This time is a function of velocity and therefore provides  $m/z$  information.

### 2.5.1 Ion Velocity

The theory of TOF separation can be explained by calculating the difference between ion velocities. Depending on the strength of the electric field and the charge of the particle, the potential energy can be defined as follows:

**Eq. 1** 
$$E_p = qU$$

Independent of the ionization method, an ion with a mass of  $m$ , a charge of  $q$  and a voltage of  $U$  has the potential energy of  $E_p$ . As the particle is accelerated into the TOF tube, the former potential energy is converted into kinetic energy.

Eq. 2 
$$E_k = \frac{1}{2} m v^2$$

Assuming the ion had no initial speed:

Eq. 3 
$$E_k = E_p$$

Eq. 4 
$$\frac{1}{2} m v^2 = qU$$

And knowing that the ion's velocity is inversely proportional to the square root of its mass:

Eq. 5 
$$v = \sqrt{\frac{2qU}{m}}$$

Considering  $q = ze$ , where  $z$  is the charge of the ion and  $e$  is the elementary charge:

Eq. 6 
$$v = \sqrt{\frac{2zeU}{m}}$$

Eq. 7 
$$\frac{m}{z} = 2eU/v^2$$

This is how the  $m/z$  ratio is calculated in the TOF mass analyzer.<sup>42</sup>

Considering  $v = d/t$  where  $d$  is the flight length and  $t$  is the flight time, then time-of-flight is:

Eq. 8 
$$t = d/\sqrt{\frac{2zeU}{m}}$$

### 2.5.2 Reflectron Time-of-Flight Analyzer

In reality, the starting time, initial kinetic energy, starting location and initial direction of the movement of the charged particles is not the same. These differences make Eq. 3 incorrect, because they result in differing times-of-flight. This variance is corrected by using a reflectron (Figure 4),

which is made of a series of ring-shaped electrodes with a voltage gradient and is located in the field-free drift tube. Ions of the same mass but different velocities penetrate the reflectron to various depths. It takes longer for ions with more energy to become ejected in the opposite direction due to their longer flight paths. Therefore, ions of the same mass arrive at the detector, which is slightly offset from the initial ion beam path. Using this feature, the time-of-flight of ions with different initial levels of kinetic energy is corrected while their kinetic energy remains unaffected. By using two- or multi-stage reflectrons, the performance of the mass analyzer can be further improved. This substantially enhances the resolving power of the TOF mass analyzer and provides a longer flight path for a given length of the TOF instrument.<sup>42</sup>

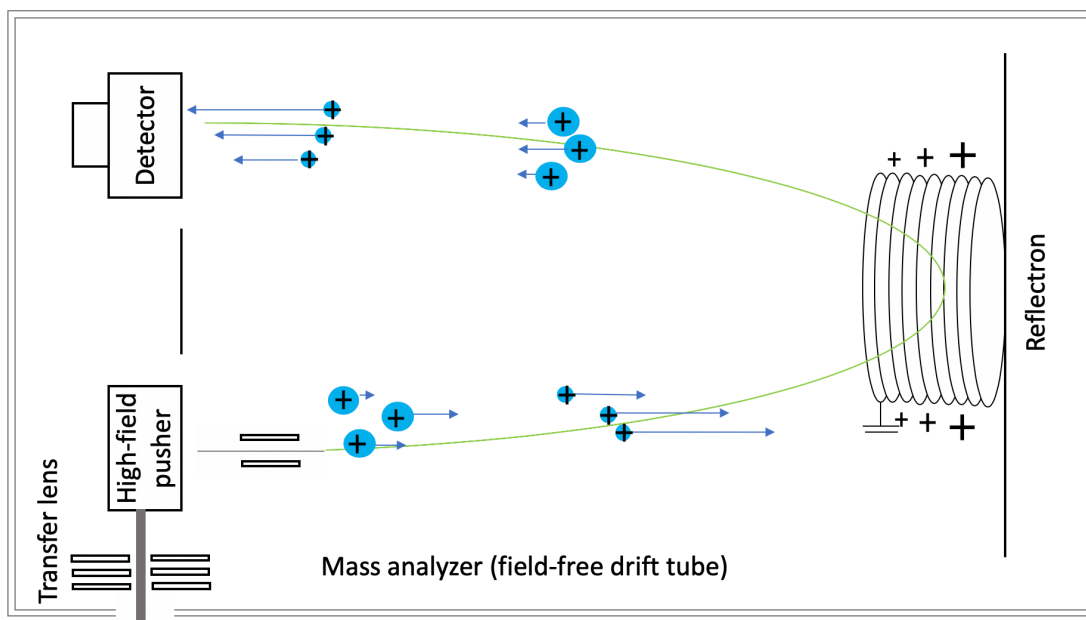


**Figure 4.** Principle of operation of a reflectron TOF mass analyzer.

## 2.6 Synapt G2-S

The Synapt G2-S high definition mass spectrometry (HDMS) system is a hybrid, quadrupole, ion mobility, orthogonal acceleration, time-of-flight mass spectrometer controlled by MassLynx software. The main components of this instrument are: (1) the source with the StepWave ion guide, (2) a quadrupole, (3) the TriWave device and (4) the TOF mass analyzer. A sample is introduced at atmospheric pressure into the ionization source, undergoes expansion, and then reaches the

StepWave. In the StepWave, neutral material is extracted from the system. In the next stage, ions enter the quadrupole and are filtered based on different  $m/z$  ratios. The mass-separated ions undergo collision-induced dissociation (CID) in the TriWave. In the TOF analyzer, using high-voltage pulse orthogonal acceleration, ions of different mass-to-charge ratios have different flight times. These times are recorded and converted into  $m/z$ .

The orthogonal acceleration and dual reflection features provide high-resolution detection capabilities. The TOF analyzer can be operated in sensitivity, resolution and high-resolution mode depending on the purpose of the experiment. Figure 5 shows the Synapt G2-S ion optics overview.<sup>69</sup>

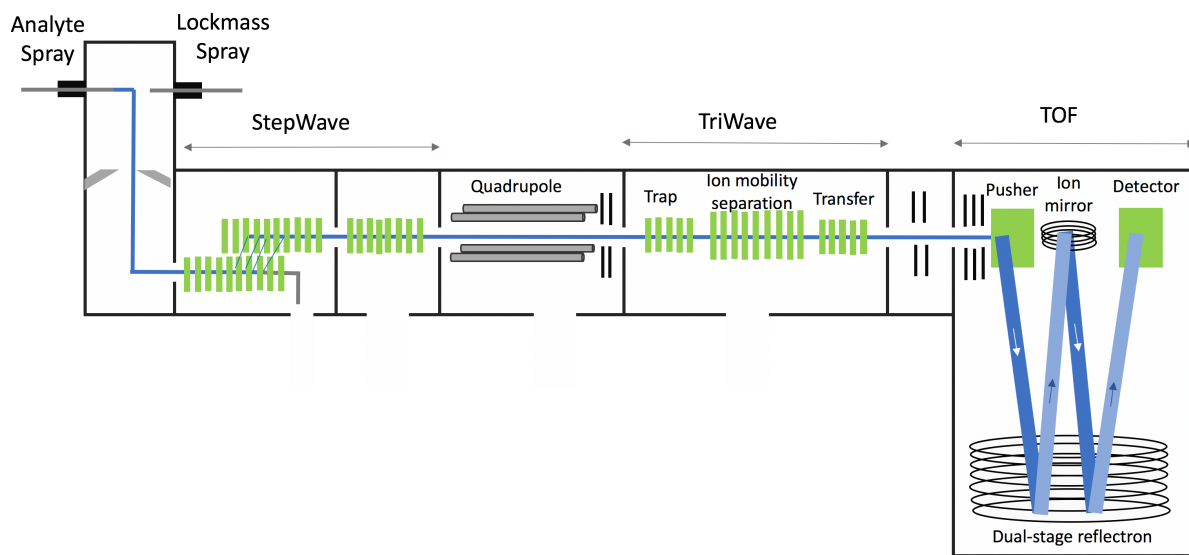


**Figure 5.** Synapt G2-S ion optics overview, including ion source, StepWave, TriWave and TOF mass analyzer.

This page intentionally left blank.



# Chapter 3

## A Comparative Study Between a Miniaturized Liquid Junction Built in a Capillary Gap versus Semi-open Capillaries for nL Sample Infusion to Mass Spectrometry

*This chapter is adapted from:*

Ghiasikhou, S., Marchand, A. & Zenobi, R. A comparative study between a miniaturized liquid junction built in a capillary gap and semi-open capillaries for nL sample infusion to mass spectrometry. *Microfluid Nanofluid* **23**, 60 (2019).

### 3.1 Abstract

This study introduces a novel design for the microfluidic element used in a high-throughput screening (HTS) mass spectrometer autosampler. The original design of the sampler consists of a liquid bridge formed by a micrometer gap between two capillaries. This liquid bridge is used to receive the sample, which downstream is ionized and analyzed by MS. The advancements described here consists in replacing the hardly maintainable liquid bridge by a single pierced capillary called a semi-open capillary. The fabrication of semi-open capillaries is explained. To achieve an optimum structure, two different machining methods were investigated, laser ablation and electro-discharge micromachining (EDM). The advantages of this design over the previous one are reduction of the dead volume and sample dilution, as well as higher stability. Characterization of the repeatability and limit of detection (LOD) show that the optimized semi-open capillary leads to nearly two-fold lower LOD when compared to the liquid bridge.

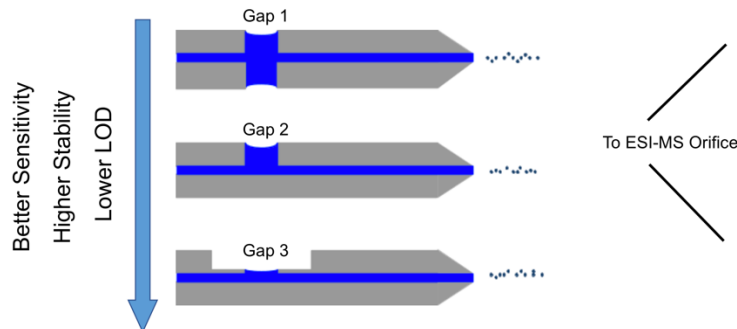


**Figure 6.** Different liquid connector configurations.

### 3.2 Introduction

HTS-MS is a powerful tool to analyze a large number of compounds. During the last decades, the development of high-throughput samplers for MS attracted a lot of attention. Most of them are based on microfluidic technology.<sup>70-73</sup> Microfluidics allows better control of fluids and physical parameters. Second, using minimal amounts of the sample will enable one to decrease the screening cost considerably, and finally, the possibility for automation and parallelization increases the throughput. Well-established microfluidic devices with a right level of maturity already provide rapid and high-throughput compounds analysis.<sup>11-13, 74, 75</sup> However, there remains room for improvement, for example, by decreasing the sample volume, even more, increasing the speed and the robustness of the experiment, and developing multitasking approaches in terms of sample preparation. When it comes to high-throughput drug screening of complex biological samples, an extra step of separation is often needed. Conventionally, MS is combined with gas or liquid chromatography<sup>76-79</sup> or capillary electrophoresis<sup>80, 81</sup> in order to extract the compounds of interest. However, such methods are often incompatible with HTS needs and can be expensive. In 2014, Jin *et al.* introduced the Swan-probe as an inexpensive tool for electrospray ionization (ESI)-MS HTS. It consists of a U-shaped capillary with a horizontal emitter tip. The probe is vertically grounded at the bottom of the U-shaped section such that a hole of about 100  $\mu\text{m}$  forms as sample inlet. By pumping carrier solution through the capillary and placing the inlet on the droplet arrays on a multi-well plate, the sample will infuse inside the capillary and later get mixed and sprayed to ESI-MS. This probe can be dipped into an array of samples and therefore provides continuous sample screening. Sampling speed is about 21 seconds per sample. The main drawback of this autosampler is the lack of precision in the hole fabrication method.<sup>23</sup> In 2004, Ozbal *et al.*<sup>82</sup> developed an ESI-APCI technique and hardware for HT discovery applications. In this method, an integrated microfluidic system is designed in a way that 1–5  $\mu\text{L}$  of sample gets delivered to a chromatography system for purification. The purified sample is then directed to a mass spectrometer for analysis. One injection cycle takes 5 seconds, and the sample carryover issue is addressed using materials such as Teflon, PEEK and fused silica in the microfluidic circuits, as well as chemically modified surfaces. In addition, the entire system is flushed with aqueous and organic buffers between different samples, which increases the analysis time. Screening of

different inhibitors for acetylcholinesterase was performed as a proof of concept, and several potent inhibitors were identified. In 2012, Chen *et al.*<sup>83</sup> developed a stable isotope labelling method performed in a microfluidic chip that is coupled to ESI-MS (SIL-chip-ESI-MS) for HT online analysis of cell metabolism. This platform combines a cell culture chamber and on-chip sample clean-up methods, including a micro-SPE column, connected via a microfluidic network. Such an integration followed by ESI-MS provides a multifunctional chip-based MS platform that has been used for qualitative and quantitative analysis of the metabolism of drug and cell interactions.

In this thesis we introduce the CGS as a HTS platform, which consist of a liquid bridge as the sample receptor. The formation and stability of the liquid bridge depends on different factors such as the surface tension of the solution, the spray capillary voltage, the solution flow rate, the distance between the capillaries, the overpressure inside the chamber, the surface composition of the capillaries and their geometries.<sup>14</sup> The optimization of these parameters can be time taking and difficult.

In this chapter, we present a comparative study between different configurations of the sample receptor in the CGS. We present a new design, where instead of being injected into a liquid bridge between two different capillaries, the sample is introduced into a semi-open capillary. The stability of the device is enhanced, which increases the robustness of the method. In addition, by optimizing the gap shape we could minimize the dead volume of the system, which allows the sample to be less diluted, which therefore increases the limit of detection (LOD). The advantages of the new liquid connector shapes, as well as the production of a semi-open capillary are discussed in the following sections.

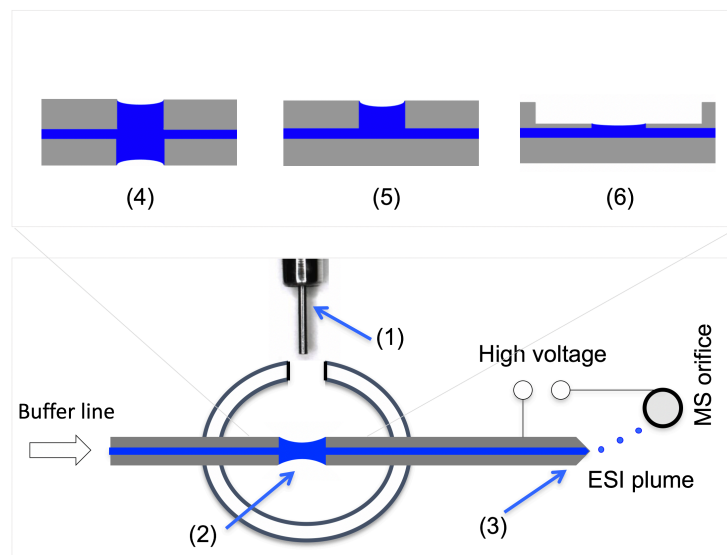


**Figure 7.** Key parts of the Capillary Gap Sampler: sampling tool held by the robot arm (1), liquid bridge (2), ESI spray tip (3), capillary gap so-called “Gap 1” (4), semi-open capillary (fabricated by laser ablation) called “Gap 2” (5), semi-open capillary (fabricated by EDM) introduced as “Gap 3” (6) sample receptors.

### 3.3 Experimental Section

#### 3.3.1 Chemicals and Materials

Acetonitrile  $\geq 99.9\%$  (LC-MS CHROMASOLV), water (LC-MS grade), acetazolamide and leucine enkephalin were purchased from Sigma Aldrich (St Louis, MO, USA). Also, diazepam, diazepam-d5 and nor-diazepam were obtained from Sigma Aldrich (The Woodlands, TX, USA) and stored at  $4^{\circ}\text{C}$ . Methanol (LC-MS grade) was purchased from Fisher scientific (Loughborough, U.K). Formic acid (98-100%) and rhodamine B were purchased from Merck (Darmstadt, Germany). The stainless-steel capillaries for three different configurations have  $320\ \mu\text{m}$  O.D. and  $50\ \mu\text{m}$  I.D. (New Objective, Woburn MA, USA) with the same opening at the end, only different lengths for Gap 1 (50 mm) and Gap 2 and 3 (150 mm).

#### 3.3.2 Equipment for Detection, Software, Buffer Delivery

A synapt G2-S high definition (Waters, Manchester) mass spectrometer operated in positive mode was used for the experiments. The source temperature was set to  $30^{\circ}\text{C}$  and the capillary voltage to

3.2 kV. The Masslynx 4.1 software was used for acquiring data. Buffer delivery was performed via a syringe pump (neMesys, Cetoni, Korbuss, Germany).

### 3.3.3 Preparation of Semi-open Capillaries

Two different micromachining methods, laser ablation and electro discharge machining, were used to drill a hole into stainless-steel capillaries. The process and optimization will be discussed in detail in the results and discussion section.

## 3.4 Results and Discussion

### 3.4.1 Design of the Semi-open Capillary

Long stainless-steel single capillaries (total length of 15 cm) were pierced using two different machining methods, laser ablation and electro discharge machining (EDM).

First, to produce a semi-open capillary with an opening angle of approximately  $90^\circ$ , hereafter called Gap 2, we used laser ablation. In laser ablation, by irradiating the surface with a laser beam, material evaporates. The amount of material removed by the laser depends on the laser wavelength, the pulse length and duration as well as the material's optical properties. This method was chosen since the laser pulse can be precisely controlled over a wide range of time (from milliseconds to femtoseconds).<sup>84</sup> Laser ablation was performed at CSEM (Neuchâtel, Switzerland) using a TRUMICRO 5350 instrument with a 343 nm laser wavelength and 10W mean power. The result of this fabrication method is shown in the following SEM images in Figure 8a. They show redeposited material from the laser ablation. The tilted image displays the open channel. The other method used to make a hole was EDM, whereby a desired shape is obtained by rapid sparks on a surface. The sinker EDM process uses an electrically charged electrode that is configured to a specific shape to burn the geometry of the electrode into a metal component.<sup>85</sup> EDM is a useful method to achieve such a configuration without residues left on the surface. For optimizations of the hole geometry, we used the results from Neu *et al.*<sup>14</sup> who described the influence of the capillary dimensions on the sample flush-out at the liquid bridge and along the spray capillary. They concluded that a reduction in the capillary wall thickness causes a significant decrease in

peak width. The reason is the large dead zone in the liquid junction between two thick walled capillaries. Clearly, smaller capillary inner diameters allow less samples dilution due to a smaller dead volume in the liquid connector. Therefore, the optimum configuration should provide the smallest dead zones possible. Accordingly, the structure of the hole was optimized. Using wire-EDM, a part of the surface is then removed in order to reduce the thickness of the wall and by sinker-EDM a hole was then machined in the center. The SEM images of such a structure is presented in the Figure 8b and called hereafter Gap 3.

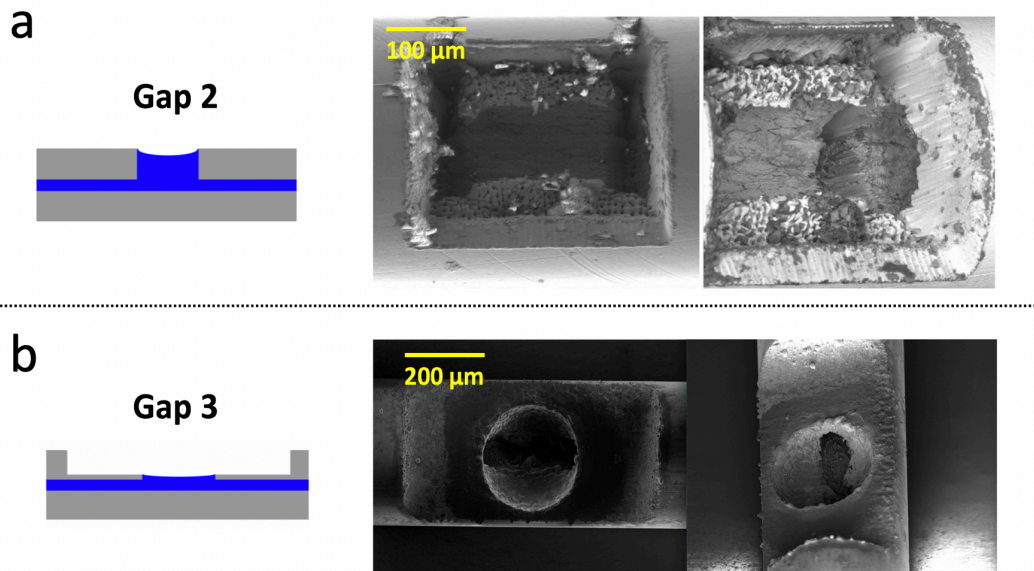


**Figure 8.** SEM images of the different holes in the stainless-steel capillary made by (a) laser ablation ( $300\ \mu\text{m} * 200\ \mu\text{m}$ ) and (b) a combination of wire and sinker EDM method.  $115\ \mu\text{m}$  of the thickness is removed by wire EDM and a hole ( $r=115\ \mu\text{m}$ ) is made inside.

Initially, a  $115\ \mu\text{m}$  section of the capillary was removed by wire EDM followed by sinker EDM for making a hole ( $r=115\ \mu\text{m}$ ) in it. Although surface roughness of the openings did not have any influence on the performance of the system, the fabrication quality improved a lot by using EDM method compared to laser ablation.

To prevent spilling of the liquid, the outer surface of the stainless-steel capillaries was coated. In case of major fluctuations in pressure or flow rate, the liquid junction can be controlled by altering the flow rate or over pressure inside the chamber.

### 3.4.2 Capillary Coating

The capillaries were coated with a hydrophobic protein repelling agent, perfluoro-alkyl-nitro dopamine (PFAND).<sup>86</sup> Success of the coating procedure was evaluated by comparing X-ray photoelectron a surface-sensitive spectroscopic technique that measures the elemental composition spectra before and after the coating. (Figure 9).

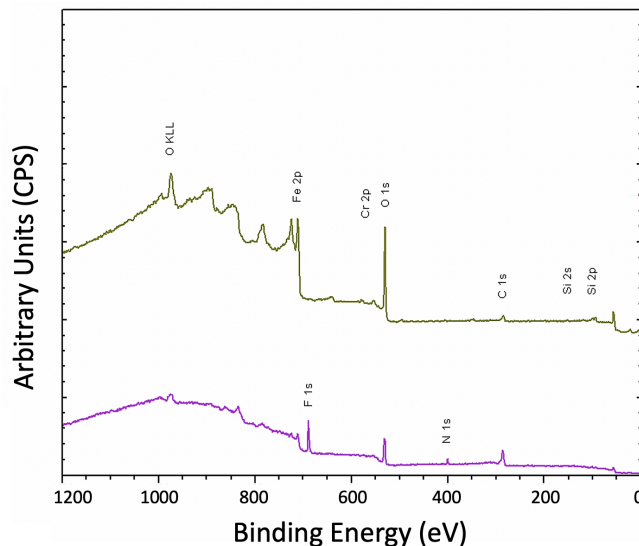


**Figure 9.** XPS survey spectra on the stainless-steel capillary before (upper curve) and after (lower curve) coating.

According to the Figure 9, Fe and O are the main elements present beside a small amount of Cr as well as a trace of Ca before coating. The success of the PFAND coating can be seen from the same figure. A decrease in substrate signals Fe and O, an increase in C and the presence of N and F show a successful coating. Also, water was not wetting the surface anymore, which was qualitatively tested with water droplets placed on the outside of the capillaries. All the coating procedure should be performed prior to making a hole on the capillary.

### 3.4.3 Increased Liquid Junction Robustness with the Semi-open Capillaries

To characterize the robustness of the gap sampler, we sprayed different solutions with different surface tensions, using various combinations of flow rates and pressures, using the different capillaries. Two different buffer compositions were tested; a relatively high (water: methanol 1:1 (V/V), surface tension of 48 J/m<sup>2</sup>) and a low (pure acetonitrile, surface tension of 22 J/m<sup>2</sup>)<sup>87</sup> surface



tension liquid. Experiments were performed under different chamber pressures (0, 12, 25, 100 mbar). The flow rate of the buffer inside the capillary was set to 1  $\mu\text{L}/\text{min}$  and increased by 1  $\mu\text{L}/\text{min}$  every 100 seconds. Usually 100 s is long enough to collect an acceptable spectrum, and empirically, if a spray can stay stable for 100 s, then it can be considered stable for a long time. The stability of the system can be directly assessed by the stability of the spray. Therefore, this evaluation was done based on the TIC as a function of time. Experiments were stopped whenever flooding of the liquid out of the hole was observed by the real-time monitoring. The times reported in Figure 12 correspond to the times during which the spray was stable. Figure 12 is prepared based on the experimental data presented in the Figure 10 and 11.

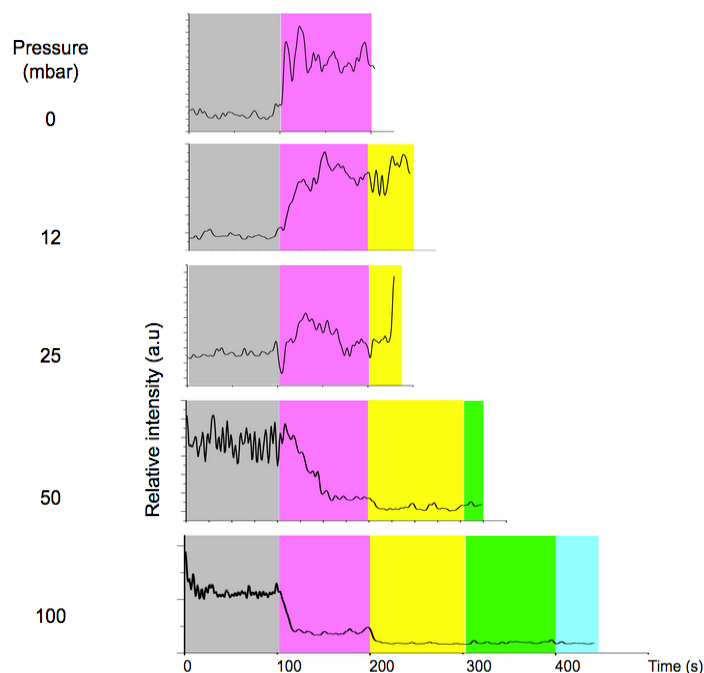


**Figure 10.** TIC of the spray stability tests which was evaluated as a function of the flow rate and chamber pressure for high surface tension liquid (MeOH/Water 1:1 (V/V)).

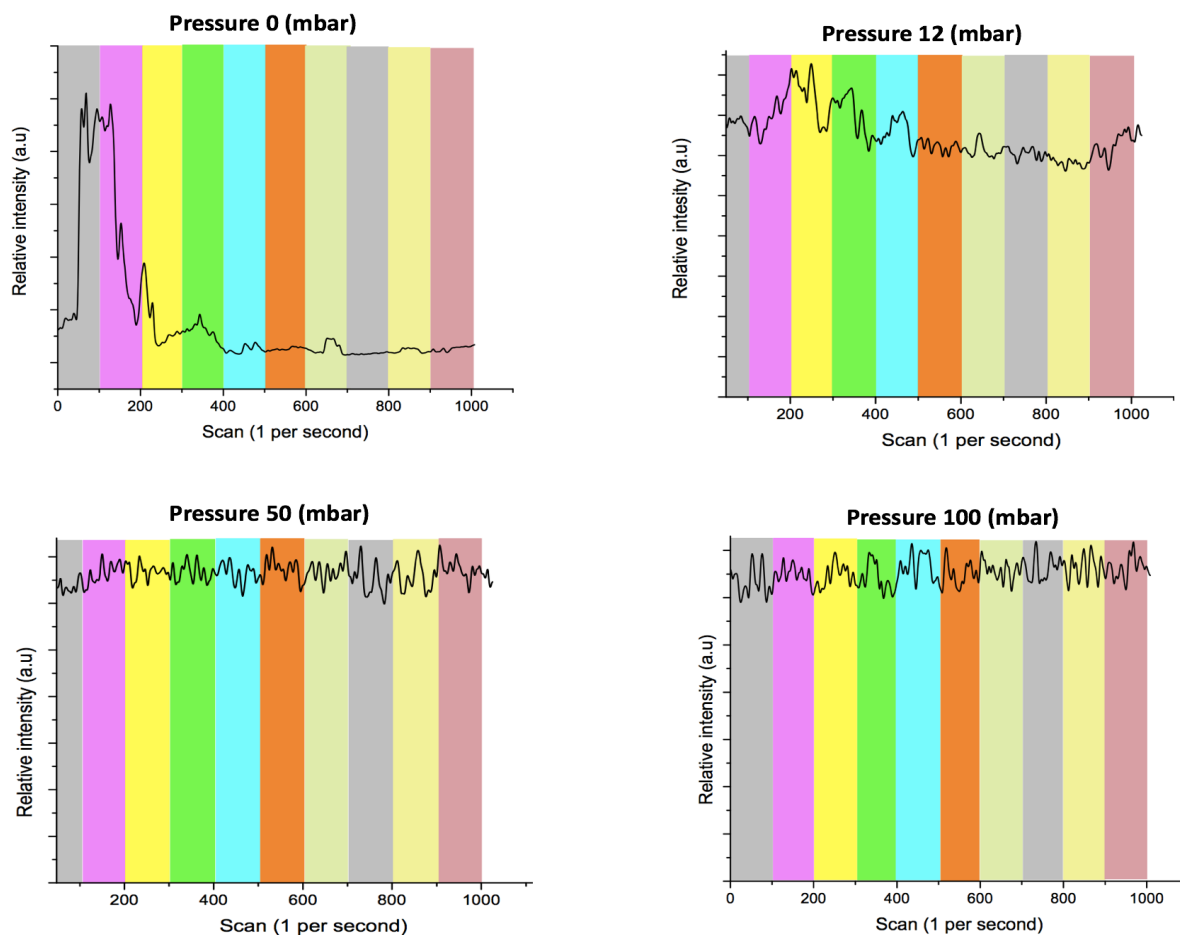


**Figure 11.** Results of the spray stability as a function of the flow rate and chamber pressure for low surface tension liquid (Pure ACN).

Using the original system with an optimized gap distance ( $300\ \mu\text{m}$ ), the liquid bridge is most stable between 27-29 mbar for low surface tension solutions. Using the semi-open capillary, the pressure and flow rate range at which the signal is stable, and the liquid connector is not flooding is significantly increased. Indeed, for low surface tension solutions, almost any combination of pressure (0-100 mbar) and flow rate ( $< 10\ \mu\text{L}/\text{min}$ ) tested were giving stable signals. (Figure 12)

In addition, for high surface tension solutions, where it was almost impossible to get a stable spray with the previous design, the Gap 3 gives very good results. For example, depending on the flow rate, overpressures from almost 0 to 100 mbar can be used with flow rates of 1–4  $\mu\text{L}/\text{min}$ . In

general, the results show that the system is compatible with a significantly wider range of flow rates at high chamber pressures. This can be explained by the fact that the back pressure caused by the high flow rate can be compensated by a high chamber pressure.

At flow rates less than 1  $\mu\text{L}/\text{min}$ , broad peaks were observed and with flows higher than 4  $\mu\text{L}/\text{min}$ , the back pressure needed, exceeded the system tolerance back pressure compensation (max 400 mbar).

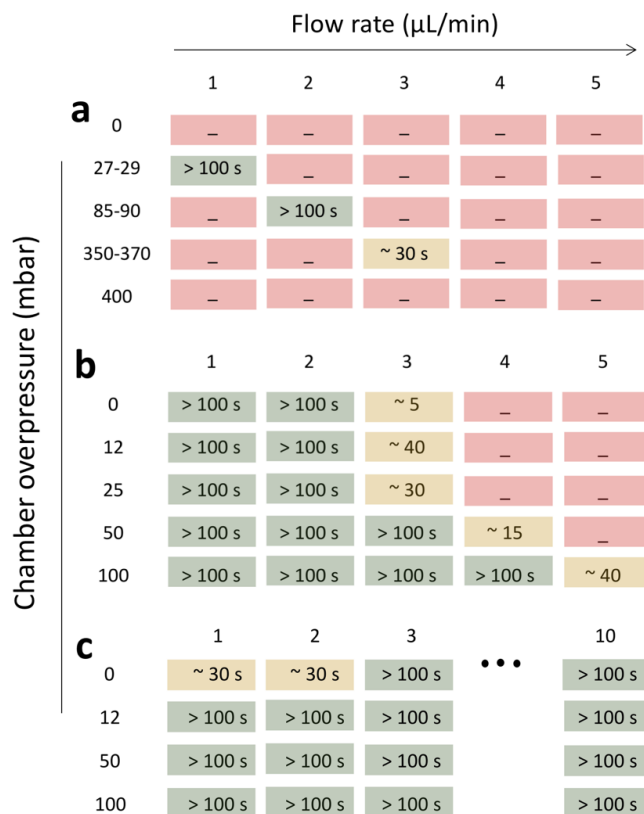


**Figure 12.** Pressure dependence experiment for Gap 1 and Gap 3, (a) Gap 1 (low surface tension solution), (b) Gap 3 (high surface tension solution), (c) Gap 3 (low surface tension solution). Different colors correspond to the liquid connector stability (Green=stable, yellow=short term stability, red= not possible to make liquid connector).

We believe the higher stability of Gap 3 compared to Gap 1 to be due to the fact that in Gap 1, the liquid junction is entirely made up by liquid (called a “liquid bridge”). For Gap 1, if we assume formation of a liquid cylinder with a diameter of  $320\mu\text{m}$  (=capillary diameter) and a length of

300 $\mu\text{m}$  (=gap distance), then roughly an area of  $6.03 \times 10^{-7} \text{ m}^2$  is exposed to atmosphere, which is therefore very sensitive to small fluctuations in pressure and flow rate. More effort and control are required to build and maintain such a liquid bridge, whereas the liquid in Gap 3 is flowing over a metal surface, which supports the uniformity of the liquid surface against variations in flow rate, pressure or voltage. The open surface area of the liquid in Gap 3 is  $4.15 \times 10^{-8} \text{ m}^2$ , almost 14.5 times smaller than that the exposed area for Gap 1.

### 3.4.4 Repeatability of Sample Infusion Using Semi-open Capillary

In order to illustrate the robustness of the new injection system using Gap 3, we performed 27 injections of rhodamine B (1.5  $\mu\text{M}$ , in acetonitrile/water 80:20 (V/V) + 0.1% formic acid) as shown in Figure 13. The EIC of rhodamine B is recorded at  $m/z$  443.4  $\pm$  0.3. The experimental conditions a, b and c are described in Figure 13. The capillary voltage, the flow rate and the chamber pressure were varied for each part of the experiment.

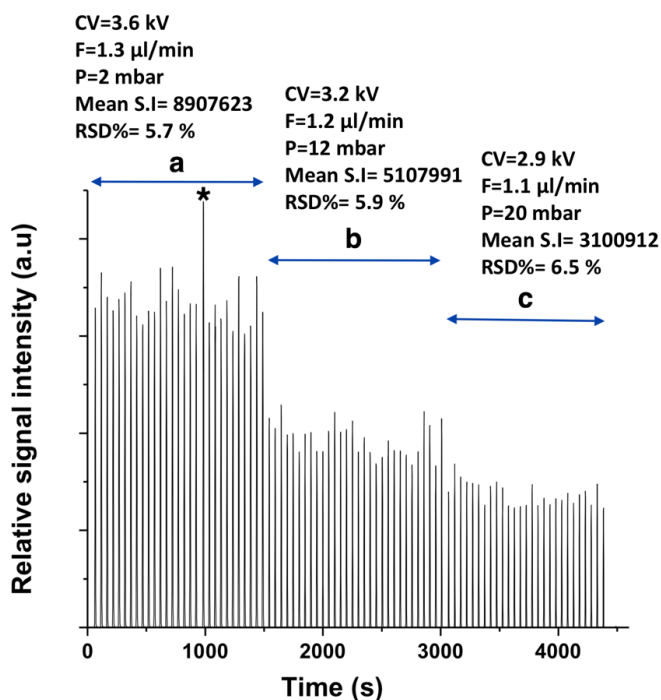


**Figure 13.** Representative injection sequence of Rhodamine B [1.5  $\mu\text{M}$ ], used for determining the repeatability of injections in different experimental conditions. (CV=capillary voltage, F=Flow rate, P=chamber overpressure, S.I.=signal intensity, RSD=relative standard deviation). \*A data point was

excluded in RSD and mean value calculation in part a (due to instrumental error). Considering the excluded point RSD and the average are 9.9% and 9055738 respectively.

The repeatability was evaluated from the relative standard deviation (RSD) of the peak intensities. For 27 injections at different experimental conditions using Gap 3, the RSD was less than 7%. This is an acceptable RSD and illustrates the repeatability of the experiments performed with Gap 3. The variations in the relative signal intensities in Figure 13 are mainly coming from variations in the sample volume taken up by the sampling tool. This variation in volume uptake cannot be easily reduced. However, its effect on the signal intensity can be corrected using an internal standard directly mixed with the sample.

### 3.4.5 Less Sample Dilution and Dead Volume

In order to figure out the influence of the gap shape on the sample flush out, we injected a mixture of cortisone, leucine enkephalin and rhodamine B (1.5  $\mu\text{m}$  each) inside the liquid bridges formed between two capillaries and in the liquid connectors formed in the semi-open capillaries. To ensure that the liquid connector volume difference in three different gap shapes is only due to the different gap shapes, we kept the gap length (distance between two capillaries) the same as the lengths of the holes ( $\sim 300 \mu\text{m}$ ). All other experimental parameters including flow rate and capillary voltage were kept constant for all experiments.

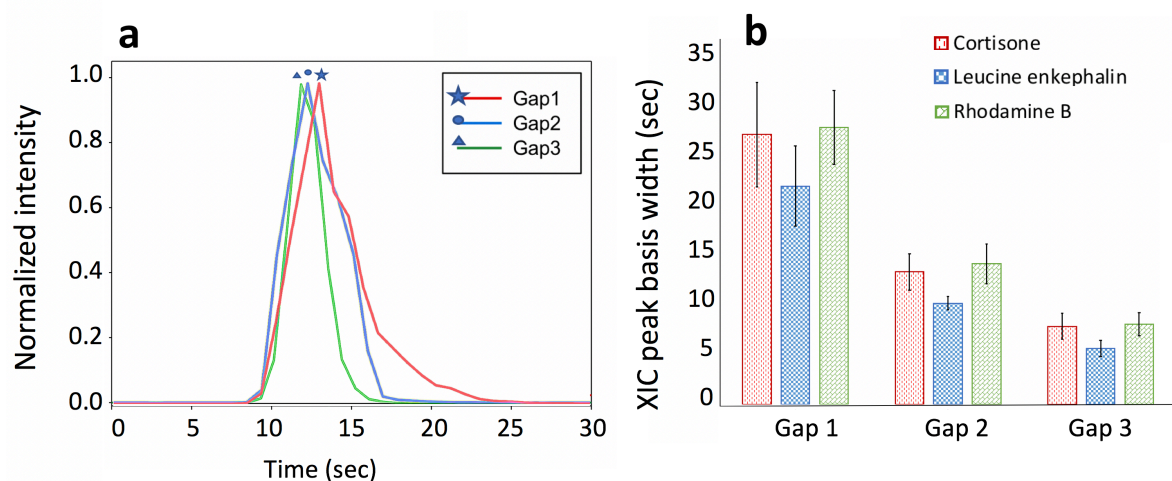


**Figure 14.** Comparison of different sample peak widths for three gap configurations.

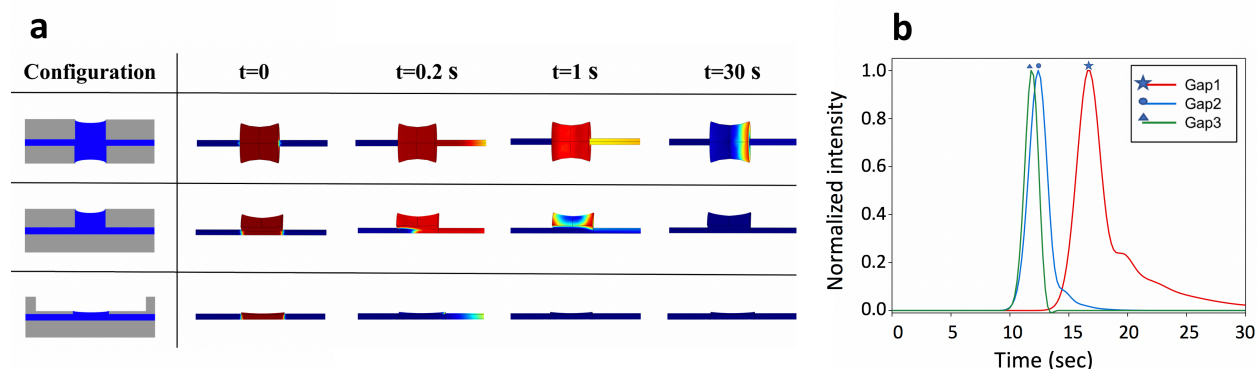
Figure 14 shows representative elution peaks for cortisone for the three tested configurations. In Figure 14a, the normalized intensities of the extracted ion current are shown. These represent the normalized signal intensity of the ions reaching the detector as a function of time. The TIC sums the intensity of the entire mass range being detected at every point in the analysis, whereas an EIC shows the intensity of a certain  $m/z$  value versus time. An interesting result is that with the semi-open capillaries, the peak widths are smaller compared to the dual capillary setup. In addition, there is a significant tailing with the latter that can be avoided using semi-open capillaries.

The results of 20 repetitions of the injections of the three different compounds is shown in Figure 14b. The average peak width for cortisone for the dual capillaries system (Gap 1) and the semi-open capillary (Gap 3) is 27.7 and 7.7 seconds, respectively. Gap 2 gives intermediate peak widths. A similar effect is observed for leucine enkephalin and rhodamine B. This decrease in peak width corresponds to about 70%.

To explain why the peak elution widths are affected by the gap shape, we performed 3D COMSOL Multiphysics simulations for the different configurations (Figure 15). These results show the elution of an analyte from the gap to the outlet of the capillary. The legend is from dark red to blue, with dark red for the highest and blue for the lowest sample concentration and is identical for all three Gaps. At  $t=0$ , the sample is uniformly dispersed in the liquid junction. For all designs the liquid flows from left to right with a 1  $\mu\text{L}/\text{min}$  flow rate. The flow is assumed to be laminar.

Different junction volumes yield various dead zones and diffusion lengths for sample to reach the solution flow. Compared to the gap sampler with two capillaries, both monolithic designs have much smaller dead volumes. A rough calculation shows the volume for Gap 3 hole to be about 1.5 nL, much less than the volume in the CGS model (25 nL). More importantly, after removing a 115  $\mu\text{m}$  of the capillary wall, and considering the capillaries' outer and inner diameter of 320 and 50  $\mu\text{m}$ , respectively, the diffusion distance for analyte to reach the main flow is only 20  $\mu\text{m}$ . Already at  $t=0.2$  s, the difference in performances is clear: Gap 3 is almost empty whereas Gap 1 still contains the majority of the sample. Gap 2 is similar to Gap 1 but its volume is only 25% of

that of Gap 1. Large dead volumes caused by the thick capillary walls in Gap 1 makes it more difficult for the analyte to move and diffuse into the solution flow. Some molecules are trapped inside the dead zone in the liquid bridge and remain there for more than 30 seconds.



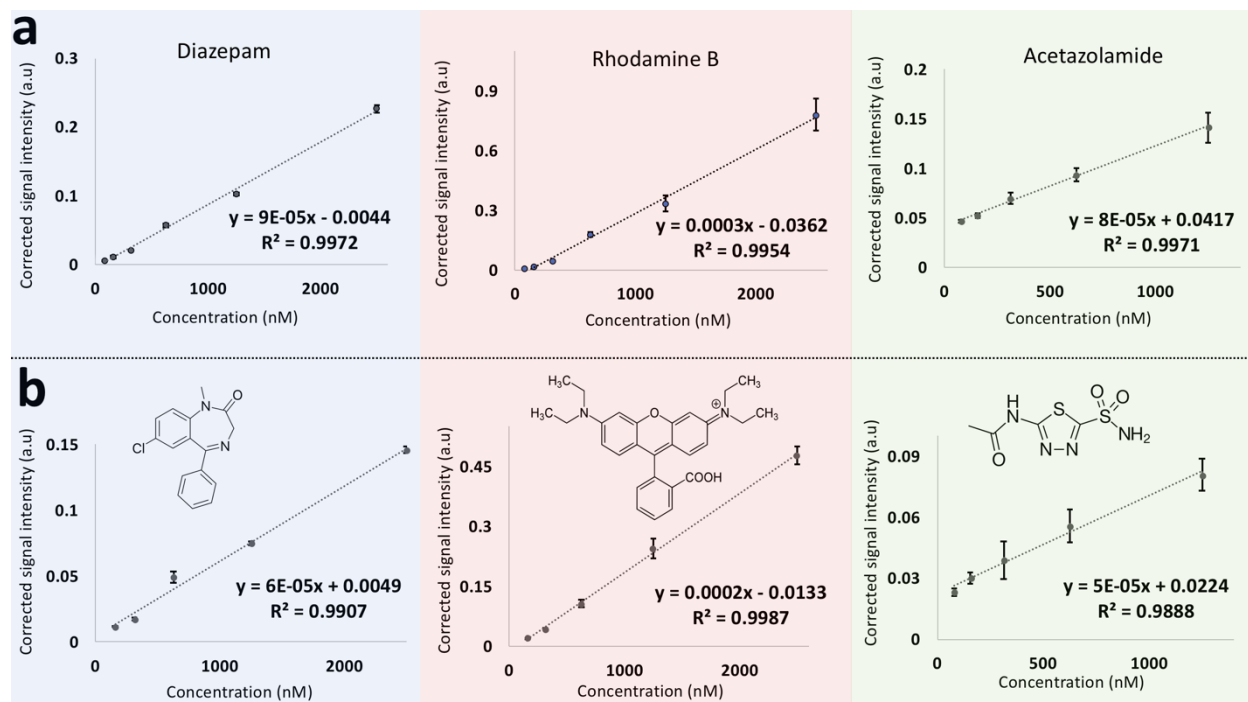
**Figure 15.** (a) Flow COMSOL simulation for Gap 1, 2 and 3 at different times. Color code is from dark red to blue, with dark red for the highest and blue for the lowest sample concentration and is identical for all three gaps. (b) Normalized extracted ion current for small molecules.

Figure 15b shows the simulated normalized extracted ion current of a small molecule representing (cortisone, leucine enkephalin or rhodamine B) for different gap configurations. The EIC was stimulated by considering small molecule diffusion coefficients and a flow rate of 1  $\mu\text{L}/\text{min}$ . The results from Figure 15b explains the tailing of the peaks for Gap 1 in Figure 15b. Gap dimensions are explained in Figure 8. The elution peak width obtained from the simulations are in good agreement with the experimental results. Replacing two capillaries with the single capillary thus benefits from less dead volume and therefore, less memory effects.

### 3.4.6 System Sensitivity

For the same amount of sample delivered to the gap, the signal is higher for semi-open capillary. The linearity and sensitivity of the system were investigated using diazepam, rhodamine B and acetazolamide. Diazepam d5 was used as internal standard. Nordiazepam was used in the buffer line to account for changes in ionization efficiency. The compounds were chosen based on current applications of the sampler. For instance, acetazolamide and diazepam are two compounds of interest for performing SPME using the sampler. A dilution series of the mixture was injected into

Gap 1 and the Gap 3, four times each. Figure 16 shows the corrected mean signal intensities versus sample concentration for each analyte and capillary configuration.



**Figure 16.** Corrected signal intensity (a.u) versus concentration (nM) of diazepam, rhodamine B, acetazolamide using (a) Gap 3 and (b) Gap 1.

Replacing Gap 1 (Figure 16b) with Gap 3 (Figure 16a), the LOD values for diazepam, rhodamine B and acetazolamide changed from 50, 28 and 87 nM to 27, 12 and 50 nM respectively, which corresponds to nearly a factor of 2. LOD values were calculated based on the signal-to-noise ratio of 3:1 in EICs for each analyte. As Figure 16 presents, a nice linearity was achieved for all of the compounds using Gap 3. By performing more tests for low concentrations, good system sensitivity was obtained, which was improved by 40-60% for the three compounds. By comparing the results, one can conclude that the semi-open capillary provides a better sensitivity for the system due to less sample dilution at the injection spot, which is very important for low concentration sample screening.



### 3.4.7 Injection Cycle

A contact-free injection test was implemented with the stainless-steel pin (diameter=356  $\mu\text{m}$ ). The applied voltage helps the sample droplet infusion into the liquid junction. It takes 2 seconds for the liquid junction to get back to its initial and stable shape after sample injection. An injection step is shown in Figure 17.

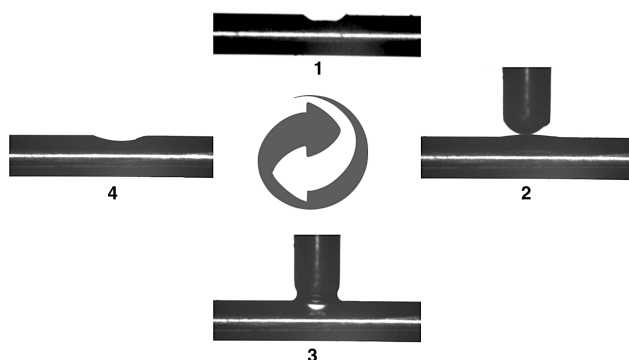


**Figure 17.** Injection cycle into semi-open capillary which takes 2 seconds (from step 1 to step 4).

## 3.5 Conclusion

The classic sample receptor (the liquid bridge) involves some drawbacks. Firstly, building and maintaining a stable liquid bridge is user-dependent and requires online adjustment of the experimental parameters (e.g. pressure, flow rate, voltage). Secondly, aqueous solutions are essential media for protein studies because they keep the polypeptide chains folded. However, the operation of the sampler is even more user-dependent and time-consuming when using aqueous solution and it is almost impossible to keep an aqueous bridge stable. Therefore, in this chapter, I focused on the use of a new configuration of the sample receptor that overcomes these obstacles. The new design offers greater stability, user-independent operation and a stable platform for delivering high surface tension solutions. It is composed of a semi-open capillary in which a hole is fabricated into a monolithic capillary by two different methods (laser ablation and EDM). This design has several advantages over the classic configuration. The most significant advantages are discussed in this chapter. One of the major achievements of this new system is that replacing the original design with the optimized structure causes less dependence on chamber overpressure and

flow rate fluctuations. The sampler was observed to be more robust. It can be operated more easily and quickly, and it is almost user independent. Repeatability of sample introduction in different conditions was also tested. The RSDs of sample injection in different conditions were found to be less than 7% and support the reproducibility of the sampling process. Reduction in sample dilution prior to ESI-MS results in higher sensitivity. Peak widths of individual analytes were compared for different configurations. A reduction of approximately 70% in peak width and about 50% in LOD are advantages of the new design. Experimental results correspond to those simulated by COMSOL. Using the new design, less peak tailing was observed, as predicted by COMSOL flow simulations. Also, the dead volume was drastically reduced, and based on the COMSOL simulation, there was almost no sample in the liquid junction after 0.2 seconds, whereas in the conventional design, the sample was trapped close to the capillary walls and edges even 30 seconds after sample injection. Compared with the capillary gap model, much less time is needed for capillary alignment and almost no time is required for building the liquid connector. Therefore, the new system can be operated more quickly. Improving this sampler to be more user-friendly and stable for high surface tension solutions opens the door for many new applications, which will be discussed in detail later in Chapter 6.<sup>27</sup> The main focus of the thesis, after increasing the system robustness, is the introduction of SPME as a new application to the CGS.

# Chapter 4

## The Capillary Gap Sampler, a New Microfluidic Platform for Direct Coupling of Automated Solid-phase Microextraction with ESI-MS

*This chapter is adapted from:*

Ghiasikhou, S., da Silva, M. F., Zhu, Y. & Zenobi, R. The capillary gap sampler, a new microfluidic platform for direct coupling of automated solid-phase microextraction with ESI-MS. *Analytical and Bioanalytical Chemistry* **409**, 6873–6883 (2017).

#### 4.1 Abstract

In this study, a new technology for rapid, automated SPME-MS interfacing is introduced. Employing the CGS for automated SPME and direct delivery of the extracted analytes to a mass spectrometer provides certain advantages over existing technologies: coupling of the CGS to mass spectrometric analysis offers quick, automated and site-specific extraction from very low-volume samples. High stability, reusability, and repeatability were achieved through systematic optimization. Diazepam, oxazepam and nordiazepam were used as test compounds in all experiments. The ability of the sampler to extract benzodiazepines from human plasma (limit of detection 0.3  $\mu\text{g/ml}$ ) in the therapeutic range was confirmed. A linear dynamic range from 1 to 1000  $\text{ng/ml}$  for all three analytes was found. The relative standard deviation of twenty extractions was between 11 and 17%, for oxazepam, nor diazepam and diazepam, respectively, indicating an acceptable repeatability of the method.

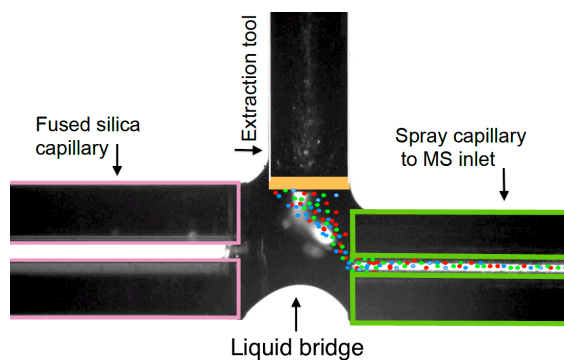


**Figure 18.** The CGS as an automated SPME-MS interface.

## 4.2 Introduction

There is a growing need for automated sample extraction in different areas, including clinical and pharmaceutical sciences.<sup>88-96</sup> In this context, extraction from complex matrices and automation of Solid Phase Extraction (SPE) has drawn a lot of attention during the last two decades. A 96-well plate SPE method was introduced in 1996 providing simultaneous analysis of wide variety of samples.<sup>97-99</sup> Further improvements in automated SPE such as developing new workstations for 384 and 1536 well plates, increased the rate of parallel sample preparation.<sup>100-102</sup> In recent years, the Pawliszyn group has reported a C<sub>18</sub>-coated 96-blades system, which was successfully tried for extraction of drugs from biological samples.<sup>103-105</sup> Vuckovic *et al.* also used the same concept for whole blood analysis.<sup>106</sup> However, these automated processes may still face some challenges. Large, heavy and expensive robots are used for parallel sample analysis. All of the techniques mentioned require a separation method such as LC or GC prior to MS analysis, which introduces more limitations and makes the method more expensive and time-consuming. It is possible to couple SPME directly to MS without employing chromatographic separations. This can be achieved using different ionization methods: (1) electron impact (EI-MS); (2) inductively-coupled plasma (ICP-MS); (3) atmospheric-pressure ionization (API-MS); (4) laser-desorption/ionization (LDI-MS); and, (5) ambient MS (AMS).<sup>107</sup>

Ambient MS techniques are currently of greatest interest. Marsili *et al.* used a GC injection port to couple SPME with EI-MS.<sup>108</sup> A 75- $\mu$ m-carboxen-polydimethylsiloxane fiber was used for the extraction of volatile analytes from milk. The same type of fiber was used by Peres in 2001 for extraction and characterization of volatile fraction of cheese.<sup>109</sup> Qualification and quantification analysis based on 70 eV EI mass spectra are complicated and time-consuming. In 1997, Möder *et al.*<sup>110</sup> for the first-time reported coupling of SPME with API-MS using a SPME desorption chamber as an interface. These authors analyzed acylcarnitine in aqueous solution, blood plasma, and urine samples. A similar 70  $\mu$ m SPME desorption chamber with some modifications was later used by Chen and Pawliszyn for coupling SPME directly with ESI-MS.<sup>71</sup> Ceglarek *et al.* used the same interface design to ESI-MS for determination of linear alkylbenzene sulfonates (LASs) in wastewater samples. Desorption took 15 minutes and was performed using isopropanol methanol

1:1 (*V/V*) ratio.<sup>111</sup> McCooey *et al.* developed a custom SPME desorption chamber in which a SPME fiber was inserted through a graphite-filled vessel ferrule into the desorption area.<sup>112</sup> Using 1.5  $\mu\text{L}/\text{min}$  of buffer solution, the analyte gets desorbed carried to the ESI needle for delivery to the MS. Further investigations by Van Hout *et al.*<sup>113, 114</sup> coupled SPME with atmospheric pressure chemical ionization (APCI-MS). They could determine lidocaine in a sample of urine by directly immersing a 100- $\mu\text{m}$  Polydimethylsiloxane (PDMS) fiber. In their other study, higher temperatures were applied in a modified desorption chamber that allowed temperature control. They concluded that elevated temperatures increased the speed of extraction. Using SPME at non-equilibrium conditions allows high speed extraction. This is interesting for high-throughput applications. Recently, our group has developed an ionization source that couples SPME to MS directly using thermal desorption of analytes extracted on the fiber, followed by ionization in a described barrier discharge ionization (DBDI) source. This method showed LODs below the pg/ml level.<sup>115</sup>

In this chapter we introduce the CGS as a novel technology for interfacing SPME with MS. The main focus of the current work is the proof of concept of this interface, as well as development, optimization and evaluation of coupling SPME with MS using the CGS. We believe that this addresses many challenges for small volume sample clean-up prior to ESI-MS analysis. For the purpose of performing SPME using the robotic sampling component of the CGS, a specialized extraction tool was prepared by immobilizing an octadecyl-silica-based stationary phase ( $\text{C}_{18}$ ) on the surface of a very thin stainless-steel rod. By dipping this extraction tool into the sample, an extraction is performed. The extraction tool is then transferred to a chamber where an elution solution is flowing through a microfluidic platform into an ESI-MS spray capillary. The liquid bridge was used here for the extraction tool to enter and desorb the extracted analyte.

## 4.3 Experimental Section

### 4.3.1 Chemicals and Materials

Diazepam, oxazepam, nordiazepam, diazepam- $\text{d}_5$  (internal standard) were purchased from Sigma-Aldrich (Texas, USA) and were stored as 1 mg/ml solutions in methanol in the fridge at 4°C. These

solutions were used as stock solutions for all experiments in the following sections. Phosphate-Buffered Saline (PBS); pH 7.4 (Life technologies, Thermo Fisher Scientific, (New York, USA) was used for dilution of stock solutions. Acetonitrile  $\geq 99.9\%$  (LC-MS CHROMASOLV), water (LC-MS grade) and N, N-dimethylformamide anhydrous (DMF), 99.8% were purchased from Sigma Aldrich (Saint Louis, USA). Human plasma was purchased from Sigma Aldrich (Saint Louis, USA), and stored at 2–4°C. Silica-based C<sub>18</sub> (3  $\mu$ , pore size 100Å) particles, which were used as extraction phase, were purchased from Phenomenex, (California, USA). Polyacrylonitrile (PAN), which was used as biocompatible glue to immobilize the C<sub>18</sub> beads on the stainless-steel pin, was purchased from Acros (New Jersey, USA).

#### **4.3.2 Preparation of Biocompatible C<sub>18</sub>-PAN SPME Coatings**

0.5 g PAN particles were mixed with 4.5 g DMF in a glass vial (10% w/w). The mixture was heated to 90°C for 1h, until a yellowish clear solution was obtained.<sup>116</sup> The vial should be sealed tightly to avoid the evaporation of DMF. Prior to coating the extraction tool, a stainless-steel pin, it was cleaned by sonication in 2-propanol and methanol for 10 minutes each and using two minutes of O<sub>2</sub>-Plasma in order to remove impurities and contaminants from the surface. Pins were coated by a dipping method that is described in details later.

#### **4.3.3 Mass Spectrometry Conditions**

A commercial electrospray ionization mass spectrometer (Synapt G2-S high definition, Waters, Manchester) was used for all experiments. It was operated in positive mode. The source temperature was set to 30°C and capillary voltage to 3.2 kV. The Masslynx software V4.1 was used for acquiring data.

#### **4.3.4 Operation with a Miniaturized SPME Tool**

we mainly focus our description on the operation of an SPME pin tool in connection with the CGS. A solid stainless-steel pin is used as the extraction tool. The extraction tool is held and moved by the arms of the micro robot with a positioning precision of 3  $\mu$ m. The sampling tool moves with a constant speed to different wells of a microwell plate to perform different steps of the

microextraction and further enters the pressure chamber for desorption. Operation cycle of a sample extraction and desorption consists of several automated steps.

1) Conditioning: conditioning is a two-step process, with the aim of maximizing the efficiency and capacity of extraction by the silica-based materials. During the first step of the conditioning with an organic solution, the dry, non-polar functional C<sub>18</sub> chains become solvated and activated. Next, the extraction phase is equilibrated with an aqueous solution in order to displace the organic environment with an aqueous one so that the particles can interact with the sample. Conditioning was applied using a 1:1 (V/V) mixture of methanol and water for one hour in the beginning of each set of experiments and five minutes prior to the rest of the extraction series. It is also important that the C<sub>18</sub> phase does not dry out once it has been conditioned.

(2) Loading: this is the step of adsorbing the analyte of the interest on the extraction phase. The extraction phase should be chosen based on the physical characteristics of the analyte. The silica-based phase with nonpolar C<sub>18</sub> chains is an appropriate option to extract benzodiazepine compounds.<sup>117</sup>

3) Washing: this refers to the process of cleaning the interfaces from the remaining matrix without removing the analyte of interest. This step is accomplished by dipping the pin into pure water for 5 seconds after loading.

4) Elution: this is the step in which the compound is eluted from the extraction phase by a desorption solution. Using the CGS as the experimental setup, elution occurs in the gap while pin is flushed by the organic desorption solution.

5) Pin cleaning: The extraction tool was left in the gap in exposure to the desorption solution (ACN/H<sub>2</sub>O 80% (V/V) +0.1% formic acid) for 3 minutes after the EIC signal reached the baseline. Followed by 5 minutes dipping in the well filled with MeOH/H<sub>2</sub>O 50% (V/V) prior to each experiment, then 1-minute dipping in H<sub>2</sub>O to replace the organic phase with water.



## **4.4 Automation and User Interface**

Automation of the sampling procedures was programmed for easy user operation in order to increase reliability, throughput, reproducibility and precision of chemical analysis with the MS. The functionality obtained thus for automated sampling with the device allows for rapid SPME. The speed with which data are obtained is greatly increased compared to manual operation. The programming language used for the control software was Microsoft's Visual Basic. The Visual Studio 14 integrated development environment (IDE) was used directly on the robot's workstation. A graphical user interface (GUI) was programmed in order to allow the user to define and tune parameters pertaining to the sampling procedure. It is thus possible to define the coordinates of the process, the grid spacing of the sampling plate and tune other quantities such as the stirring of the robot's sampling pin inside micro wells, the speed and radius of this stirring, as well as the speed of movement of the pin itself. Furthermore, it is possible to define a number of repetitions for the same process, as well as repetitions starting at different micro wells relative to the first one. In order to save the parameters of the sampling procedure and other quantities, a database, programmed in SQL Express Server 2014 this database was adapted to contain reference micro well coordinates. These were defined in order to map the sampling plate. To avoid accidents and consequent damage to the robot's end-effector containing the sampling pin, the software was imbued with certain safety features. Implementation of these features allowed the user to define a handful of parameters and to initiate sampling procedures on any given position in the sampling plate, leaving the robot to sample and deliver to the MS automatically and reproducibly. Introduction of full automation allowed thus for much greater flexibility and precision in the performing of these sampling tasks, with more safety due to the decrease in sources of human error.

## **4.5 Results and Discussion**

### **4.5.1 Optimization of Coating Preparation**

It is important to develop a biocompatible and long-lasting coating, which can provide reproducible extraction with high efficiency. Based on a survey of previous studies done in Ref.29,

a C<sub>18</sub> (octadecyl) silica-based stationary phase was found to be applicable for extraction of a wide range of compounds with high efficiency.<sup>29, 117</sup> To prepare the extraction tool, C<sub>18</sub> particles were immobilized on the stainless-steel pin using the PAN glue. Biocompatibility is given because the PAN glue is a polymer that does not trigger infections or immune reactions, and is therefore widely used in the biomedical area, e.g. in dialysis.<sup>116, 118, 119</sup> The C<sub>18</sub> particles were mixed with 20% V/V PAN glue. The tip of the pin was dipped into a very thin layer (50 μm) of the mixture and then transferred to an oven at 180°C for two minutes for thermal curing.<sup>117</sup> This method is frequently used for coating of stainless-steel by C<sub>18</sub> beads and reported to provide a uniform and mechanically stable coating.<sup>117</sup> Unfortunately, using this method, beads were found to be covered by the glue as shown in the following SEM image (Figure 19a). To avoid that, the coating procedure was divided into two discrete steps: first covering the stainless-steel with a very thin layer of the glue and then touching a monolayer of beads, followed by curing the glue in the oven. A thin layer of beads was dispersed on a microscopic slide, using cover slips on the top. As Figure 19b demonstrates, using the second method particles are not covered with glue and expose a maximum surface area for extraction. This method was then selected for generating the coating in all further experiments. In order to get a thicker layer, the coating cycle is repeated. It will be shown below that although the underneath layers were covered by glue, increasing the thickness of the extraction phase enhanced the extraction.

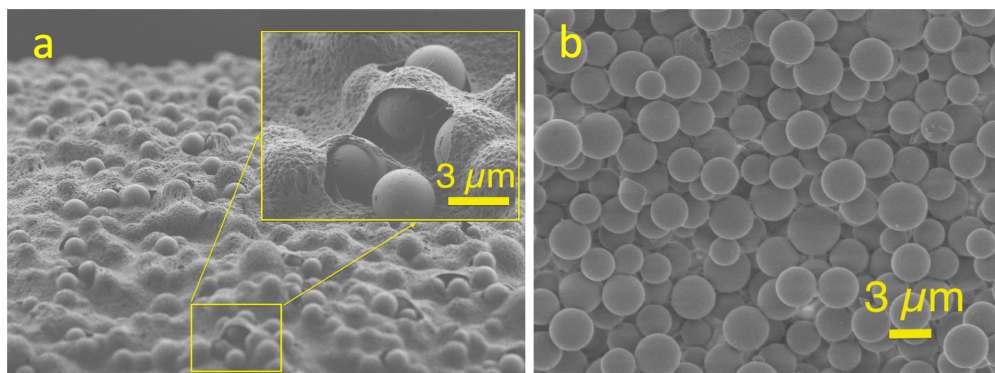


**Figure 19.** SEM imaging of bead coatings using two different procedures. (a) result of immobilizing C<sub>18</sub> using a mixture of glue and particles. This SEM image clearly shows that C<sub>18</sub> particles are covered by glue. (b) using discrete steps, beads are free of glue on the surface.

To show the influence of the PAN polymer on the extraction profile, the following test was performed. In this test, two pins were both coated three layers, using the coating methods explained in the previous sections. They were then used for extraction of 500 ng/ml diazepam from PBS. The thickness, the number of beads, and the amount of the accessible C<sub>18</sub> coating will not be same for the two pins. A clear difference in the desorption profile was found (Figure 20), demonstrating that there is a difference in accessibility of the C<sub>18</sub> beads for the two coating methods.

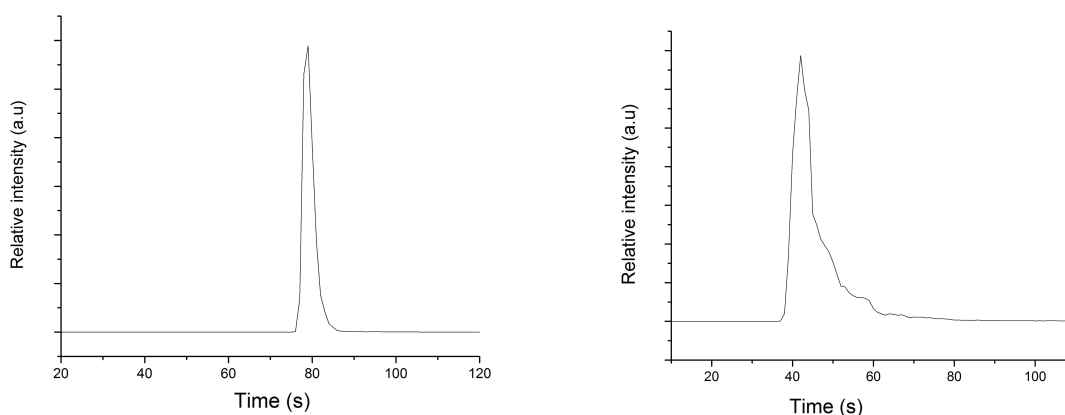


**Figure 20.** EIC for diazepam ( $m/z=285.1$ ) using a pin coated with free beads (left), and a pin coated by a mixture of PAN glue and C<sub>18</sub> beads 20% (w/w) (right).

As Figure 20 shows, it takes more time for the analyte to get desorbed from the beads that are partially trapped inside the glue than the free beads.

At equilibrium, the amount of extracted analyte is proportional to the volume of the extraction phase according to the following formula:<sup>120</sup>

$$\text{Eq. 9} \quad n = K_{eS} V_e C_0 / K_{eS} V_e + V_s$$

where  $n$  is the amount of extracted analyte,  $C_0$  the initial concentration of analyte in the matrix,  $V_e$  and  $V_s$  are the volumes of the extraction phase and the sample, respectively, and  $K_{eS}$  is the partition coefficient between the sample matrix and the extraction phase. An experiment was performed to

investigate the effect of increasing the volume of the extraction phase on the profile and kinetics of the extraction. Three pins with different coating thicknesses were prepared by the optimized coating method. The coating cycle mentioned was performed one, three and seven times for preparation of thin, mid and thick extraction phases, respectively. All were conditioned for 30 minutes and loaded in 40  $\mu\text{L}$  of a 500 ng/ml diazepam solution in PBS for 30 minutes (much smaller sample volumes are possible, down to a few  $\mu\text{L}$ , but were not used for these experiments). Then the extracted analyte was eluted with acetonitrile/water (80:20 *V/V*) + 0.1% formic acid as the desorption solution with a 0.6  $\mu\text{L}/\text{min}$  flow rate. Figure 21 shows the effect of the extraction volume on the performance. In this figure, the intensity of the diazepam signal (at  $m/z=285.09$ ) averaged over five replicates is plotted for all three different thicknesses.

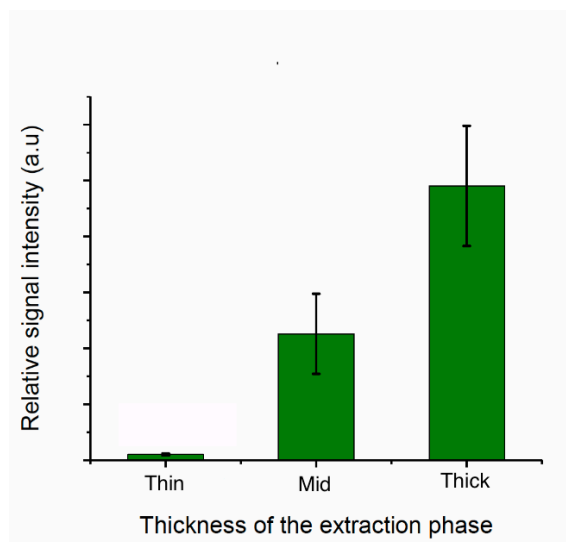


**Figure 21.** Average diazepam signal intensity ( $n=5$ ) extracted by pins covered by single, triple and multiple layers of  $\text{C}_{18}$  which were fabricated by using one, three, and seven coating cycles.

The key result from experiments shown in Figure 21 is that by increasing the volume of the extraction phase, the amount of extracted analyte rises. In order to interpret the results obtained, the thickness and volume of the extraction phase should be considered. The thicknesses of the coatings were 10, 30, and 90  $\mu\text{m}$ , and the volumes were roughly 0.42, 1.26, and 3.78 nL for “thin”, “mid” and “thick” coatings, respectively. Because the extraction phase thickness is not linearly proportional to the number of coating cycles, the extracted amount is not expected to be linearly proportional to the thickness (or volume) of the coating. This is corroborated by the findings in

Figure 21. Desorption times for thin, mid and thick extraction phase volume were found to be  $8.2 \pm 1.2$ ,  $8.7 \pm 0.8$  and  $18.2 \pm 3.4$  seconds, respectively. According to these results, the desorption kinetics is slower as the coating gets thicker. Therefore, the best approach to increase the sensitivity of the method without compromising the kinetics is to have a maximum surface area to volume ratio. This provides maximum extraction and fast rate of extraction and desorption, thus a short analysis time. Based on this experiment, a pin with a medium coating thickness was selected as the optimum coating thickness.

#### **4.5.2 Kinetics**

Speeding up the extraction process is crucial for many applications. One of the factors that can help is agitation or stirring of the solution.<sup>29</sup> To shorten the analysis time, vibrational and circular movements were applied to the extraction tool. In order to study the influence of stirring on the rate of extraction, 500 ng/ml nor-diazepam, diazepam, oxazepam were extracted from PBS by increasing the extraction time. The experiments were performed with and without stirring of the extraction tool. The rotation speed was set to 250 rpm. The intensity of the analyte peaks was then plotted against the time. Results are shown in Figure 22.

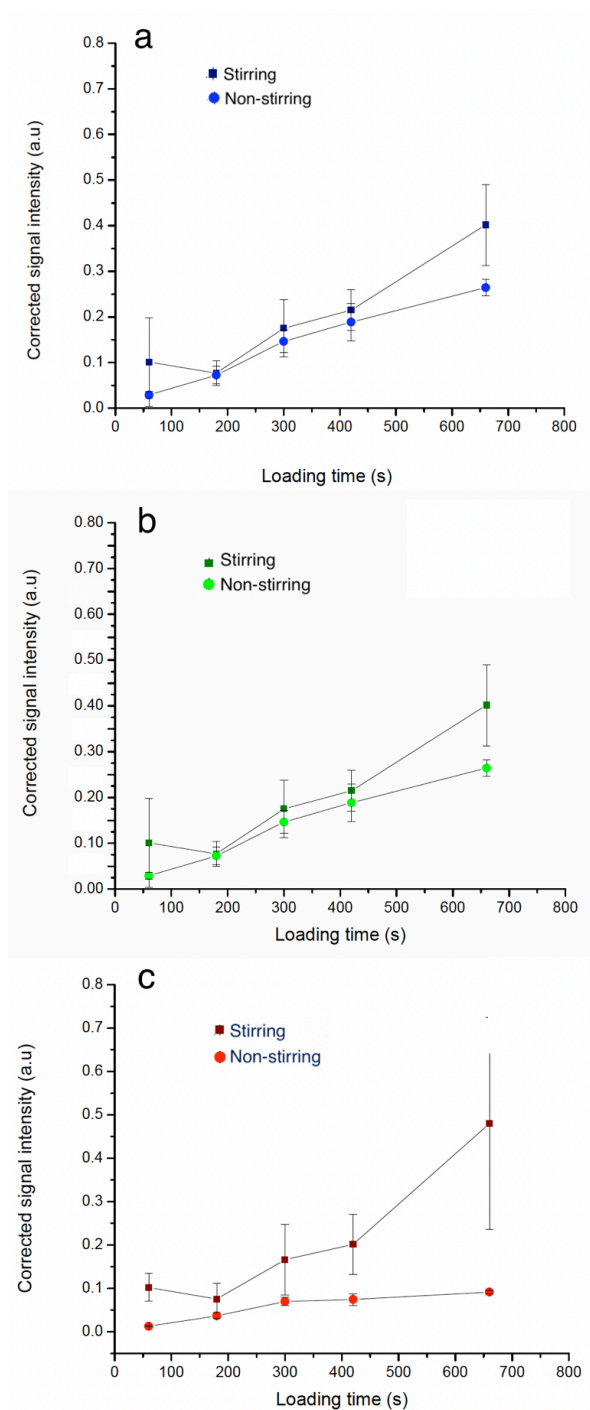


**Figure 22.** Extraction kinetics of 500 ng/ml of, (a) nordiazepam, (b) diazepam, (c) oxazepam from PBS. Each drug was extracted with and without stirring. Then the extracted analyte was eluted with

acetonitrile/water (80:20 *V/V*) + 0.1% formic acid as the desorption solution, using a 0.6  $\mu\text{L}/\text{min}$  flow rate

All three plots confirm that stirring of the extraction tool increases the extraction rate. As shown by the results, this influence grows with time. Mass transfer through the solution to the extraction phase has been modeled.<sup>121</sup> It occurs either by convection from bulk or via diffusion from a boundary layer to the extraction phase. The boundary layer is defined as a zone surrounding the extraction phase where no convection occurs. The thickness of the boundary layer is defined by the rate of agitation or stirring of the solution.<sup>121</sup> A higher stirring rate gives rise to a thinner boundary layer, which renders the extraction process quicker.

#### 4.5.3 Effect of Desorption Solution Flow Rate and Position of the Pin Within the Gap on Desorption Profile

When it comes to very low analyte concentrations, then not only maximizing the extraction matters, but optimizing the desorption is also important to enhance sensitivity. In other words, it is important to elute more analyte within a shorter time. In this section, the effect of the flow rate and pin position in the liquid bridge was investigated. Higher flow rates ensure more rapid desorption of the analyte. According to the limitations of the set up in terms of stability of the liquid bridge and spray, as well as the ionization in the spray, the flow rate can be adjusted between 0.5 and 3  $\mu\text{L}/\text{min}$ . A set of experiments were performed in which diazepam was extracted from PBS and eluted with ACN/H<sub>2</sub>O 80:20 (*V/V*) + 0.1% formic acid with different flow rates (0.5, 1, 1.5, 2.5)  $\mu\text{L}/\text{min}$ . Table 1 shows the desorption profile and stability of the liquid bridge.

**Table 1.** Comparison of the effect of desorption solution flow rate on the desorption profile.

	0.5 $\mu\text{L}/\text{min}$	1 $\mu\text{L}/\text{min}$	1.5 $\mu\text{L}/\text{min}$	2.5 $\mu\text{L}/\text{min}$
<b>Desorption time (s)</b>	7.7 $\pm$ 1.1	3.6 $\pm$ 0.6	4 $\pm$ 0.1	9.7 $\pm$ 4.7
<b>Stability of liquid bridge</b>	Bridge was hardly formed	Stable	Stable	Overflooding of the bridge

Based on the observations during these experiments, flow rates of 0.5  $\mu\text{L}/\text{min}$  and 2.5  $\mu\text{L}/\text{min}$  disturb the stability of the liquid bridge. A flow of 0.5  $\mu\text{L}/\text{min}$  is not sufficient to create a stable liquid bridge, and when applying flow rates more than 2  $\mu\text{L}/\text{min}$ , the overpressure inside the chamber cannot compensate the back pressure caused by the spray tip, thus the bridge grows and floods the capillaries. In conclusion, 1–1.5  $\mu\text{L}/\text{min}$  is the optimum flow rate in terms of desorption profile and system stability. During the desorption process, analytes diffuse from the coating into the flow of the fluid in the liquid bridge. The flow profile of the bridge was simulated using COMSOL Multiphysics and is shown in the Figure 23. The flow and concentration profile simulation were performed by Pablo Dörig using COMSOL Multiphysics (version 4.4, Burlington, MA, USA). Capillary dimensions are 360  $\mu\text{m}$  O.D., 50  $\mu\text{m}$  I.D., and the distance between the capillaries is 200  $\mu\text{m}$ . Several assumptions were made in order to simplify the simulation. For instance, the injection step is not covered by the simulation, therefore a start “injection zone” has to be chosen. A complete dispersion of the probe in the gap was also assumed.

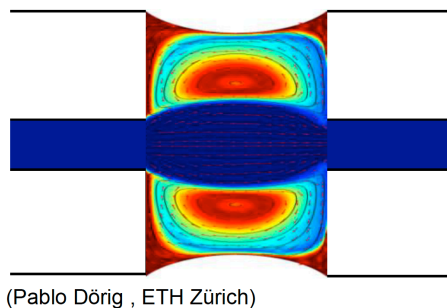


**Figure 23.** COMSOL Multiphysics simulation of the flow profile in a liquid bridge.

The flow profile in the capillaries is laminar (blue). The flow inside the gap can be separated into two zones, an active zone, where there is laminar flow (blue) and dead zones where there is very little or no flow (red) and acts as a laminar trap. Vortexes surround the laminar flow inside the bridge. Material transport is mostly controlled by diffusion and additional factors such as convection (vortex) also should be also considered.



This flow profile obviously changes after insertion of the pin inside the bridge. To have a better understanding of how the pin position in the liquid bridge can affect the desorption profile, a test was performed as described in the next section.

#### **4.5.4 Influence of the Pin Position Inside the Gap on the Extraction Profile**

To understand the effect of the extraction tool inside the different zones of the liquid bridge in the desorption step, pin position was changed from top (150-200  $\mu\text{m}$  above the gap) to the middle of the bridge (for gap distance 290  $\mu\text{m}$ ).

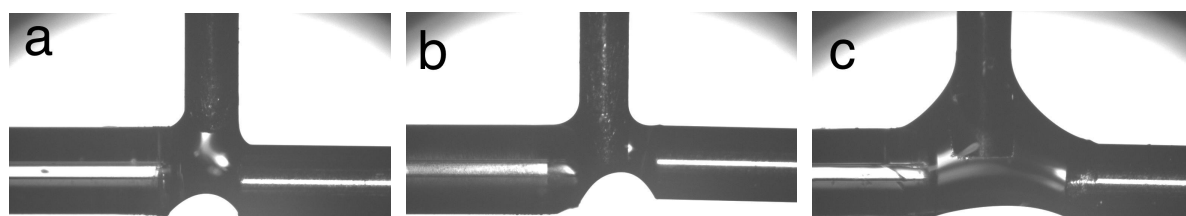


**Figure 24.** Different pin positions inside the liquid bridge, (a) Top (gap distance=290  $\mu\text{m}$ ), (b) Gap (gap distance=290  $\mu\text{m}$ ), (c) Gap (gap distance=560  $\mu\text{m}$ ).

Then extractions of three benzodiazepines drugs (oxazepam, diazepam, nordiazepam) 500 ng/ml from PBS were performed for both positions. The intensity of the peaks was plotted for the different positions.

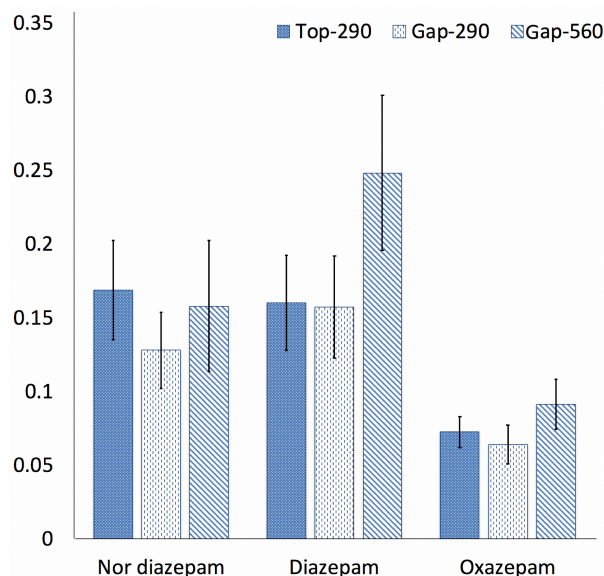


**Figure 25.** Benzodiazepines peak intensities extracted from different pin positions inside the gap. Solid fill) Top (gap distance=290  $\mu\text{m}$ , dotted) Gap (gap distance=290  $\mu\text{m}$ , hatching) Gap (gap distance=560  $\mu\text{m}$ ).

The results indicate that there is no noticeable change in the amount of extracted analyte and considering the error bars, the results are in the same range. Therefore, the results are not significantly influenced by the pin position in the gap. Thus, the desorption step is robust and is not sensitive to changes in the pin position inside the bridge, thus almost independent of the flow profile inside the gap. However, considering the bridge stability and the flush-out profile, a 290  $\mu\text{m}$  gap is preferred to higher gap distances.

#### 4.5.5 Evaluation of Time Profile of the Extraction

SPME is an equilibrium-based method, because the maximum extraction and the highest reproducibility can be achieved at equilibrium, where the results are less influenced by fluctuations of the extraction time. A set of experiments was performed, in which nor-diazepam, diazepam and oxazepam (500 ng/ml each) were extracted from PBS by varying the extraction time. Extraction times were extended until no significant increase in the extractions was observed by increasing the loading times. Results are plotted in Figure 26.

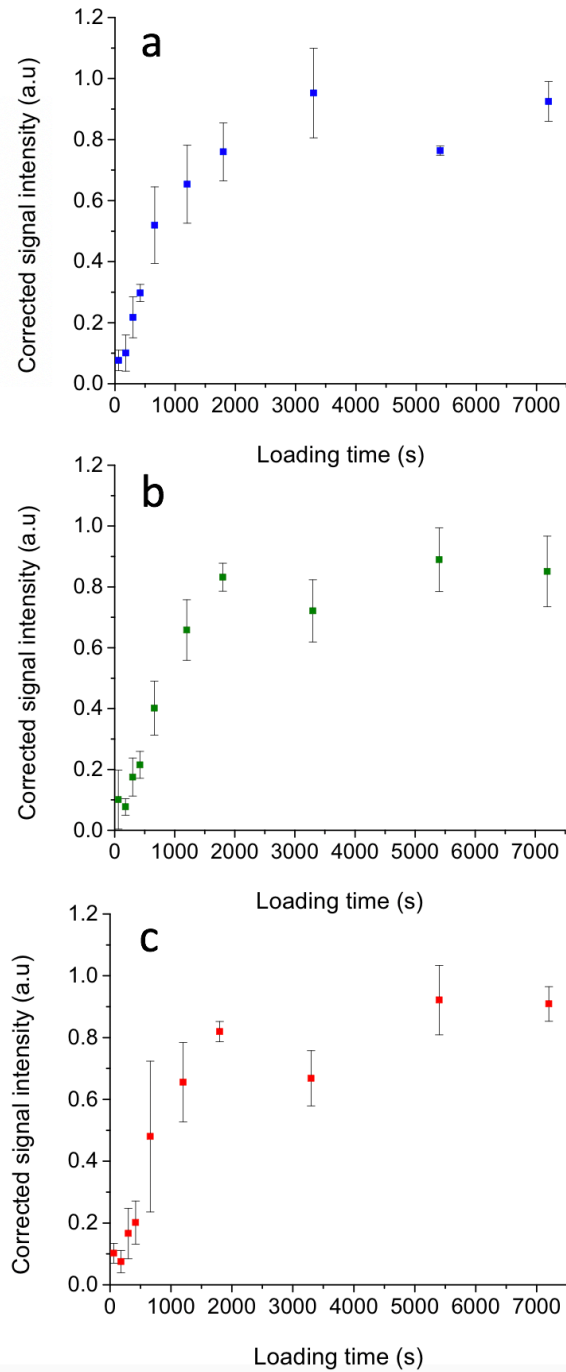


**Figure 26.** Time profiles of extraction of benzodiazepines, (a) nordiazepam, (b) diazepam, (c) oxazepam. Corrected analyte intensity is plotted against the loading time. In all experiments, no significant increase was observed after 30 minutes of loading time. The extracted analyte was eluted with acetonitrile/water (80:20 *V/V*) + 0.1% formic acid as the desorption solution with a 1  $\mu\text{L}/\text{min}$  flow rate.

There are two noticeable points in Figure 26. Firstly, equilibrium is achieved after 30 minutes of analyte loading. Compared to previous reports, the equilibrium time between the C<sub>18</sub>-based extraction tool and benzodiazepines<sup>117, 116</sup> is reduced by almost half. This can be interpreted by the high surface-to-volume ratio of the extraction phase, which contributes to the advantage of our extraction tool over traditional SPME tools. Based on Eq 10, the rate of extraction is proportional to the surface of the extraction phase,<sup>104</sup>

**Eq. 10** 
$$(dn/dt = D_s A / \delta) / C_s t$$

where  $dn/dt$  is the rate of the extraction,  $D_s$  is the diffusion coefficient for the analyte in the sample matrix,  $A$  is the surface area of the extraction phase,  $\delta$  is the thickness for the boundary layer,  $C_s$  is the analyte concentration, and  $t$  is the extraction time. As the extraction phase enters the solution, analyte enters into the extraction phase by diffusion and convection. This accumulation grows non-linearly time up to a certain level. This level is determined by  $K_{es}$ , the distribution constant.  $K_{es}$  for a solid extractant is defined by:<sup>122</sup>

**Eq. 11** 
$$K_{es} = S_e / C_s$$

where  $S_e$  is the surface concentration of adsorbed analyte on the extraction phase and  $C_s$  is the analyte concentration in the sample. The sorbent surface area is also considered in the definition of the  $S_e$ . Thus, for a higher surface-to-volume ratio, equilibrium is reached faster. Secondly, even for an extraction time of one second, the diazepam peak was clear and intense, confirming the ability of the method to be used in high-throughput screening where speed and time are important factors.

#### **4.5.6 Reproducibility of Extractions of Benzodiazepines from PBS and Dynamic Linear Range**

So far, several key factors have been optimized for efficient extraction and short analysis time. To determine the repeatability of the method the variation of the results of subsequent experiments were studied. Twenty extractions of nordiazepam, diazepam, oxazepam 500 ng/ml each were performed from PBS, stored in a standard 396 micro well plate. An automated process was defined

in the software to perform all these twenty extractions one after the other using optimized conditions. Loading time was kept constant at only 5 minutes in all tests to check the repeatability of pre-equilibrium extractions. 1-minute extractions were also possible, but the error bars were found to be larger. Peak intensities are plotted for all three compounds in Figure 27.

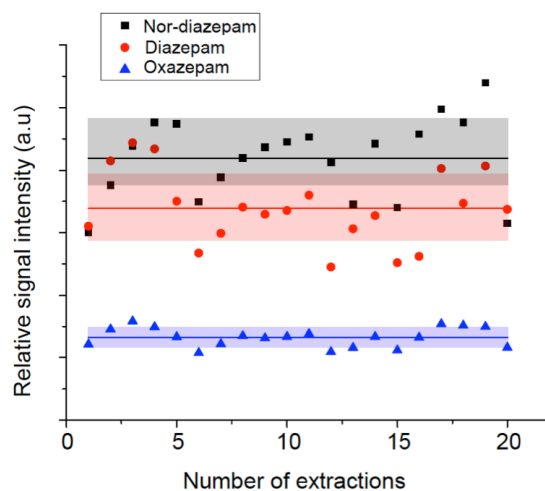


**Figure 27.** Peak intensity was obtained for twenty extractions of nordiazepam, diazepam, oxazepam (500 ng/ml from PBS). Loading time was kept constant ( $t=5$  minutes) for all experiments. The lines show the mean value for each analyte. Confidence intervals are shown as colored bands. The extracted analyte was eluted with acetonitrile/water (80:20  $V/V$ ) + 0.1% formic acid as the desorption solution, using a 1  $\mu\text{L}/\text{min}$  flow rate.

The RSD of the extractions were calculated from the acquired peak intensities for each analyte. It ranges from 11 to 17% from oxazepam to diazepam, indicating an acceptable repeatability of the method. The method also demonstrates an acceptable linear range from 1 to 1000 ng/ml for all three analytes. The regression coefficients of the calibration curves ranged between 0.9905 and 0.9957.

#### 4.5.7 Evaluation of the Method for Extraction of Benzodiazepines from Human Plasma

In the final step, the capability of the CGS to extract benzodiazepines from a complex matrix was evaluated. To that end, human plasma was spiked with 600 ng/ml of nordiazepam, diazepam and oxazepam and was left in the fridge overnight to ensure binding of proteins and drugs. Extraction

was performed using optimized conditions. Extraction from human plasma is more challenging compared to PBS. Two main complications can be pointed out when extracting analytes from complex matrices: firstly, unspecific adsorption of macromolecules to the C<sub>18</sub> beads' surfaces and pores, and competition of proteins in plasma and the C<sub>18</sub> phase for the drugs. The second point depends strongly on the difference of the competitor's affinity for the target analyte and concentration of each.<sup>123-126</sup> Figure 28 illustrates the extraction of a mixture of benzodiazepines (600 ng/ml) from human plasma. The LOD was determined with a dilution series test and was found to be 0.3 µg/ml.

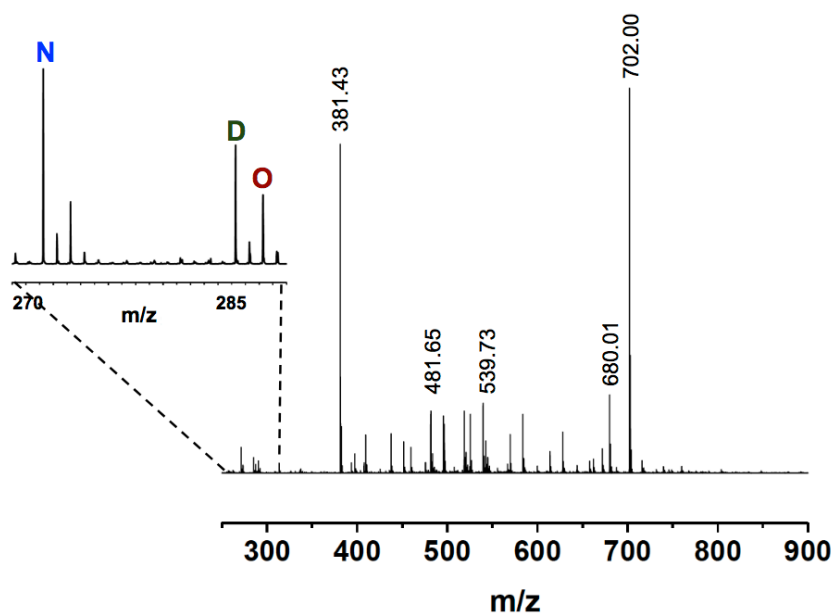


**Figure 28.** Shows the extraction of benzodiazepines from, human plasma 600 ng/ml. Peaks observed at  $m/z=271.1$ , 285.1, 287.1 corresponds to nordiazepam (blue), diazepam (green), and oxazepam (red) respectively. The spectrum was acquired from  $m/z=250$ . The extracted analyte was eluted with acetonitrile/water (80:20 *V/V*) + 0.1% formic acid as the desorption solution with a 1 µL/min flow rate.

The spectrum was acquired starting from  $m/z=250$ . Peaks between  $m/z$  380 and 800 mostly originate from the coating of the extraction tool, and some from human plasma. For example, the strong peak at  $m/z=381.43$  was observed while extracting from PBS and human plasma both, therefore it is coming from the coating material. The peaks observed at  $m/z=271.1$ , 285.1, and 287.1 correspond to nordiazepam, diazepam, and oxazepam, respectively.

EIC of the spectrum and spectrum of blank sample is shown below, both indicating the success of the extraction.

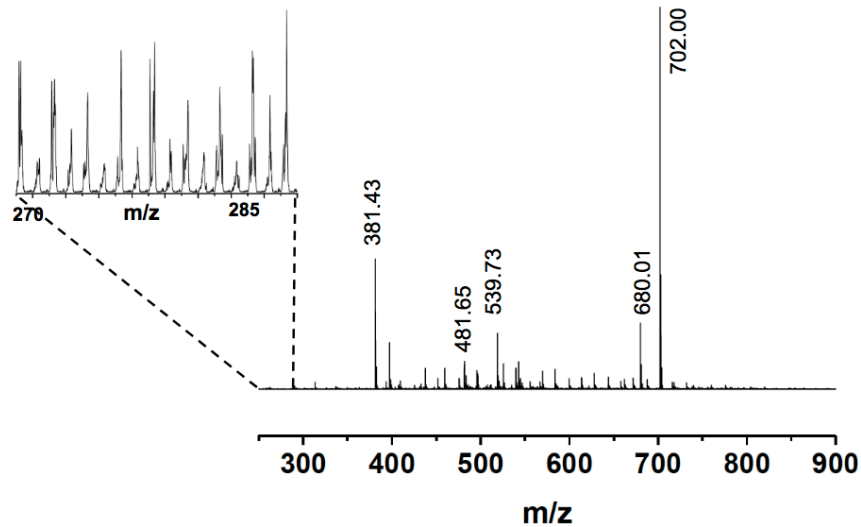


**Figure 29.** Extraction from human plasma (blank sample). The extracted analyte was eluted with acetonitrile/water (80:20 *V/V*) + 0.1 % formic acid as the desorption solution with a 1  $\mu\text{L}/\text{min}$  flow rate.

#### 4.5.8 Extracted Ion Chromatogram

The following figures show the EIC of diazepam, oxazepam and nordiazepam.

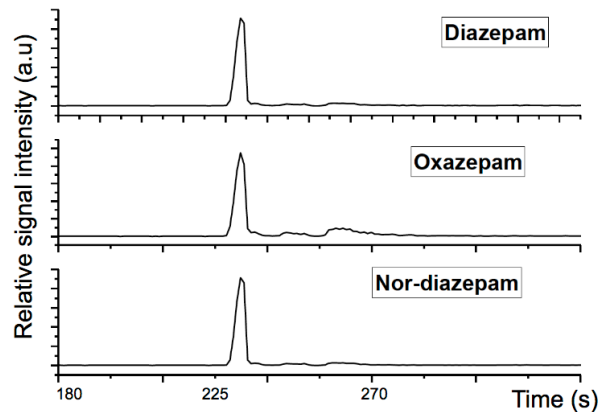


**Figure 30.** EICs from extraction of 600 ng/ml benzodiazepines from human plasma.

Residuals in the EIC are due to the delay of sample flush out of the spray, which happens when the bridge grows (rarely happens) and sample is trapped in the dead zones. To avoid any problem in quantifications, all of the peak intensities are obtained by summing up a constant range (100 seconds) of the chromatogram, to make sure that all of the analyte has reached the MS.

The average therapeutic concentration of diazepam in human plasma is 0.08–2.05  $\mu\text{g}/\text{ml}$ , based on several studies.<sup>127-132</sup> Our limit of detection is sufficient for the sampler to be used in the mid-to upper range of the therapeutic concentrations of nordiazepam, diazepam, and oxazepam in human plasma.

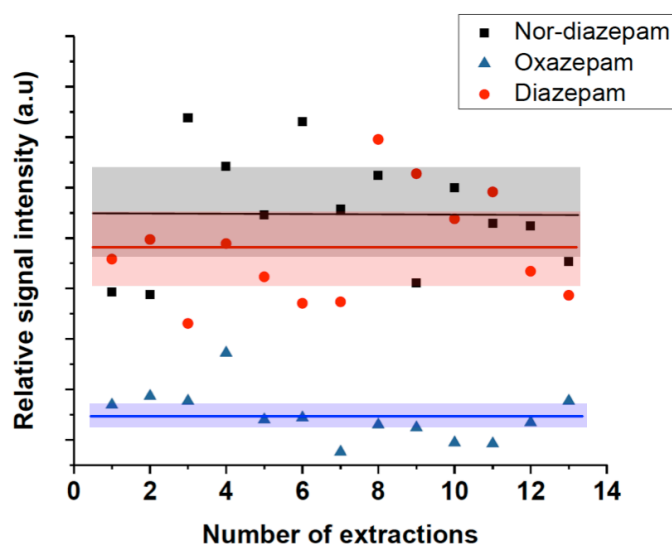


**Figure 31.** Signal intensities obtained for thirteen extractions of nordiazepam, diazepam, oxazepam (700 ng/ml) from human plasma. Loading time was kept constant ( $t=5$  minutes) for all experiments. The lines show the mean value for each analyte. Confidence intervals are shown as shaded bands. The extracted analyte was eluted with acetonitrile:water 80:20 ( $V/V$ ) + 0.1% formic acid as the desorption solution with a 1  $\mu\text{L}/\text{min}$  flow rate.

The RSD of the extractions were calculated from the measured peak intensities for each analyte. RSD values ranged from 18 to 21%, indicating an acceptable repeatability of the method. A linear dynamic range of nearly 3 orders of magnitude was achieved. The LOQ was about 500 ng/ml.



## 4.6 Conclusions

This Chapter introduced the CGS as a new device for sample up-concentration via SPME, before MS analysis. Compared to existing methods (such as thermal desorption followed by GC), the direct interfacing of SPME to MS has several benefits. A key advantage is that there are fewer limitations in terms of coating material selection. When using separation methods, thermal and physical stability restrict the extraction coating material choices.

The small size of the extraction tool of the CGS is beneficial in cases where only tiny sample volumes or expensive samples are available. This setup allows high-throughput SPME due to the high sampling speed and automation. In this chapter a well-studied system ( $C_{18}$  beads and benzodiazepines compounds) was chosen to as a proof of concept case study. Coatings were found to be reusable (for at least 30 extractions) and showed excellent physical and chemical stability. The reasonably low RSD ( $< 18\%$ ) of extraction repeatability confirms the robustness of this method. It is predicted to be straightforward to develop more specific extraction coatings that can be used in the quantitative analysis of target compounds. Moreover, the capability of the sampler to extract compounds from complex matrices rapidly (within a few minutes) and with high spatial accuracy render this tool interesting for bioimaging applications. For such uses, the definition of the customized loading coordinates for the SPME procedure can be improved, which would require knowing the coordinates of the microwells and each of the mechanical structures in the workspace - information that is not yet available.<sup>4</sup>

Bioimaging is one of the potential future applications of the CGS and semi-open capillary sampler. This application consists of basic SPME and specific SPME. One of the examples of basic SPME is when analytes are extracted with modified silica beads based on their Van der Waals interactions ( $C_{18}$ ,  $C_8$ ,  $C_4$ , etc.). When a compound of interest is specifically extracted using affinity interactions with a solid extraction phase, the method is called specific SPME. The main purpose of a specific extraction is to minimize non-specific interactions as much as possible. Thus, the next step in improving the sampler for future bioimaging applications is to prove and optimize its capabilities

in both categories. In Chapter 4, a basic SPME system was studied. A more challenging and complex system was chosen in Chapter 5 to perform specific SPME.

# Chapter 5

## Automated and Enhanced Extraction of a Small Molecule- drug Conjugate Using an Enzyme-inhibitor Interaction Based SPME Tool Followed by Direct Analysis by ESI-MS

*This chapter is adapted from:*

S. Ghiasikhou, S. Cazzamalli, J. Scheuermann, D. Neri, and R. Zenobi, Automated and Enhanced Extraction of a Small Molecule-Drug Conjugate using an Enzyme-Inhibitor Interaction based SPME Tool Followed by Direct Analysis by ESI-MS, *Analytical and Bioanalytical Chemistry* (2019). (ABC-00770-2019.R1 - Accepted)

## 5.1 Abstract

We report a novel, fast and automatic SPME-based method capable of extracting a small molecule-drug conjugate (SMDC) from biological matrices. Our method relies on the extraction of the drug conjugate followed by direct elution into an electrospray mass spectrometer (ESI-MS) source for qualitative and quantitative analysis. We designed a tool for extracting the targeting head of a recently synthesized SMDC, which includes acetazolamide (AAZ) as high-affinity ligand specific to carbonic anhydrase IX. Specificity of the extraction was achieved through systematic optimization. The design of the extraction tool is based on noncovalent and reversible interaction between AAZ and CAII that is immobilized on the SPME extraction phase. Using this approach, we showed a 330% rise in extracted AAZ signal intensity compared to a control, which was performed in the absence of CAII. A linear dynamic range from 1.2–25  $\mu\text{g/ml}$  was found. The limits of detection (LOD) of extracted AAZ from phosphate-buffered saline (PBS) and human plasma were 0.4 and 1.2  $\mu\text{g/ml}$ , respectively. This with a relative standard deviation of less than 14% ( $n=40$ ) covers the therapeutic range.

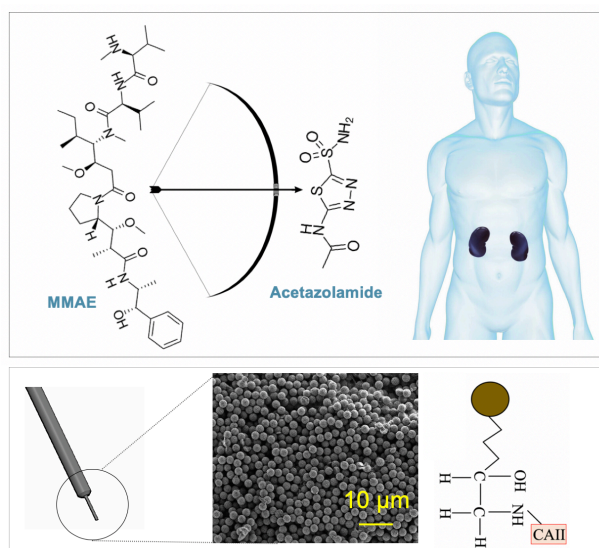


**Figure 32.** CAII-based extraction tool to evaluate MMAE targeted delivery to kidney cancer cells.

## 5.2 Introduction

Different targeting moieties have been proposed, including tumor-specific antibodies,<sup>133, 134</sup> aptamers,<sup>135- 137</sup> peptides<sup>138- 141</sup> and low-molecular-weight non-peptidic ligands.<sup>142- 145</sup> The use of antibodies as targeting head has several limitations: antibodies are large molecules, and thus have problems penetrating deeply into solid tumors.<sup>146</sup> Other disadvantages are the drug's long circulation times.<sup>147</sup> This has shifted the focus to small molecule-drugs, as they have advantages in terms of pharmacokinetics,<sup>138</sup> in vitro and in vivo stability,<sup>148</sup> antigenicity,<sup>149, 150</sup> conjugate chemistry and cost of manufacturing. Folate Receptor,<sup>151</sup> Prostate Specific Membrane Antigen,<sup>152</sup> Somatostatin Receptors,<sup>153</sup> and Carbonic Anhydrase IX,<sup>154</sup> have been successfully targeted with small molecules.

Carbonic anhydrase IX (CAIX) is a metalloenzyme and transmembrane protein involved in cell adhesion, pH homeostasis, and upregulated by hypoxia during tumor development and progression. The excellent tumor-targeting performance of AAZ, a small organic ligand for CAIX, was demonstrated by quantitative biodistribution in a murine model of Renal Cell Carcinoma.<sup>154</sup> AAZ showed good tumor-penetrating properties and fast targeting kinetics. AAZ derivatives of cytotoxic payloads have been generated and characterized for their potent in vivo anti-tumor activity against Carbonic Anhydrase IX expressing solid tumors in mice. Chemically defined ADC and SMDC products targeting CAIX have been generated and compared in terms of tumor-homing properties and therapeutic effect.<sup>155</sup> In quantitative biodistribution experiments performed with radiolabeled drugs administered intravenously to tumor bearing, the small organic ligand showed about 40% injected dose per gram (%ID/g) 6 hours after injection, while the anti-CAIX antibody only displayed a 4%ID/g after 24 hours.

Moreover, fluorescently labelled SMDC and ADC were analyzed for their diffusion properties in solid tumors. While the antibody-based product only localized nearby vascular structures, the anti-CAIX small ligand homogeneously accumulated over the tumor mass in a very short period of time (1 h after injection). Therapy experiments indicated the potent antitumor effect of both ADC and SMDC products. In order to evaluate the targeting performance, experiments that do not

require labeling and modification of the drugs are required. This might simplify sample preparation and lower generation of experimental artifacts. There is also a great demand for techniques capable of quick, site-specific and low-volume sample analysis, which would render the drug biodistribution screening in the tissue possible.

In this chapter, we report the development of a label-free SPME-based method, which allows analysis of the of anti-CAIX SMDCs, specifically AAZ-VC-MMAE, in biological matrixes. We present the capillary gap sampler as a platform for direct coupling of site-specific solid phase microextraction (SPME) with ESI-MS. Using such a sampler, SMDC products (in this case AAZ-VC-MMAE) can be selectively and quickly extracted from low volumes of different matrices and later quantified by ESI-MS analysis. The extraction step is based on the interaction between immobilized CAII, a commercially available and inexpensive isoform of CA, and the targeting moiety of AAZ-VC-MMAE, i.e., AAZ. Therefore, for the optimization experiments we focused on the extraction of AAZ using CA and later applied the optimized parameters to the extraction of the AAZ-VC-MMAE (whole drug). This approach was selected to minimize the use of expensive AAZ-VC-MMAE due to its long and complicated synthesis.

## 5.3 Material and Methods

### 5.3.1 Chemical and Materials

Acetonitrile  $\geq 99.9\%$  (LC-MS CHROMASOLV), water (LC-MS grade), bovine carbonic anhydrase II, human plasma, bovine serum albumin, myoglobin Dimethyl sulfoxide (for acetazolamide solution preparation) were purchased from Sigma Aldrich (St Louis, MO, USA). Also, diazepam and diazepam-d5 were obtained from Sigma Aldrich (The Woodlands, TX, USA) and stored at 4°C. Acetazolamide  $\geq 99\%$  and Methazolamide  $\geq 98\%$  were purchased from Sigma (Steinheim, Germany). Methanol and ethanol (HPLC grade) were purchased from Fisher Scientific (Loughborough, U.K). Formic acid (98-100%) and rhodamine B were purchased from Merck (Darmstadt, Germany). Acetone was provided by Aldrich (Milwaukee, WI, USA). Dynabeads M-270 Epoxy was purchased from Thermo Fisher Scientific (Baltics, Norway) and

stored at 2–4°C. 8-Anilino-1-naphthalenesulfonic acid was bought from Fluka-Chemie AG (Buchs, Switzerland). Polyacrylonitrile (PAN), which was used as a biocompatible glue to immobilize the beads on the stainless-steel pin, was purchased from Acros (New Jersey, USA). AAZ-VC-MMAE was synthesized as described in Ref. 156.

### **5.3.2 Equipment for detection, Software, Buffer Delivery**

A Synapt G2-S high definition mass spectrometer (Waters, Manchester) operated in positive ion mode was used for the experiments. The source temperature was set to 30°C and the capillary voltage to 3.3 kV. Masslynx 4.1 software was used for acquiring the data. Buffer delivery was performed via a syringe pump (neMesys, Cetoni, Korbuss, Germany).

### **5.1 Preparation of the SPME tool.**

The stainless-steel pin (229 µm in diameter; V&P Scientific, San Diego/CA, US) was washed and sonicated with isopropanol/methanol, followed by a O<sub>2</sub> plasma cleaning procedure. Silica beads carrying epoxide functionalization on their surface were then fixed to the metal tip using polyacrylonitrile (PAN) polymer (the approximate ratio of beads : glue is 1 : 1), and this PAN glue was later cured in the oven at 180°C for two minutes and later cooled down to room temperature. The same process was repeated 3 times. Afterwards, the epoxy-modified beads were immersed in a saturated CAII solution for 48 hours at 2–4°C. The CAII was immobilized on the beads through an amine-epoxy reaction. The unreacted active epoxy groups were quenched by incubation in Tris 20 mM buffer for half a day. A SEM image of the coated extraction tool is shown in Figure 33. The coating thickness was found to be around 50µm. This extraction tool can be used for multiple extractions (50 extractions in this work) without replacement.

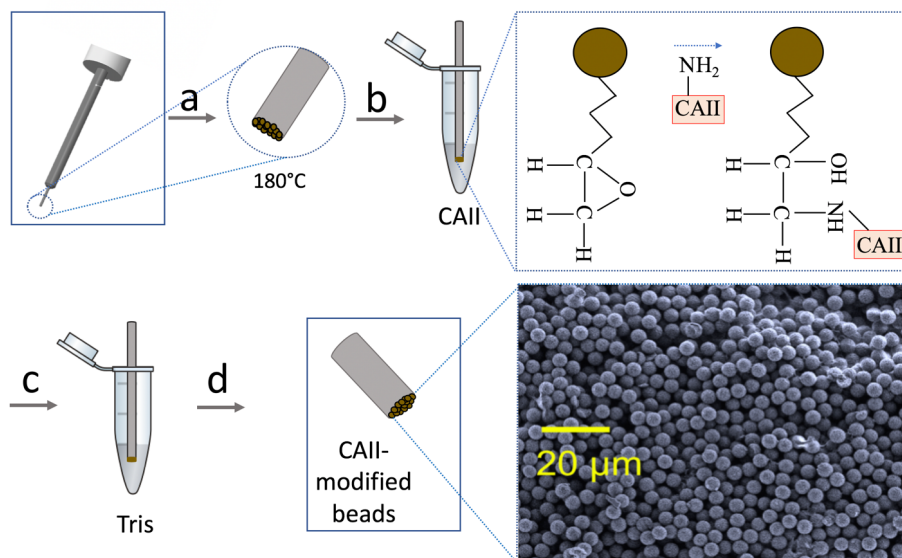


**Figure 33.** Extraction tool preparation steps, (a) gluing epoxy-modified beads onto the solid pin and curing at 180°C, (b) incubation with CAII and amine-epoxy reaction, (c) incubation in Tris buffer, (d) SEM image of the CAII-modified beads after immobilization on the extraction tool, confirming that beads are not covered with PAN glue.

### 5.1.1 Workflow for Sample Extraction and Elution

(1) Loading: in this step, the extraction tool is dipped into the sample solution and binds with the analyte of the interest noncovalently (Figure 36). CAII and AAZ were found to bind best at a pH of ~7.2 (Figure 37). The rate of extraction increases by performing agitation in this step. This is achieved by quick movements of the extraction tool inside the sample well using a 250 rpm rotation speed.<sup>4</sup>

(2) Washing: this refers to the step of removing the remaining matrix off the pins, with minimum loss of the analyte of interest. In this case, washing occurs in water at a pH of 7.4.

(3) Elution: this is the step of desorption of the analyte using an appropriate elution solution. Using the CGS, elution is performed inside the liquid bridge. The eluted compound is then sprayed directly into the MS inlet. The extraction tool is left in the gap exposed to the desorption solution for 2 minutes, until the EIC signal has reached baseline level again (explained in Figure 39).



(4) Conditioning: after the elution step and prior to the next round of the experiment, the extraction tool moves into water at a pH of 7.4 to keep the CAII folded.

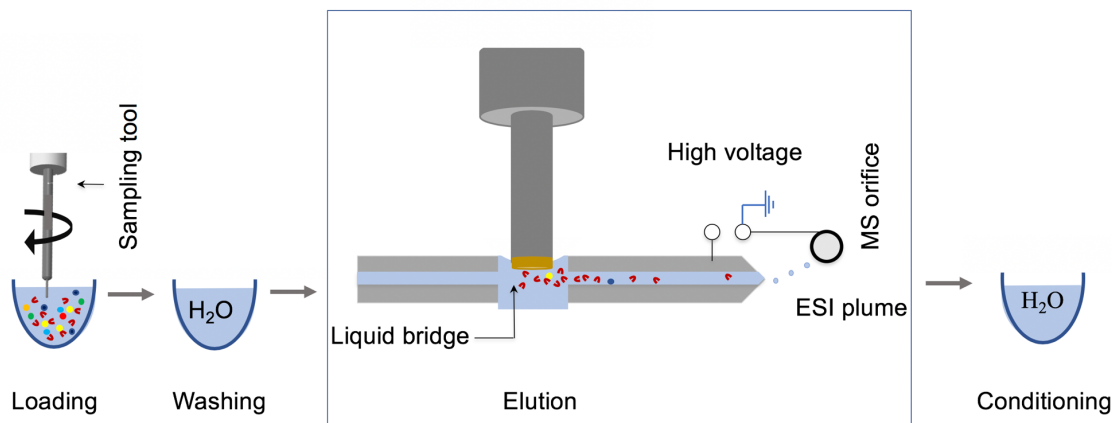


**Figure 34.** In this figure extraction workflow including loading, washing, elution, conditioning is shown. The elution step happens in the liquid bridge formed in between two capillaries.

## 5.2 Results and Discussion

### 5.2.1 Proof of CAII Immobilization

In order to evaluate whether the immobilization of CAII on the epoxy beads was successful, a well-established protein identification test with 8-anilino-naphthalene-1-sulfonic acid (ANS) was performed. ANS is a hydrophobic organic dye containing both a sulfonic acid and an amine group. Non-covalent binding of ANS and peptides/proteins in solution largely occurs through the negatively charged sulfonate groups and the positively charged side chains of the arginine residues of the proteins.<sup>157, 158</sup> Fluorescence enhancement results from ion pairing between the arginine from CAII with the ANS sulfonate group.<sup>159</sup> In this test, epoxy-modified beads were glued onto two microscope slides (one as a control experiment) with different densities and incubated with a buffer solution with and without CAII for 48 hours at 4°C. In order to remove non-specifically bonded ANS while keeping proteins in their correct folding, beads were rinsed with water, incubated with an ANS solution for one hour and washed with saline buffer at pH 7.4 to remove any non-specifically bonded ANS while the proteins were kept folded. Both slides were observed

under a fluorescent microscope. Several areas were imaged using both the blue fluorescence emission channel and bright field modes. The results are shown in Figure 35.

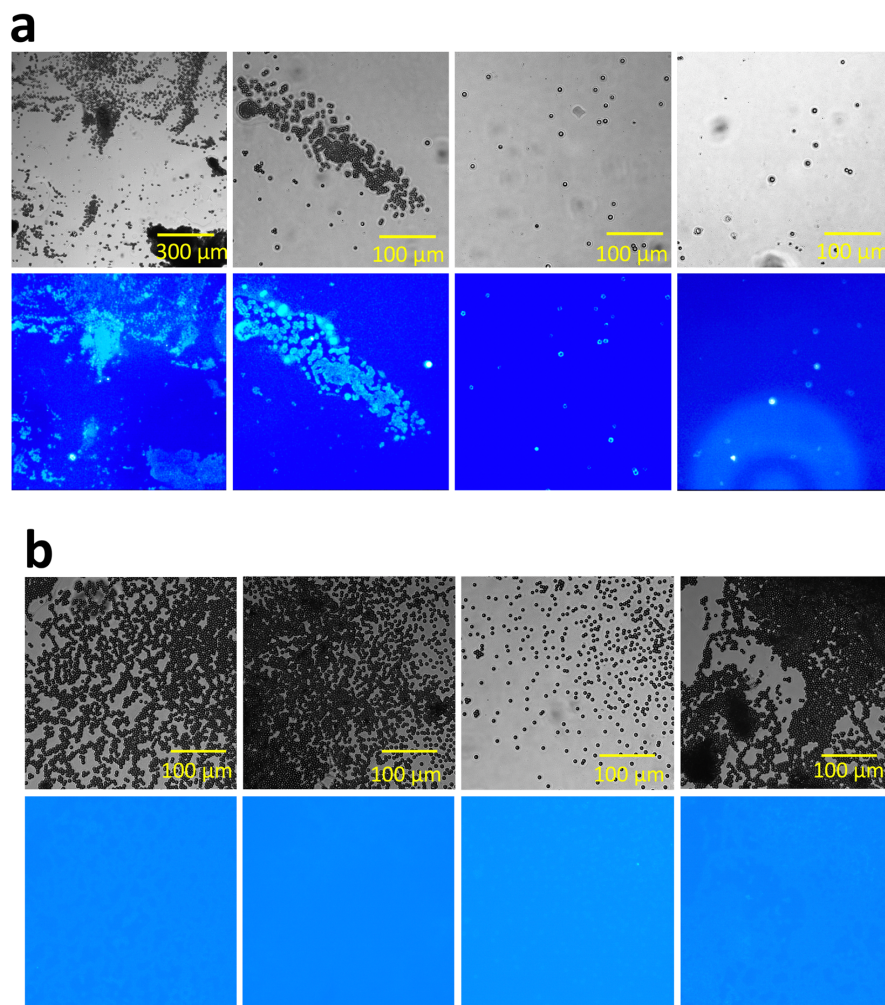
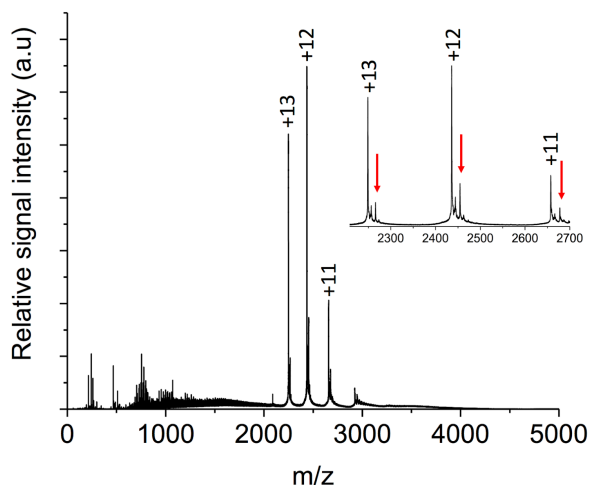


**Figure 35.** Bright field and blue channel images from the epoxy-modified beads (incubated (a) with, (b) without CAII) after reacting with ANS.

The results shown in Figure 35 confirm the binding of CAII to the beads. Images were selected from areas with different bead densities. Comparison of the fluorescent enhancement among series a and b confirms the presence of CAII proteins on the beads in Figure 35a.

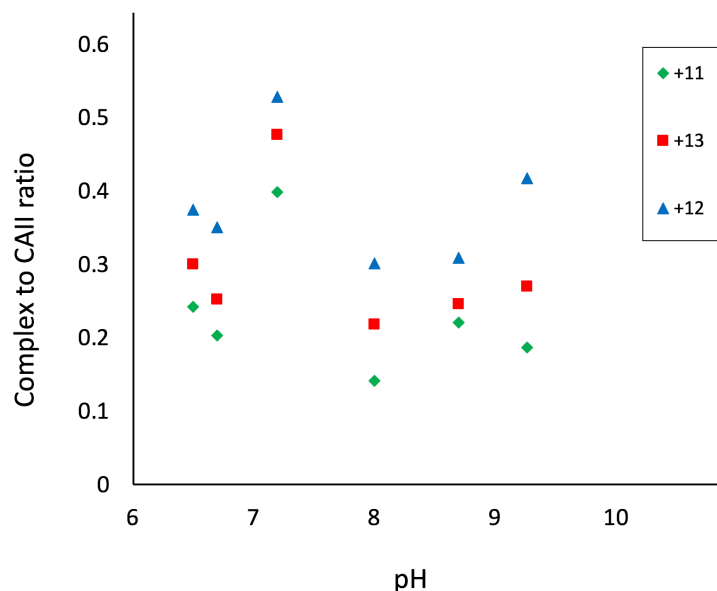
### 5.3 Carbonic Anhydrase II and Acetazolamide Binding

Acetazolamide is a sulfonamide and known to be an inhibitor for CAII. In this section we present a spectrum (Figure 36) showing the CAII-AAZ complex. To achieve this spectrum, AAZ 10  $\mu\text{m}$  and CAII 15  $\mu\text{m}$  in 100 mM ammonium acetate were mixed. After 2 minutes it was loaded into a borosilicate nano-emitter and was sprayed to MS.



**Figure 36.** Showing the 1:1 ratio of the CAII and AAZ complex ESI-MS spectrum.

As shown in the Figure 36 the pointed peaks in the zoomed section represents the different CAII-AAZ complex charge states in the native form. The AAZ binds to the metal cofactor ( $\text{Zn}^{\text{II}}$ ) of the enzyme. In the later step, the influence of the pH on the ligand-enzyme binding was investigated. In this case the pH of the AAZ-CAII reaction were varied from 6.5 to 9.3. The solutions were loaded in the borosilicate nano-emitters and later sprayed into the MS. The 3 minutes of data acquisition for each solution of different pH, was summed and the signal intensities were used to plot the Figure 36. In the Figure 36 complex to protein ratio is plotted for each charge state versus the pH.



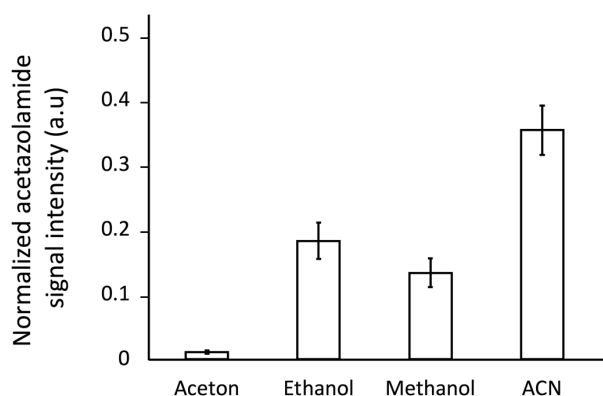
**Figure 37.** The pH profile of AZZ-CAII binding.

Figure 37. illustrates two important points. Firstly, the physiological pH provides the most desirable condition for AAZ and CAII binding. The second point is that the native form of the complex is observed through a wide range of pH (6–9). In general, the global structure of CAII undergoes minimum changes in the mentioned pH window. The observed changes in complex to protein ratio as pH changes is mainly due to the chemical effects of the active site such as protonation of the ligand or enzyme. The other small but noticeable reason is the change in the active site environment for instance presence and location of water molecules as a function of pH.

### 5.3.1 Influence of the Desorption Solution on the Acetazolamide Signal

Selection of the right desorption solution is crucial to have a complete elution of the analyte and to keep the CA protein properly folded for the next extractions. In order to separate the analyte from the enzyme, different mixtures of organic solvents acetonitrile, methanol, ethanol and acetone and water were tested. Restrictions such as the pH or organic solvent content of the mixture should be considered. Decreasing the pH or increasing the organic solvent-to-water ratio of the solution increases the release of the inhibitor from CAII, but also increases the probability of protein denaturation. On the other hand, the stability of the liquid bridge in the double capillary system is

significantly enhanced by increasing the organic ratio of the mixture. The reason is their low surface tension in comparison with water. Possible denaturation during the elution process can be overcome by placing the extraction tool in a buffer solution with physiological pH immediately after elution and prior to the next extraction (conditioning step). Solutions containing 50% of the mentioned organic solvent and water, plus 0.1% formic acid for enhancing ionization were prepared. Methazolamide (1  $\mu\text{M}$ ) was added to the solution in order to normalize the acetazolamide signal intensity. Normalization was performed based on dividing the summed intensity of AAZ to the summed intensity of methazolamide over the same desorption time window. Methazolamide was chosen as the normalizing agent because it originates from the same family of compounds (sulfonamides) and has a very similar chemical structure, size and functionality to AAZ. It can therefore be used to correct for fluctuations in the ionization of AAZ. Also, the AAZ concentration was chosen based on its therapeutic concentration in human plasma. Extraction of acetazolamide 5  $\mu\text{M}$  from PBS was performed 10 times for each solution. Results are shown in Figure 38.



**Figure 38.** Average amount of eluted acetazolamide ( $n=10$ ) using acetonitrile, methanol, ethanol and acetone 50% mixed with water (plus 0.1% of formic acid) as the desorption solution. The results are normalized to methazolamide (1  $\mu\text{M}$ ).

As shown in Figure 38, water containing 50% acetonitrile elutes more acetazolamide compared to the other organic solvents, which can be explained by the higher solubility of AAZ in ACN and its lower pH value in comparison with other solutions. RSD values for acetone, ethanol, methanol

and ACN were 22%, 15%, 17% and 11% respectively. The use of 50% ACN also results in a smaller RSD, most probably due to lower carry-over from the previous 120 seconds of elution. We also expected the protein to be more prone to becoming denatured after dissociation of the acetazolamide. This expectation is supported by a study by Almstedt *et al.*<sup>160</sup> who showed that sulfonamide ligands, bound to the metal cofactor (the active site of the enzyme), can further stabilize CA against denaturation. Therefore, after acetazolamide elution, CAII is more prone to denaturation, i.e., long elution times should be avoided. Considering our experimental parameters, such as coating thickness, acetazolamide concentration, etc., and in accordance with the EIC of the acetazolamide, a 2-minute elution was found to be enough for the chromatogram to return to baseline. An example of an EIC of acetazolamide is shown in Figure 39 (the extraction tool enters the liquid bridge only at  $t=3.2$  min), which confirms that 2 minutes is long enough for the elution step.

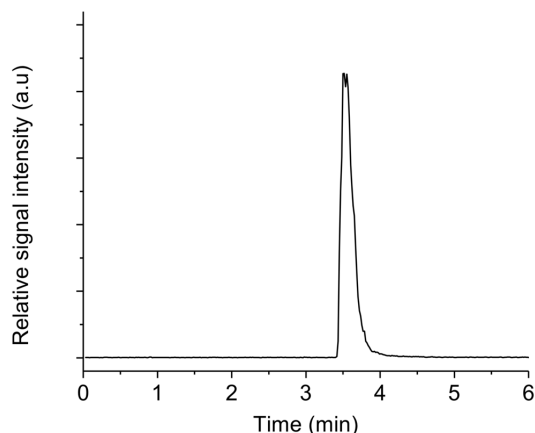


**Figure 39.** EIC ( $m/z=223.25 \pm 5$  ppm) of acetazolamide ( $20 \mu\text{M}$ ) after extraction from PBS.

In order to confirm that CAII is not denatured during the desorption step, CAII  $20 \mu\text{M}$  was incubated in 50 % ACN:  $\text{H}_2\text{O}$  for 2 minutes and sprayed directly into MS using borosilicate nano-emitters. Figure 40 represents the resulting spectrum. The peaks marked in Figure 40 correspond to a native charge state distribution of CAII (which has been performed as a control), thus confirming the high stability of CAII against denaturation in 50% ACN:  $\text{H}_2\text{O}$ .

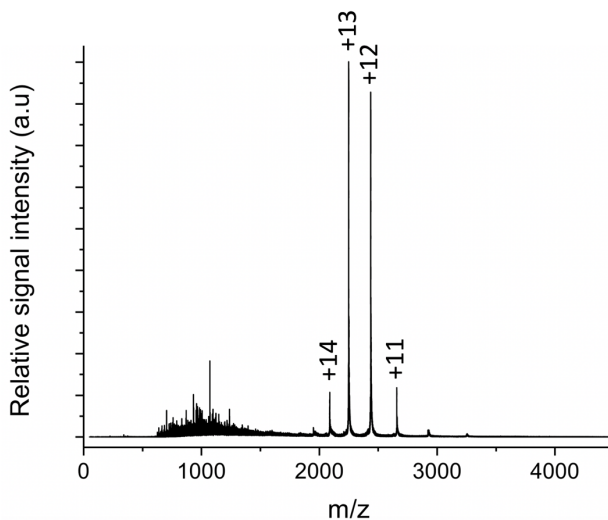


**Figure 40.** The nano-ESI spectrum of CAII 20  $\mu\text{m}$  incubated in 50% ACN: H<sub>2</sub>O for 2 minutes.

### 5.3.2 Extraction of AAZ-VC-MMAE from Human Plasma by the CGS

After understanding and optimizing different experimental parameters such as pH, desorption solution and time, an evaluation of the technique for drug extraction was performed. A solution of AAZ-VC-MMAE of 2.5  $\mu\text{g}/\text{ml}$  was directly sprayed by a borosilicate nano-emitter, and the spectrum shown in Figure 41a was collected. Then, using a CAII modified pin, the 2.5  $\mu\text{g}/\text{ml}$  drug was extracted from PBS (Figure S14b, supplementary information) and human plasma. The human plasma (8% by volume, in water) was spiked with the drug and left overnight in the fridge at 2–4°C. A control experiment was performed, in which 2.5  $\mu\text{g}/\text{ml}$  AAZ-VC-MMAE was extracted from PBS using bare beads (Figure 42). The results are shown in Figure 41b. The peaks corresponding to the drug are marked in the spectra.

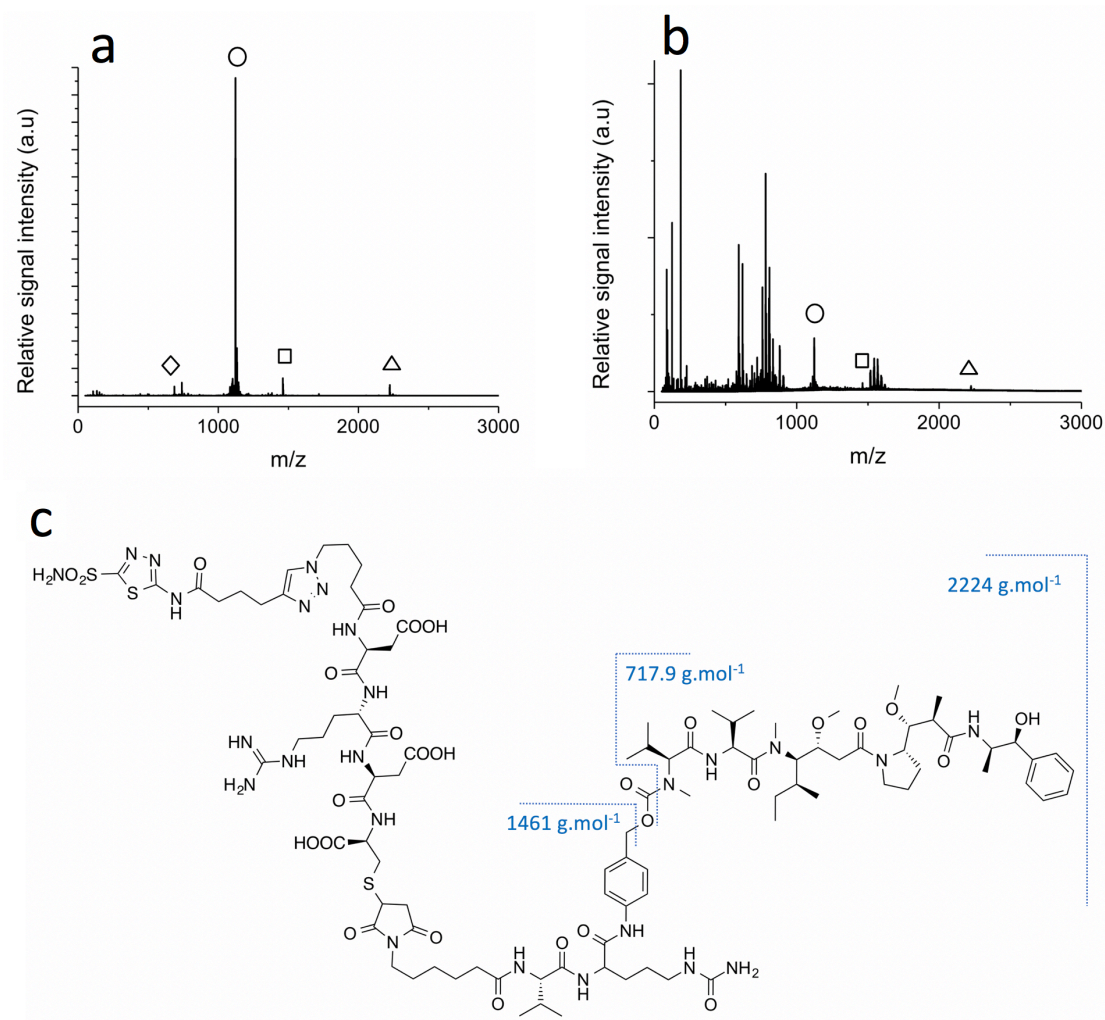


**Figure 41.** Spectrum of AAZ-VC-MMAE, (a) direct infusion by nanospray, (b) extraction from human plasma. The following peaks were observed in both spectra: ( $\diamond$ ) MMAE +  $H^+$  = 718.51  $m/z$ , ( $\circ$ ) AAZ-VC-MMAE +  $2H^+$  = 1113.03  $m/z$ , ( $\circ$ ) AAZ-VC-MMAE +  $H^+$  +  $Na^+$  = 1123.53  $m/z$ , ( $\square$ ) AAZ-VC-MMAE – MMAE –  $CO_2$  = 1461  $m/z$ , ( $\Delta$ ) AAZ-VC-MMAE<sup>+</sup> = 2224.05  $m/z$ . Part (c) shows the chemical structure of AAZ-VC-MMAE.

Five identical peaks in both spectra indicate the success of the drug extraction from human plasma. Peaks between 50 and 800  $m/z$  mostly originate from the coating glue of the extraction tool, and some from human plasma. For example, the strong peaks at 780.7 and 591.7  $m/z$  were observed while extracting from both PBS (Figure 42b) and human plasma (Figure 41b), therefore they must originate from the coating material. The peaks observed at 718.51, 1113.03, 11123.53, 1461 and



2224.05  $m/z$  correspond to  $\text{MMAE} + \text{H}^+$ ,  $\text{AAZ-VC-MMAE} + 2\text{H}^+$ ,  $\text{AAZ-VC-MMAE} + \text{H}^+ + \text{Na}^+$ ,  $\text{AAZ-VC-MMAE} - \text{MMAE} - \text{CO}_2$ , and  $\text{AAZ-VC-MMAE}^+$ , respectively. Extraction of the drug from human plasma is more challenging due to matrix effects: firstly, unspecific adsorption of macromolecules to the beads' surfaces and pores, competition between the proteins in the plasma and the extraction phase for the drug can occur. The second point depends strongly on the differences of the competitor's (extraction phase and plasma) affinity for the target analyte and the concentration of each.

A control experiment was performed in which  $\text{AAZ-VC-MMAE}$   $2.5 \mu\text{g/ml}$  was extracted from PBS using bare beads and the result is shown in the Figure 42a. Later using a CAII modified pin, the same concentration of the drug was extracted from PBS (Figure 42b).

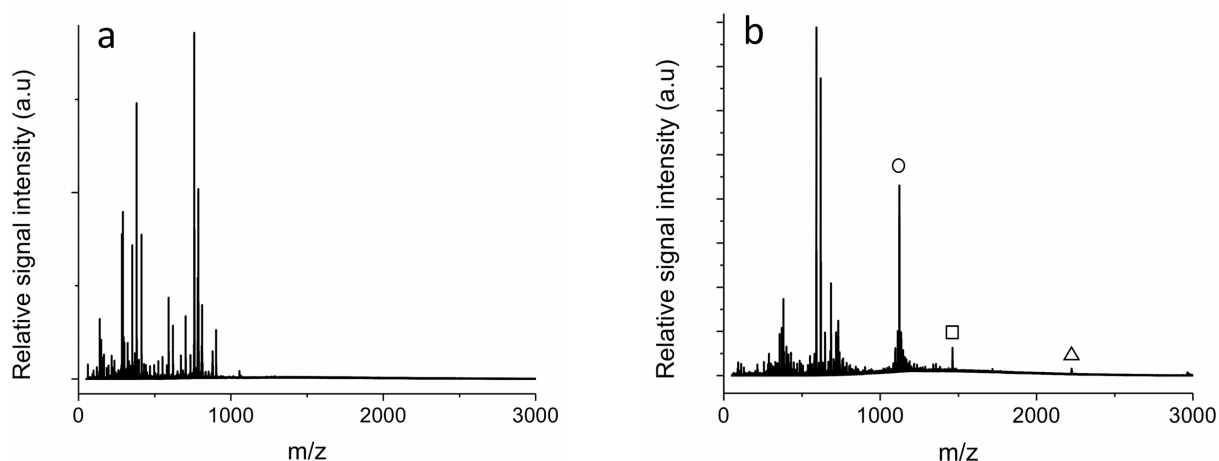


**Figure 42.** The  $\text{AAZ-VC-MMAE}$   $2.5 \mu\text{g/ml}$  extraction spectrum from PBS using, (a) bare beads (control), (b) CAII beads. The following peaks were observed in both spectra: (◇)  $\text{MMAE} + \text{H}^+ = 718.51 \text{ m/z}$ , (○)  $\text{AAZ-VC-MMAE} + 2\text{H}^+ = 1113.03 \text{ m/z}$ , (◉)  $\text{AAZ-VC-MMAE} + \text{H}^+ + \text{Na}^+ = 1123.53 \text{ m/z}$ , (□)  $\text{AAZ-VC-MMAE} - \text{MMAE} - \text{CO}_2 = 1461 \text{ m/z}$ , (Δ)  $\text{AAZ-VC-MMAE}^+ = 2224.05 \text{ m/z}$ . Part c shows the chemical structure of  $\text{AAZ-VC-MMAE}$ .

None of the mentioned peaks were observed in the control test spectrum.

### 5.3.3 Specificity of the Extraction

The specific extraction approach is crucial to discriminate against other compounds in a biological sample. In this context, the term specific means enhancing the extraction of the analyte of interest as much as possible while minimizing interferences from unwanted compounds, to make the data interpretation as clean and simple as possible. In most cases, nonspecific extraction cannot be avoided but can be minimized. To investigate the specificity of the AAZ extraction, three different proteins including CAII, BSA and myoglobin, were immobilized on the extraction tool (serum albumin representing a blood plasma protein and myoglobin presenting a muscle protein). They represent important proteins in homogenized tissue where this method is going to be applied in the future. Then, using these three pins and a pin without immobilized protein (as a control), seven extractions of acetazolamide 6.7  $\mu\text{M}$  from PBS were performed. Results are plotted in Figure 43.

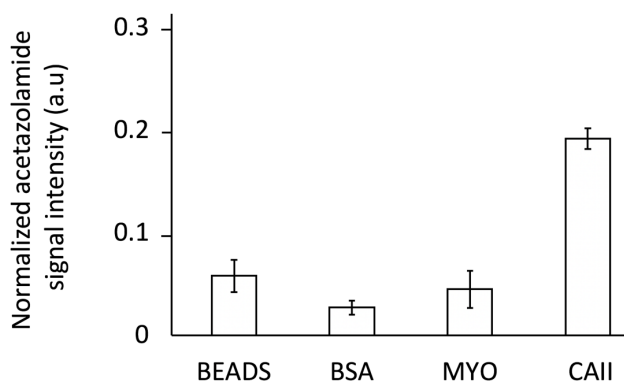


**Figure 43.** Extraction of acetazolamide using three different proteins (bovine serum albumin, myoglobin and carbonic anhydrase II) immobilized on the pins, plus a control experiment (bare beads). The acetazolamide signal intensities are normalized to methazolamide 2  $\mu\text{M}$ . ( $n=7$ )

Although nonspecific binding was observed for all the pins, extraction was significantly enhanced using CAII modified beads, which means that carbonic anhydrase II binds AAZ specifically and therefore provides an enhanced extraction. Nonspecific binding can be minimized by a longer washing time after extraction and prior to the desorption step. Epoxy-modified beads are hydrophilic and pH neutral. AAZ is also hydrophilic, which explains the nonspecific extraction in the control experiment. Immobilization of BSA and myoglobin render the surface more

hydrophobic and they do not bind AAZ specifically, therefore less extraction of AAZ was observed. According to the future application of this extraction tool in the real samples including tissue and blood, one can use this test results to define the matrix effect. Based on the results competition of the other existing proteins for AAZ in compare to the CAII is not considerable, since they extract less than 30% of what can be extracted using CAII. In another test, extraction of AAZ from a mixture of different analytes using a CAII modified pin was evaluated. The mixture consisted of three compounds, acetazolamide, diazepam and MMAE, each at a concentration of  $6.7 \mu\text{m}$  in PBS. Diazepam was chosen because of its similar molecular weight to AAZ, and MMAE was chosen as the therapeutic head of the drug (AAZ-VC-MMAE). This allowed us to gauge how much of the compound is extracted because of the affinity of CAII to AAZ vs. non-specific binding of the MMAE to the extraction tool.

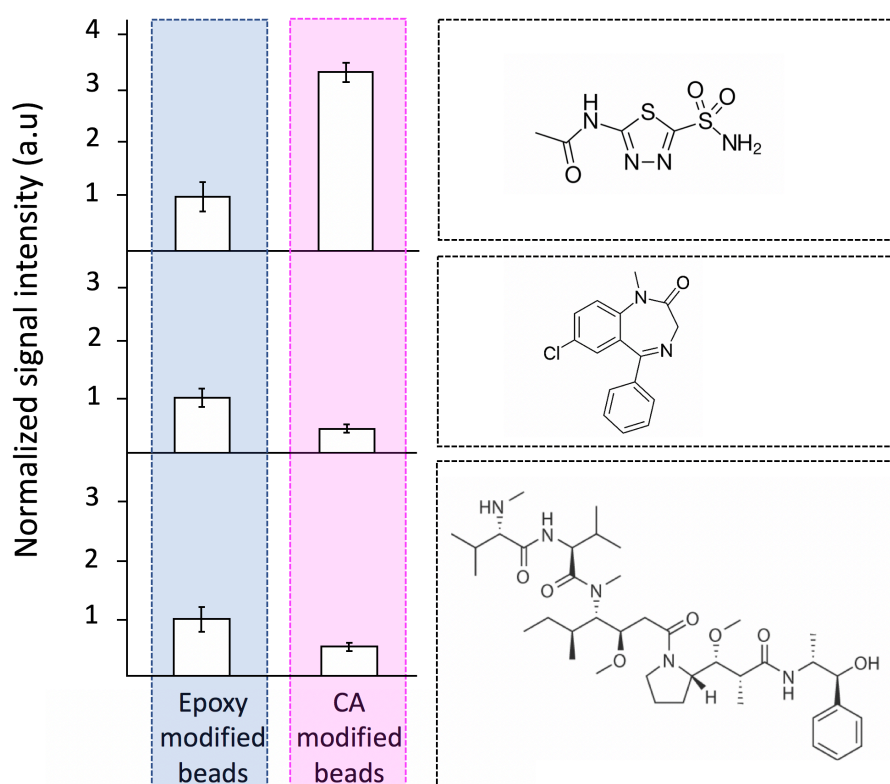


**Figure 44.** Comparison of the extraction of three different analytes, (a) acetazolamide, (b) diazepam, (c) MMAE, using CAII and epoxy-modified beads. ( $n=5$ )

Figure 44 shows the results. For each analyte peak, intensities were normalized to the analyte intensity extracted by the epoxy-modified beads. The normalized intensity of the peaks is compared for each extracted analyte using CAII modified pins, plus a control using bare epoxy-modified beads. According to Figure 44, modification of the pin with CAII greatly enhances the extraction of acetazolamide and decreases the extraction of diazepam and MMAE. The high affinity of CAII to acetazolamide is the main reason for the 330% enhancement of the extraction.

### 5.3.4 Time Profile of the Extraction

The concept of SPME was developed to address the need for fast sample clean-up. The SPME extraction phase is in contact with the sample matrix for a well-defined amount of time. Depending on several factors such as temperature, the affinity of the extraction phase with the analyte, the volume of the extraction phase and sample volume, analyte concentration, and agitation, the amount of the extracted sample may vary. The extraction strategy can either be designed on the basis of pre-equilibrium or equilibrium conditions. The former is accomplished by stopping extraction before equilibrium has been reached. In the equilibrium-based approach, convection/agitation conditions do not affect the extracted amount. However, when using the pre-equilibrium method, high reproducibility, which is especially important for the purpose of quantification, can be achieved only if convection/agitation is controlled. Pre-equilibrium extraction is quicker compared to equilibrium-based extraction and, pending acceptable level of sensitivity, accuracy and reproducibility, it would be the preferred method. In this section, several extractions from a 20  $\mu\text{M}$  acetazolamide solution in 40  $\mu\text{L}$  PBS were performed by a CAII modified pin. The extraction time was varied to find the equilibration time. Each experiment was repeated 3 times. Agitation was performed in all the extractions. The time profile of the extraction is shown in Figure 45.

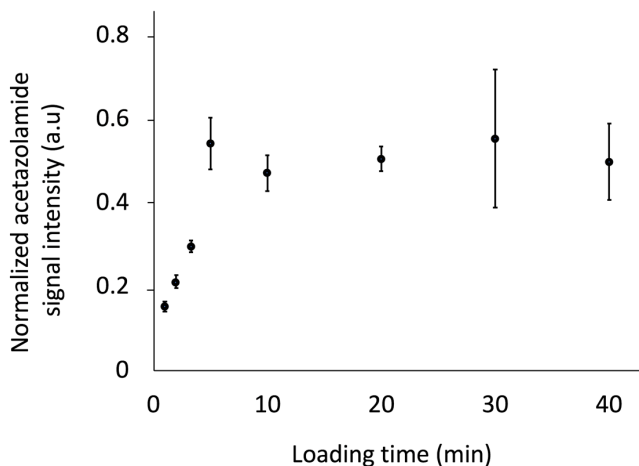


**Figure 45.** The time profile of the extraction acetazolamide (20  $\mu\text{M}$ ) from PBS ( $n=3$ ). The results are normalized to methazolamide (2  $\mu\text{M}$ ). "Loading time" (x axis) is equal to "Extraction time".

By increasing the extraction time, the signal intensity of the extracted acetazolamide increases. This increase continues for the first five minutes, after which no considerable change is observed. Therefore, equilibrium is reached within five minutes in this case. The equilibrium is determined by the distribution constant  $K_{es}$  for a solid extractant defined as  $K_{es} = S_e / C_s$ ,<sup>122</sup> where  $S_e$  is the surface concentration of the adsorbed analyte on the extraction phase and  $C_s$  is the analyte concentration in the sample. The sorbent surface area is also considered in the definition of  $S_e$ . Thus, for a higher surface-to-volume ratio, equilibrium is reached faster, i.e. this method can be designed for high-throughput screening where speed and time are important factors. An efficient agitation technique during extraction reduces the equilibration time by making the boundary layer thinner.<sup>161, 162</sup>

### 5.3.5 AAZ Extraction Linearity, Sensitivity, Limit of Detection, and Recovery

One of the advantages of SPME-based methods over traditional sample preparation methods is their ability to quantify free concentration of a drug in a biological fluid or tissue. According to the therapeutic concentration of acetazolamide in human plasma, which is about 5–10  $\mu\text{g}/\text{ml}$ ,<sup>163</sup> the linear dynamic range and limit of detection should be evaluated. Equilibrium-based extraction of the acetazolamide is shown in Figure 46. Using simple linear regression model and considering error bars as weighing factors, extraction linearity from plasma spiked with different sample

concentrations was found over the entire calibration range of 1.2–25  $\mu\text{g/ml}$  ( $n=4$ ), with a regression coefficient of 0.997. Methazolamide at a 1.5  $\mu\text{g/ml}$  concentration was used for normalization, to correct the AAZ signal intensity.

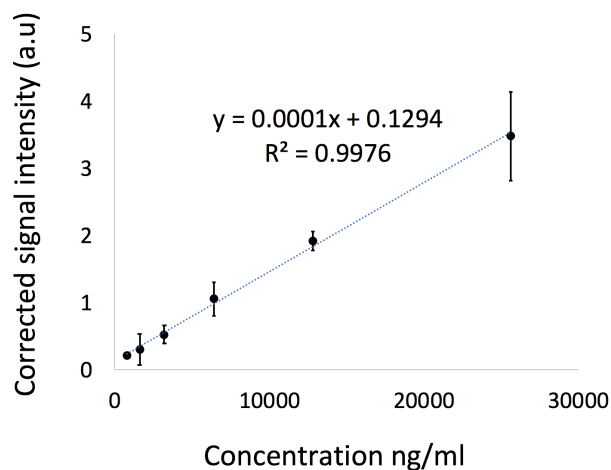


**Figure 46.** Linear range of AAZ extraction ( $n=3$ ). Results are normalized to methazolamide 1  $\mu\text{M}$ .

The range mentioned is a function of immobilized CAII concentration on the beads, LOD, extraction recovery and dilution of the sample in the desorption step. The linearity range covers a broader range than the therapeutic AAZ concentration range. By optimizing the washing and desorption steps, carryover from one extraction to the next round was kept below 0.1%. Sample carryover was checked by three extraction series, each consisting of extraction of a high analyte concentration followed by a blank extraction using a microwell filled with water. Evaluation of sample carryover was performed by summing the AAZ peak intensity over the defined desorption time obtained for the blank extraction relative to the previous sample extraction. For a signal-to-noise ratio of 3:1, the LOD was 0.4  $\mu\text{g/ml}$  from PBS and 1.2  $\mu\text{g/ml}$  from human plasma, respectively ( $n=4$ ).

In another set of experiments, different concentrations of AAZ were sprayed into the MS inlet. From these data, a calibration curve was constructed, and the recovery of the equilibrium-based extraction was calculated. Considering the extracted AAZ signal intensity, knowing the initial AAZ concentration and using an AAZ calibration curve, recovery of the extractions was found to be 5% ( $n=3$ ). In the calibration curve, the sum of the AAZ signal intensity over 3 minutes (AAZ

spraying directly from buffer line to MS) was plotted against the AAZ concentration. In accordance with the therapeutic range and achieved LOD, this method provides enough sensitivity for AAZ quantifications.

### 5.3.6 Repeatability

To confirm the repeatability of the extraction, forty tests were performed. In each test, 500 nM acetazolamide was extracted from PBS solution.

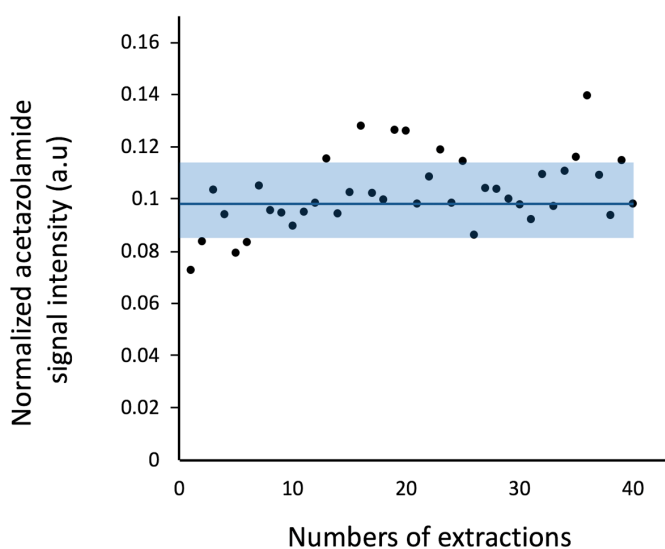


**Figure 47.** Repeatability test. RSD for forty extractions of 500 nM acetazolamide from PBS was found to be 13.5%. The solid blue line represents the mean value. The data were normalized to methazolamide (200 nM).

The relative standard deviation of 13.5% for forty extractions (Figure 47) represents an acceptable reproducibility of the process.

## 5.4 Conclusion

In this chapter, a novel affinity SPME tool to improve the capabilities of SPME is described. Here, we attempt to extract an acetazolamide conjugated drug using a CAII-based extraction tool. Acetazolamide is the inhibitor for CAII; therefore, the extraction is based on the interaction between CAII and acetazolamide. The study started with the preparation of the extraction tool, and

the CAII immobilization on epoxy modified beads was demonstrated. The critical steps of analyte elution were studied. The desorption solution was optimized to elute the highest possible amount of the extracted sample efficiently and to keep the protein in its active folded structure. The specificity of the extraction was studied in a two-step evaluation. Firstly, acetazolamide was extracted using different protein-modified beads, and then in the second step, acetazolamide was extracted from a mixture using CAII modified beads. Using both methods, extraction with CAII-altered beads showed considerable enhancement in the affinity extraction of acetazolamide. Further experiments on extraction performance were conducted. In accordance with the available biodistribution data on acetazolamide-based compounds, this model proved to be sensitive enough to satisfy the linearity range and detection limit requirements.



# Chapter 6

## Outlook

In this chapter, necessary improvements and possible future applications of the current setup are introduced and discussed.

## 6.1 Technical Improvements

### 6.1.1 Sensitivity

The sensitivity of the autosampler-ESI is lower than nano-ESI. Two phenomena can explain this. The first reason is the sample dilution during the injection into the gap and during the mixing into the main buffer flow. The second reason is the low ionization efficiency of the autosampler-ESI. The borosilicate emitter with a 3–5  $\mu\text{m}$  outlet diameter and the stainless-steel capillary with a 50  $\mu\text{m}$  outlet diameter generate different droplet sizes. One possible solution to increase the ionization efficiency is to use a curtain gas around the spray capillary. Using a curtain gas not only accelerates the solvent evaporation rate, but also induces an additional sucking effect which makes the spray formation and consequently the liquid junction more stable. A nebulizer for this purpose has already been built. It can use elevated gas temperatures (for specific applications) by utilizing a heating cartridge and a power supply. The existing nebulizer can be improved and used mainly for ligand-ranking applications where high surface tension solutions are essential.

### 6.1.2 Robustness

The robustness of an analytical instrument is one of its most important performance features. The robustness of the current setup has been increased significantly and is now much more user-friendly than that of the original CGS. Still, there is room for further improvements, such as the sample injection system. There are several drawbacks to the solid stainless-steel sampling pin, which is used for sample uptake and delivery. The volume of the sample that has been taken up by the pin depends on the physical properties of the solution such as surface tension and pin geometry. In order to increase the hanging drop volume, a pin with a larger diameter must be chosen. Using a large pin can be a limitation for a sample delivery of more than 20 nL, where the pin size is almost double of the gap size. Using “slot pin” as shown in Figure 48a, the sample volume can vary while the pin size remains the same. Also, the drop uptake mechanism is more robust than with solid pins (Figure 48b). The only challenge is the intensive cleaning procedure required to avoid sample carry-over.

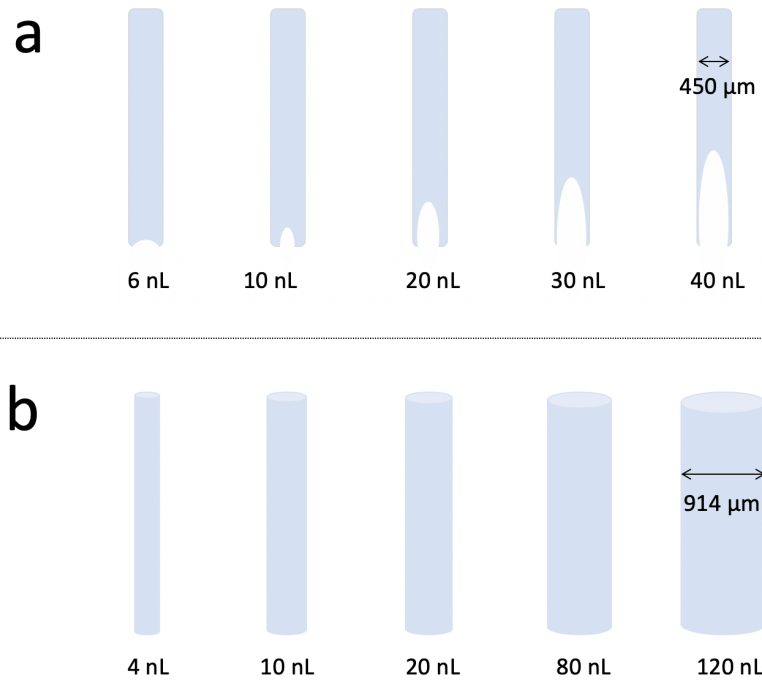


**Figure 48.** The comparison between (a) slotted hollow pins and (b) solid sampling pins.

The second drawback of the current system is the pressure shock to the hanging sample droplet and liquid connector during the sample injection step when the chamber opens. This shock is caused by the difference between the chamber and ambient pressure. When using the semi-open capillary sampler, this problem does not exist because there is less dependence on pressure fluctuations. There are two ways to overcome this issue. As shown in Figure 49, the current pressure system (Figure 49a) can be replaced by keeping the sample droplet environmental pressure constant from the well plate to the injection chamber. This idea can be implemented in two ways. The first way is to isolate the system (excluding the spray capillary outlet) and keep it at overpressure  $P_2$  (Figure 49b). This idea is interesting for the cases/in situations where high chamber overpressure is essential, such as when an experiment requires high flow rates. The second is to maintain the setup at the ambient pressure and to enclose the spray tip at the reduced pressure  $P_3$  to keep the pressure difference along the capillary for liquid sucking (Figure 49c).

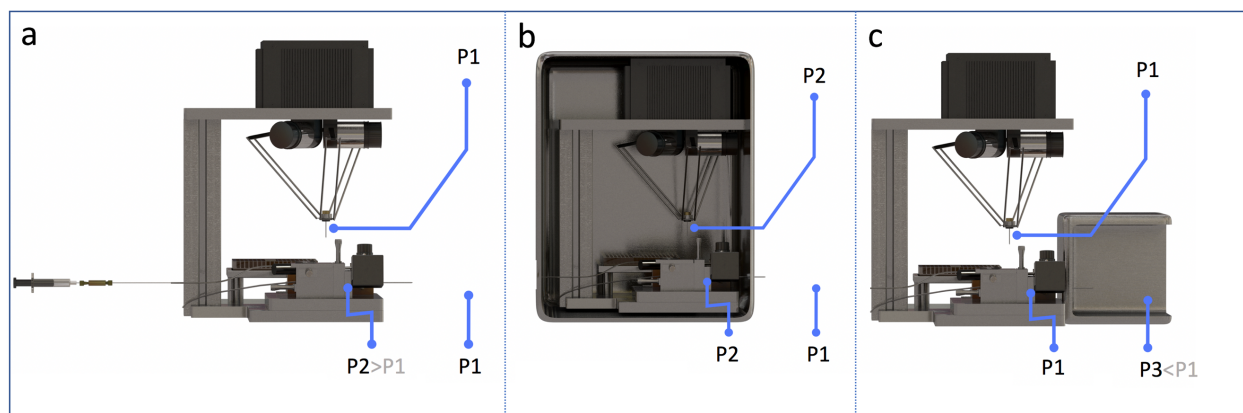


**Figure 49.** Different proposals for the system configuration, (a) the current setup where the chamber pressure  $P_2$  is higher than the ambient pressure  $P_1$ , (b) the entire system is kept under overpressure  $P_2$ , and the spray tip operates at  $P_1$ , (c) the entire system is kept at  $P_1$  and the spray tip pressure is reduced. (the idea and Figure 49 are reproduced with a few modifications from Jérôme Kaeslin).

## 6.2 Applications

### 6.2.1 Kinetic Studies

Studying the rate of transformation of reactants into products and the intermediate conformations along this path is crucial to understanding biological interactions. A crucial kinetic study pertains to the structural transformations of a protein upon denaturation. This is important due to the role of the polypeptide chains' folding patterns in defining the biological and chemical properties of a protein.<sup>164</sup> Using the semi-open capillary sampler, kinetic studies can be performed on ESI-MS compatible compounds. Having a continuous reagent line and a drop injection pin, two compounds are mixed, and the product will be detected by the MS. Adjustment of the flow rate over a broader range (in comparison to the CGS) provides a variety of sample residence times and makes it feasible to perform kinetic studies. The reagent mixing time inside the capillary can be made easier to control by defining the hole position as well as by altering the flow rate. It must be considered that the injected sample becomes diluted in the liquid bridge. I have investigated myoglobin denaturation using the CGS. Myoglobin was chosen for this study because of the different information it presents upon unfolding, including the appearance of higher-charged state conformations and the release of a heme group. This is now one of our ongoing projects.

### 6.2.2 Studying Non-covalent Interactions

One of the advantages of the semi-open capillary over the previous system is the possibility of working with high surface tension liquids such as aqueous buffers. Therefore, screening non-covalent interactions, which usually requires an aqueous media, can be easily performed using the semi-open capillary. Here, I report a discovery of a protein-ligand binding constant studied by Volker Neu, which was performed using the CGS. The studies were not continued due to the restrictions involved in using aqueous solutions. In this experiment, the lysozyme protein (4.1  $\mu\text{M}$ ) was continuously delivered via the buffer line and different concentrations of the ligand N, N', N''-triacetylchitotriose (NAG<sub>3</sub>) were infused via the sampling pin.

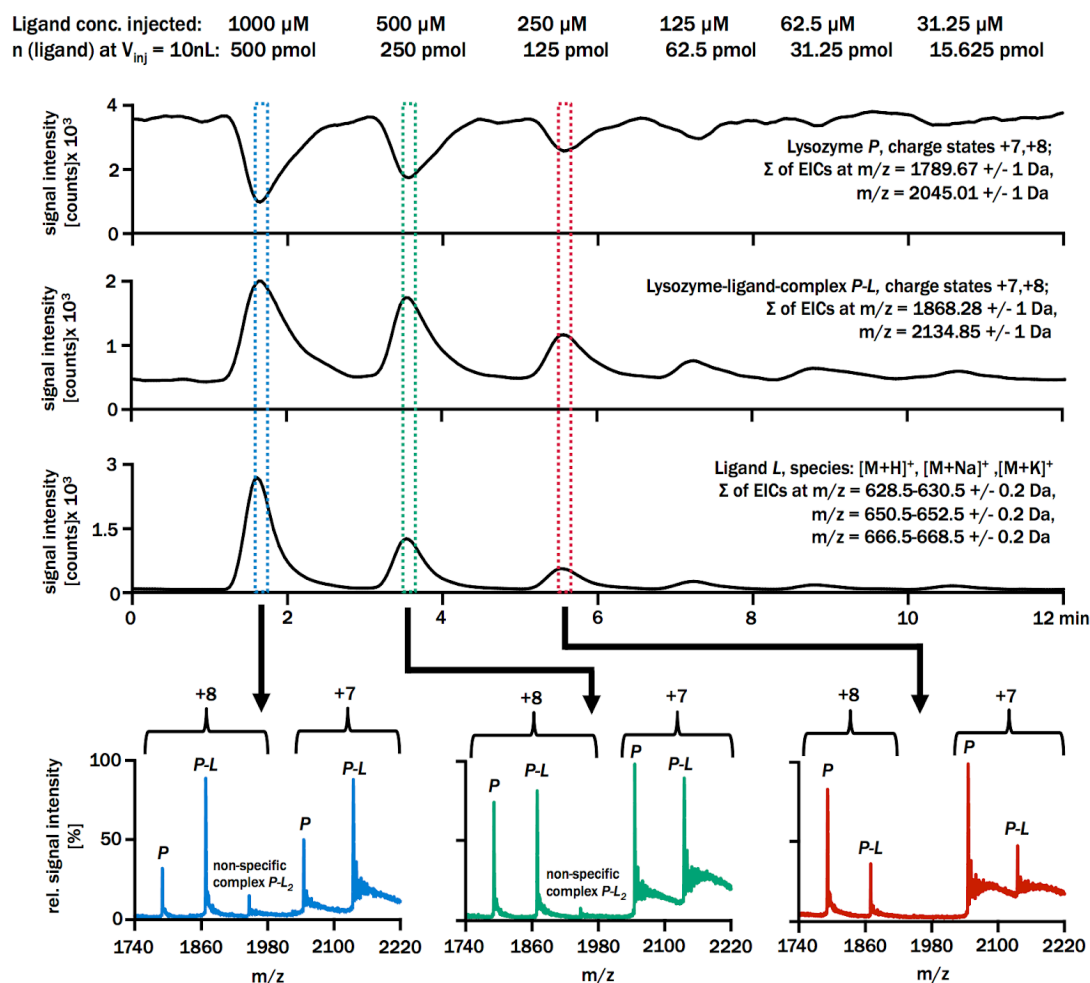


**Figure 50.** EIC of the lysozyme NAG<sub>3</sub> and the complex for different ligand concentrations and corresponding mass spectra.

The observed decrease in EIC peak area and complex-to-protein ratio is proportional to the decrease in ligand concentration. By assuming ligand concentration stays the same, the  $K_D$  was calculated and plotted against the ligand concentration in Figure 51.

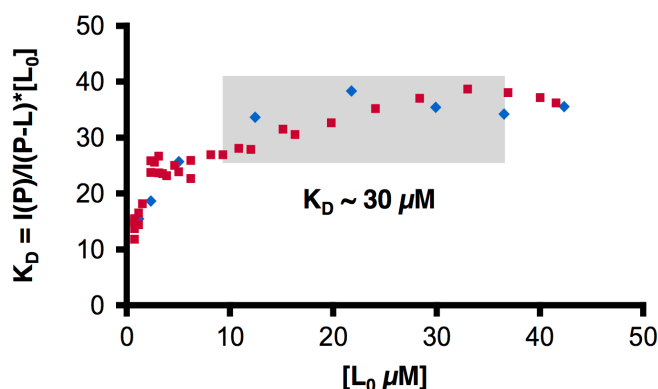


**Figure 51.** The  $K_D$  measurement plot for lysozyme – NAG<sub>3</sub> (Assumption:  $[L] \sim [L_0]$  = total ligand concentration).

The measured  $K_D$  30  $\mu\text{M}$  is comparable to the reference value of 11  $\mu\text{M}$  achieved by ITC.

### 6.2.3 Ligand Ranking

Monitoring the affinity of an extensive library of ligands to a particular protein requires a HTS method. Ligand ranking is one of the most important applications of this autosampler. A protein is continuously delivered via the syringe pump, and different ligands can be up taken from different wells by the sampling pin and diffused into the flow of the protein. Using the CGS, this study also failed due to the requirements of aqueous solutions and mixing time limitations in the spray capillary. Decreasing the flow rate in order to increase the residence time and to reach the reaction equilibrium time has limitations. On one hand, by decreasing the flow rate, the mixing time increases; and on the other hand, the peaks get broader, which reduces sensitivity. By being able to define the hole position and change the flow rate over a broader range in the semi-open capillary, both restrictions can be overcome.

### Catalyst Screening

One potential future application is catalyst screening. Two reagents can be delivered separately by two discrete syringes and can be mixed using a Y connector before they enter the liquid connector. Then a library of different catalyst candidates can be injected into the reagent mixture one by one using the sampling pin.

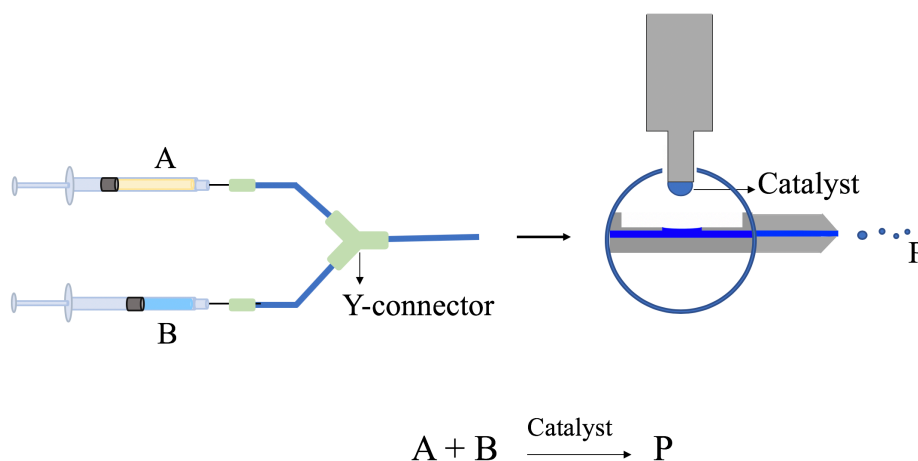


**Figure 52.** Diagram of the catalyst screening concept. Reagents A and B are mixed and form the liquid connector. A library of potential catalysts can be added via the sampling pin. The resulting product (P) will be screened by the mass spectrometer.

By observing the reaction products, one can evaluate the performance of the catalyst. There are two main limitations when performing catalyst screening using the semi-open capillary. First, the reaction solvents and reagents should be compatible with ESI-MS, and second, the reaction time should be in the range provided by the current setup. Considering that most catalysts are expensive, using the semi-open capillary and minimizing the sample usage volume reduces the cost of experiments. The two-syringe system has been already built for reaction monitoring purposes and has also been implemented into the interface software. Therefore, the setup is ready for new potential systems to be studied.

#### 6.2.4 Bioimaging

Mass spectrometry imaging (MSI) is a powerful tool in surface mapping, with applications mainly in the biological sciences and medical research.<sup>165, 168</sup> Secondary ion mass spectrometry (SIMS)-MSI and MALDI-MSI are among the most commonly used MSI techniques. TOF-SIMS is based on the bombardment of a sample by a focused ion beam. Desorption/ionization of the primary ions on the sample surface generates the secondary ions which are then analyzed by TOF-MS.<sup>169</sup> In MALDI-MSI, a laser beam irradiates the sample and generates the ions. The SIMS method has two limitations, first the generation of metal clusters coming from the ion gun and second, the undesired high fragmentation rate.

The spatial resolution of both TOF-SIMS-MSI and MALDI-MSI techniques has improved to 1–2  $\mu\text{m}$ <sup>169</sup> and 1.4  $\mu\text{m}$ <sup>170</sup> in recent years. However, both techniques non-selectively ionize the sample at the ion/laser beam irradiation spot. The semi-open capillary sampler can overcome this drawback due to its selective extraction capabilities. The unique design of the semi-open capillary sampler creates precise (3 $\mu\text{m}$ ) and fast movement of the extraction tool, which makes it potentially useful for analyzing tissue for future bioimaging applications. As an example, it can be interesting for the evaluation of targeted drug delivery performance. After a particular time from the injection of the drug, the targeted tissue can be collected, and the drug distribution can be monitored. This specific extraction approach is critical to minimize the interference from the biological sample being investigated.



---

# References

1. Ma, H. *et al.* Nanoliter homogenous ultra-high throughput screening microarray for lead discoveries and IC50 profiling. *Assay Drug Development Technology* **3**, 177–187 (2005).
2. Drug discovery market worldwide by segment 2025 forecast | Statistic. *Statista*. Available at: <https://www.statista.com/statistics/765535/drug-discovery-market-worldwide-by-segment-globally/>. (Accessed: 21st June 2018)
3. Bleicher, K. H. *et al.* Hit and lead generation: beyond high-throughput screening. *Nature Reviews of Drug Discovery* **2**, 369–378 (2003).
4. Ghiasikhou, S. *et al.* The capillary gap sampler, a new microfluidic platform for direct coupling of automated solid-phase microextraction with ESI-MS. *Analytical and Bioanalytical Chemistry* (2017).
5. Davis, A. M. *et al.* Application and Limitations of X-ray Crystallographic Data in Structure-Based Ligand and Drug Design. *Angewandte Chemie International Edition* **42**, 2718–2736 (2003).
6. Patching, S. G. Surface plasmon resonance spectroscopy for characterisation of membrane protein–ligand interactions and its potential for drug discovery. *Biochimica et Biophysica Acta (BBA) - Biomembranes* **1838**, 43–55 (2014).
7. Baranauskiene, L. *et al.* Isothermal titration calorimetry for characterization of recombinant proteins. *Current Opinion in Biotechnology* **55**, 9–15 (2019).
8. Meyer, B. & Peters, T. NMR Spectroscopy Techniques for Screening and Identifying Ligand Binding to Protein Receptors. *Angewandte Chemie International Edition* **42**, 864–890 (2003).
9. Annis, A. *et al.* ALIS: An Affinity Selection-Mass Spectrometry System for the Discovery and Characterization of Protein-Ligand Interactions. In: *Methods and Principles in Medicinal Chemistry* (eds. Wanner, K. T. & Höfner, G.) 121–156 (Wiley-VCH Verlag GmbH & Co. KGaA, 2007).
10. Qin, S. *et al.* High-throughput identification of G protein-coupled receptor modulators through affinity mass spectrometry screening. *Chemical Science* **9**, 3192–3199 (2018).
11. Ducrée, J. *et al.* The centrifugal microfluidic Bio-Disk platform. *Journal of Micromechanical Microengineering* **17**, S103 (2007).
12. Gorkin, R. *et al.* Centrifugal microfluidics for biomedical applications. *Lab on a Chip* **10**, 1758–1773 (2010).

13. Keller, M. *et al.* Automated Forensic Animal Family Identification by Nested PCR and Melt Curve Analysis on an Off-the-Shelf Thermocycler Augmented with a Centrifugal Microfluidic Disk Segment. *PLOS ONE* **10**, e0131845 (2015).
14. Neu, V. *et al.* Characterization of a miniaturized liquid bridge for nL sample infusion: a comparative study of sample flush-out behavior using flow simulations and direct ESI-MS analysis. *Microfluid Nanofluid* **20**, 62 (2016).
15. Jian, W. *et al.* Evaluation of a high-throughput online solid phase extraction-tandem mass spectrometry system for in vivo bioanalytical studies. *Analytical Chemistry*. **83**, 8259–8266 (2011).
16. Růžička, J. The second coming of flow-injection analysis. *Analytica Chimica Acta* **261**, 3–10 (1992).
17. Ohla, S. & Belder, D. Chip-based separation devices coupled to mass spectrometry. *Current Opinion in Chemical Biology* **16**, 453–459 (2012).
18. Koster, S. & Verpoorte, E. A decade of microfluidic analysis coupled with electrospray mass spectrometry: an overview. *Lab Chip* **7**, 1394–1412 (2007).
19. Oedit, A. *et al.* Lab-on-a-Chip hyphenation with mass spectrometry: strategies for bioanalytical applications. *Current Opinion in Biotechnology* **31**, 79–85 (2015).
20. Xue, Q. *et al.* Multichannel Microchip Electrospray Mass Spectrometry. *Analytical Chemistry* **69**, 426–430 (1997).
21. Bings, N. H. *et al.* Microfluidic Devices Connected to Fused-Silica Capillaries with Minimal Dead Volume. *Analytical Chemistry* **71**, 3292–3296 (1999).
22. Yin, H. *et al.* Microfluidic chip for peptide analysis with an integrated HPLC column, sample enrichment column, and nanoelectrospray tip. *Analytical Chemistry* **77**, 527–533 (2005).
23. Jin, D.-Q. *et al.* Swan probe: A nanoliter-scale and high-throughput sampling interface for coupling electrospray ionization mass spectrometry with microfluidic droplet array and multiwell plate. *Analytical Chemistry* **86**, 10796–10803 (2014).
24. Zhang, S. & Pelt, C. K. V. Chip-based nanoelectrospray mass spectrometry for protein characterization. *Expert Review of Proteomics* **1**, 449–468 (2004).
25. Constans, A. Better mass spec results off-line: Advion BioSciences' NanoMate 100 speeds up ESI-based mass spectrometry. (Tools & Technology). *The Scientist* (2003). Available at: <http://link.galegroup.com/apps/doc/A100046326/AONE?sid=googlescholar>. (Accessed: 4th May 2019)
26. Neu, V. *et al.* Development and Characterization of a Capillary Gap Sampler as New Microfluidic Device for Fast and Direct Analysis of Low Sample Amounts by ESI-MS. *Analytical Chemistry* **85**, 4628–4635 (2013).

27. Ghiasikhou, S. *et al.* A comparative study between a miniaturized liquid junction built in a capillary gap and semi-open capillaries for nL sample infusion to mass spectrometry. *Microfluid Nanofluid* **23**, 60 (2019).
28. Arthur, C. & Pawliszyn, J. Solid-phase microextraction with thermal-desorption using fused-silica optical fibers. *Analytical Chemistry* **62**, 2145–2148 (1990).
29. Pawliszyn, J. *Handbook of Solid Phase Microextraction*. (Elsevier, 2011).
30. Krall, N. *et al.* Small targeted cytotoxics: current state and promises from DNA-encoded chemical libraries. *Angewandte Chemie International Edition English* **52**, 1384–1402 (2013).
31. Srinivasarao, M. *et al.* Principles in the design of ligand-targeted cancer therapeutics and imaging agents. *Nature Reviews Drug Discovery* **14**, 203–219 (2015).
32. van der Veldt, A. A. *et al.* Biodistribution and radiation dosimetry of  $^{11}\text{C}$ -labelled docetaxel in cancer patients. *European Journal of Nuclear Medicine and Molecular Imaging* **37**, 1950–1958 (2010).
33. van der Veldt, A. A. *et al.* Towards prediction of efficacy of chemotherapy: a proof of concept study in lung cancer patients using  $^{11}\text{C}$ docetaxel and positron emission tomography. *Clinical Cancer Research* clincanres.3779.2012 (2013).
34. Aksenov, A. A. *et al.* Global chemical analysis of biology by mass spectrometry. *Nature Reviews Chemistry* **1**, 0054 (2017).
35. Wood, M. *et al.* Recent applications of liquid chromatography-mass spectrometry in forensic science. *Journal of Chromatography A* **1130**, 3–15 (2006).
36. Ojanperä, I. *et al.* Current use of high-resolution mass spectrometry in drug screening relevant to clinical and forensic toxicology and doping control. *Analytical and Bioanalytical Chemistry* **403**, 1203–1220 (2012).
37. Peters, R. J. B. *et al.* Screening in veterinary drug analysis and sports doping control based on full-scan, accurate-mass spectrometry. *Trends in Analytical Chemistry* **29**, 1250–1268 (2010).
38. Gan, H.-H. *et al.* Atmospheric pressure chemical ionisation mass spectrometry analysis linked with chemometrics for food classification - a case study: geographical provenance and cultivar classification of monovarietal clarified apple juices. *Food Chemistry* **146**, 149–156 (2014).
39. Vaclavik, L. *et al.* Liquid chromatography–mass spectrometry-based metabolomics for authenticity assessment of fruit juices. *Metabolomics* **8**, 793–803 (2012).
40. Hopfgartner, G. *et al.* High-resolution mass spectrometry for integrated qualitative and quantitative analysis of pharmaceuticals in biological matrices. *Analytical and Bioanalytical Chemistry* **402**, 2587–2596 (2012).
41. Persike, M. & Karas, M. Rapid simultaneous quantitative determination of different small pharmaceutical drugs using a conventional matrix-assisted laser desorption/ionization time-of-flight mass spectrometry system. *Rapid Communication in Mass Spectrometry* **23**, 3555–3562 (2009).

42. Gross, J. H. *Mass Spectrometry: A Textbook*. (Springer-Verlag, 2011).
43. Detection limit. *Wikipedia*,  
Available at: [http://en.wikipedia.org/wiki/Detection\\_limit](http://en.wikipedia.org/wiki/Detection_limit) (Accessed: 18th April 2019).
44. Wu, A. H. *et al.* Role of liquid chromatography-high-resolution mass spectrometry (LC-HR/MS) in clinical toxicology. *Clinical Toxicology (Philadelphia)* **50**, 733–742 (2012).
45. Schermann, J.-P. Low-Energy Electron–Molecule Interactions. *Spectroscopy and Modeling of Biomolecular Building Blocks*, 351–372 (2008).
46. Aiken, A. C. *et al.* Elemental Analysis of Organic Species with Electron Ionization High-Resolution Mass Spectrometry. *Analytical Chemistry* **79**, 8350–8358 (2007).
47. Barber, M. *et al.* Fast atom bombardment mass spectrometry. *Analytical Chemistry* **54**, 645A–657A (1982).
48. Harrison, A. G. *Chemical Ionization Mass Spectrometry*. (Routledge, 2018).
49. Fenn, J. B. *et al.* Electrospray ionization for mass spectrometry of large biomolecules. *Science* **246**, 64–71 (1989).
50. Mann, M. *et al.* Interpreting mass spectra of multiply charged ions. *Analytical Chemistry* **61**, 1702–1708 (1989).
51. Molecular Imaging of Biological Samples: Localization of Peptides and Proteins Using MALDI-TOF MS. *Analytical Chemistry* **69**, 4751–4760 (1997).
52. Karas, M. *et al.* Matrix-assisted ultraviolet laser desorption of non-volatile compounds. *International Journal of Mass Spectrometry and Ion Processes* **78**, 53–68 (1987).
53. Karas, Michael. & Hillenkamp, Franz. Laser desorption ionization of proteins with molecular masses exceeding 10,000 daltons. *Analytical Chemistry* **60**, 2299–2301 (1988).
54. Horning, E. C. *et al.* New picogram detection system based on a mass spectrometer with an external ionization source at atmospheric pressure. *Analytical Chemistry* **45**, 936–943 (1973).
55. Carroll, D. I. *et al.* Atmospheric pressure ionization mass spectrometry. Corona discharge ion source for use in a liquid chromatograph-mass spectrometer-computer analytical system. *Analytical Chemistry* **47**, 2369–2373 (1975).
56. Robb, D. B. *et al.* Atmospheric Pressure Photoionization: An Ionization Method for Liquid Chromatography–Mass Spectrometry. *Analytical Chemistry* **72**, 3653–3659 (2000).
57. Yamashita, M. & Fenn, J. B. Electrospray ion source. Another variation on the free-jet theme. *Journal of Physical Chemistry* **88**, 4451–4459 (1984).
58. Karas, Michael *et al.* Influence of the wavelength in high-irradiance ultraviolet laser desorption mass spectrometry of organic molecules. *Analytical Chemistry* **57**, 2935–2939 (1985).
59. Tanaka, K. *et al.* Protein and polymer analyses up to  $m/z$  100 000 by laser ionization time-of-flight mass spectrometry. *Rapid Communications in Mass Spectrometry* **2**, 151–153 (1988).

- 
60. Mass Spectrometry in Drug Discovery. *CRC Press*  
Available at: <https://www.crcpress.com/Mass-Spectrometry-in-Drug-Discovery/Rossi-Sinz/p/book/9780824706074>. (Accessed: 24th October 2018)
  61. Schalley, Christoph A (Ed.). *Modern Mass Spectrometry*. (Springer-Verlag, 2003).
  62. Siuzdak, G. *The Expanding Role of Mass Spectrometry in Biotechnology, Second Edition*. (MCC Press, 2006).
  63. Electrospray ionization. *Wikipedia*. Available at:  
[http://en.wikipedia.org/wiki/Electrospray\\_ionization](http://en.wikipedia.org/wiki/Electrospray_ionization) (Accessed: 18th April 2019).
  64. Iribarne, J. V. & Thomson, B. A. On the evaporation of small ions from charged droplets. *Journal of Chemical Physics* **64**, 2287–2294 (1976).
  65. Dole, M. *et al.* Molecular Beams of Macroions. *Journal of Chemical Physics* **49**, 2240–2249 (1968).
  66. Nguyen, S. & Fenn, J. B. Gas-phase ions of solute species from charged droplets of solutions. *Proceedings of the National Academy of Sciences USA* **104**, 1111–1117 (2007).
  67. Konermann, L. *et al.* Unraveling the Mechanism of Electrospray Ionization. *Analytical Chemistry* **85**, 2–9 (2013).
  68. Anonymous. Proceedings of the American Physical Society. *Physical Review* **69**, 674–674 (1946).
  69. Waters. Waters SYNAPT G2-S High Definition Mass Spectrometry System, Operator Overview and Maintenance Guide. (2011).
  70. Sun, S. & Kennedy, R. T. Droplet Electrospray Ionization Mass Spectrometry for High Throughput Screening for Enzyme Inhibitors. *Analytical Chemistry* **86**, 9309–9314 (2014).
  71. Chen, H. *et al.* Desorption Electrospray Ionization Mass Spectrometry for High-Throughput Analysis of Pharmaceutical Samples in the Ambient Environment. *Analytical Chemistry* **77**, 6915–6927 (2005).
  72. Chen, Q. *et al.* Qualitative and Quantitative Analysis of Tumor Cell Metabolism via Stable Isotope Labeling Assisted Microfluidic Chip Electrospray Ionization Mass Spectrometry. *Analytical Chemistry* **84**, 1695–1701 (2012).
  73. Mao, S. *et al.* Strategy for Signaling Molecule Detection by Using an Integrated Microfluidic Device Coupled with Mass Spectrometry to Study Cell-to-Cell Communication. *Analytical Chemistry* **85**, 868–876 (2013).
  74. van Reenen, A. *et al.* Integrated lab-on-chip biosensing systems based on magnetic particle actuation – a comprehensive review. *Lab on a Chip* **14**, 1966–1986 (2014).
  75. Strohmeier, O. *et al.* Automated nucleic acid extraction from whole blood, *B. subtilis*, *E. coli*, and Rift Valley fever virus on a centrifugal microfluidic LabDisk. *The Royal Society of Chemistry Advances* **5**, 32144–32150 (2015).

76. Sreekumar, A. *et al.* Metabolomic profiles delineate potential role for sarcosine in prostate cancer progression. *Nature* **457**, 910–914 (2009).
77. Fiehn, O. *et al.* Metabolite profiling for plant functional genomics. *Nature Biotechnology* **18**, 1157–1161 (2000).
78. Chen, Y. G. *et al.* LC/MS analysis of cellular RNA reveals NAD-linked RNA. *Nature Chemical Biology* **5**, 879–881 (2009).
79. Stark, T. *et al.* Quantitation of Resveratrol in Red Wines by Means of Stable Isotope Dilution Analysis–Ultra-Performance Liquid Chromatography–Quan-Time-of-Flight Mass Spectrometry and Cross Validation. *Analytical Chemistry* **83**, 3398–3405 (2011).
80. Wan, H. *et al.* High-throughput screening of pKa values of pharmaceuticals by pressure-assisted capillary electrophoresis and mass spectrometry. *Rapid Communications in Mass Spectrometry* **17**, 2639–2648 (2003).
81. Chu, Y.-H. *et al.* Affinity Capillary Electrophoresis–Mass Spectrometry for Screening Combinatorial Libraries. *Journal of the American Chemical Society*. **118**, 7827–7835 (1996).
82. Ozbal, C. C. *et al.* High throughput screening via mass spectrometry: a case study using acetylcholinesterase. *ASSAY and Drug Development Technologies* **2**, 373–381 (2004).
83. Chen, Q. *et al.* Qualitative and Quantitative Analysis of Tumor Cell Metabolism via Stable Isotope Labeling Assisted Microfluidic Chip Electrospray Ionization Mass Spectrometry. *Analytical Chemistry* **84**, 1695–1701 (2012).
84. Laser ablation. *Wikipedia*,  
Available at: [https://en.wikipedia.org/wiki/Laser\\_ablation](https://en.wikipedia.org/wiki/Laser_ablation) (Accessed: 28th June 2019).
85. IDS Machining. How Sinker EDM Machining Works.  
Available at: [http://www.edmmachining.com/sinker\\_edm.htm](http://www.edmmachining.com/sinker_edm.htm). (Accessed: 28th June 2018)
86. Rodenstein, M. *et al.* Fabricating Chemical Gradients on Oxide Surfaces by Means of Fluorinated, Catechol-Based, Self-Assembled Monolayers. *Langmuir* **26**, 16211–16220 (2010).
87. Wohlfarth, C. *Surface Tension of Pure Liquids and Binary Liquid Mixtures: (Supplement to IV/16)*. (Springer-Verlag, 2008).
88. Theodoridis, G. *et al.* Solid-phase microextraction for the analysis of biological samples. *Journal of Chromatography B-Analytical Technologies in the Biomedical and Life Sciences* **745**, 49–82 (2000).
89. Ulrich, S. Solid-phase microextraction in biomedical analysis. *Journal of Chromatography A* **902**, 167–194 (2000).
90. Snow, N. H. Solid-phase micro-extraction of drugs from biological matrices. *Journal of Chromatography A* **885**, 445–455 (2000).

91. Sides, S. L. *et al.* Identification of a pharmaceutical packaging off-odor using solid phase microextraction gas chromatography/mass spectrometry. *Journal of Pharmaceutical and Biomedical Analysis* **25**, 379–386 (2001).
92. Teitz, D. S. *et al.* An automated method of sample preparation of biofluids using pierceable caps to eliminate the uncapping of the sample tubes during sample transfer. *Journal of Biochemical and Biophysical Methods* **45**, 193–204 (2000).
93. Jemal, M. *et al.* Comparison of plasma sample purification by manual liquid-liquid extraction, automated 96-well liquid-liquid extraction and automated 96-well solid-phase extraction for analysis by highperformance liquid chromatography with tandem mass spectrometry. *Journal of Chromatography B* **732**, 501–508 (1999).
94. Mitani, K. *et al.* Fully automated analysis of estrogens in environmental waters by in-tube solid-phase microextraction coupled with liquid chromatography-tandem mass spectrometry. *Journal of Chromatography A* **1081**, 218–224 (2005).
95. Tong, X. C. S. *et al.* High-throughput pharmacokinetics screen of VLA-4 antagonists by LC/MS/MS coupled with automated solid-phase extraction sample preparation. *Journal of Pharmaceutical and Biomedical Analysis* **35**, 867–877 (2004).
96. Lord, H. L. *et al.* Development and evaluation of a solid-phase microextraction probe for in vivo pharmacokinetic studies. *Analytical Chemistry* **75**, 5103–5115 (2003).
97. Rule, G. *et al.* A 384-well solid-phase extraction for LC/MS/MS determination of methotrexate and its 7-hydroxy metabolite in human urine and plasma. *Analytical Chemistry* **73**, 439–443 (2001).
98. Rule, G. & Henion, J. High-throughput sample preparation and analysis using 96-well membrane solid-phase extraction and liquid chromatography-tandem mass spectrometry for the determination of steroids in human urine. *Journal of the American Society for Mass Spectrometry* **10**, 1322–1327 (1999).
99. Kaye, B. *et al.* Rapid, solid phase extraction technique for the high-throughput assay of darifenacin in human plasma. *Analytical Chemistry* **68**, 1658–1660 (1996).
100. Hutchinson, J. P. *et al.* Automation of solid-phase microextraction on a 96-well plate format. *Journal of Chromatography A* **1149**, 127–137 (2007).
101. Roddy, T. P. *et al.* Mass spectrometric techniques for label-free high-throughput screening in drug discovery. *Analytical Chemistry* **79**, 8207–8213 (2007).
102. Biddlecombe, R. A. *et al.* A clinical trial on a plate? The potential of 384-well format solid phase extraction for high-throughput bioanalysis using liquid chromatography/tandem mass spectrometry. *Rapid Communications in Mass Spectrometry* **15**, 33–40 (2001).
103. Vatinno, R. *et al.* Automated high-throughput method using solid-phase microextraction-liquid chromatography-tandem mass spectrometry for the determination of ochratoxin A in human urine. *Journal of Chromatography A* **1201**, 215–221 (2008).

104. Cudjoe, E. *et al.* Investigation of the Effect of the Extraction Phase Geometry on the Performance of Automated Solid-Phase Microextraction. *Analytical Chemistry* **81**, 4226–4232 (2009).
105. Cudjoe, E. & Pawliszyn, J. A new approach to the application of solid phase extraction disks with LC-MS/MS for the analysis of drugs on a 96-well plate format. *Journal of Pharmaceutical and Biomedical Analysis* **50**, 556–562 (2009).
106. Vuckovic, D. *et al.* Automation of solid-phase microextraction in high-throughput format and applications to drug analysis. *Analytical Chemistry* **80**, 6870–6880 (2008).
107. Deng, J. *et al.* Strategies for coupling solid-phase microextraction with mass spectrometry. *Trac-Trends in Analytical Chemistry* **55**, 55–67 (2014).
108. Marsili, R. T. SPME-MS-MVA as an electronic nose for the study of off-flavors in milk. *Journal of Agricultural and Food Chemistry* **47**, 648–654 (1999).
109. Peres, C. *et al.* Solid-phase microextraction spectrometry: A new approach to the rapid characterization of cheeses. *Analytical Chemistry* **73**, 1030–1036 (2001).
110. Moder, M. *et al.* Determination of urinary acylcarnitines by ESI-MS coupled with solid-phase microextraction (SPME). *Journal of Mass Spectrometry* **32**, 1195–1204 (1997).
111. Ceglarek, U. *et al.* Determination of linear alkylbenzenesulfonates in communal wastewater by means of solid phase microextraction coupled with API-MS and HPLC-FLD. *Fresenius Journal of Analytical Chemistry* **365**, 674–681 (1999).
112. McCooeye, M. A. *et al.* Quantitation of amphetamine, methamphetamine, and their methylenedioxy derivatives in urine by solid-phase microextraction coupled with electrospray ionization-high-field asymmetric waveform ion mobility spectrometry-mass spectrometry. *Analytical Chemistry* **74**, 3071–3075 (2002).
113. van Hout, M. W. J. *et al.* Non-equilibrium solid-phase microextraction coupled directly to ion-trap mass spectrometry for rapid analysis of biological samples. *Analyst* **127**, 355–359 (2002).
114. van Hout, M. W. J. *et al.* Ultra-rapid non-equilibrium solid-phase microextraction at elevated temperatures and direct coupling to mass spectrometry for the analysis of lidocaine in urine. *Journal of Separation Science* **26**, 1563–1568 (2003).
115. Mirabelli, M. F. *et al.* Direct Coupling of Solid-Phase Microextraction with Mass Spectrometry: Sub-pg/g Sensitivity Achieved Using a Dielectric Barrier Discharge Ionization Source. *Analytical Chemistry* **88**, 7252–7258 (2016).
116. Mirnaghi, F. S. & Pawliszyn, J. Reusable Solid-Phase Microextraction Coating for Direct Immersion Whole-Blood Analysis and Extracted Blood Spot Sampling Coupled with Liquid Chromatography-Tandem Mass Spectrometry and Direct Analysis in Real-Time Tandem Mass Spectrometry. *Analytical Chemistry* **84**, 8301–8309 (2012).



117. Mirnaghi, F. S. *et al.* Optimization of the Coating Procedure for a High-Throughput 96-Blade Solid Phase Microextraction System Coupled with LC-MS/MS for Analysis of Complex Samples. *Analytical Chemistry* **83**, 6018–6025 (2011).
118. Lavaud, S. *et al.* Optimal anticoagulation strategy in haemodialysis with heparin-coated polyacrylonitrile membrane. *Nephrology Dialysis Transplantation* **18**, 2097–2104 (2003).
119. Nie, F. Q. *et al.* Preparation and characterization of polyacrylonitrile-based membranes: Effects of internal coagulant on poly(acrylonitrile-co-maleic acid) ultrafiltration hollow fiber membranes. *Desalination* **160**, 43–50 (2004).
120. Mullett, W. M. & Pawliszyn, J. The development of selective and biocompatible coatings for solid phase microextraction. *Journal of Separation Science* **26**, 251–260 (2003).
121. Alam, M. N. *et al.* Numerical Modeling of Solid-Phase Microextraction: Binding Matrix Effect on Equilibrium Time. *Analytical Chemistry* **87**, 9846–9854 (2015).
122. Pawliszyn, J. Sample preparation: Quo Vadis? *Analytical Chemistry* **75**, 2543–2558 (2003).
123. Mulder, J. *Basic Principles of Membrane Technology*. (Springer Netherlands, 1996).
124. Zhang, Z. *et al.* Direct solid phase microextraction of complex aqueous samples with hollow fibre membrane protection. *Analytical Communications* **33**, 219–221 (1996).
125. Rasmussen, K. E. *et al.* Development of a simple in-vial liquid-phase microextraction device for drug analysis compatible with capillary gas chromatography, capillary electrophoresis and high-performance liquid chromatography. *Journal of Chromatography A* **873**, 3–11 (2000).
126. Boos, K. S. & Grimm, C. H. High-performance liquid chromatography integrated solid-phase extraction in bioanalysis using restricted access precolumn packings. *Trac-Trends in Analytical Chemistry* **18**, 175–180 (1999).
127. Stead, A. & Moffat, A. A Collection of therapeutic, toxic and fatal blood drug concentrations. *Human Toxicology* **2**, 437–464 (1983).
128. Brown, S. Clarke's Isolation and Identification of Drugs. *J Clin Pathol* **39**, 1368 (1986).
129. Winek, C. L. *et al.* Drug and chemical blood-level data 2001. *Forensic Science International* **122**, 107–123 (2001).
130. Schulz, M. & Schmoldt, A. Therapeutic and toxic blood concentrations of more than 500 drugs. *Pharmazie* **52**, 895–911 (1997).
131. Repetto, M. R. & Repetto, M. Habitual, toxic, and lethal concentrations of 103 drugs of abuse in humans. *Journal of Toxicology-Clinical Toxicology* **35**, 1–9 (1997).
132. Jones, A. W. *et al.* High concentrations of diazepam and nordiazepam in blood of impaired drivers: association with age, gender and spectrum of other drugs present. *Forensic Science International* **146**, 1–7 (2004).

133. van der Meel, R. *et al.* Ligand-targeted Particulate Nanomedicines Undergoing Clinical Evaluation: Current Status. in *Intracellular Delivery III: Market Entry Barriers of Nanomedicines* (eds. Prokop, A. & Weissig, V.) 163–200 (Springer International Publishing, 2016).
134. Chari, R.V. *et al.* Antibody–Drug Conjugates: An Emerging Concept in Cancer Therapy. *Angewandte Chemie International Edition English*, **53**, 3796–3827 (2014).
135. Wang, A. Z. & Farokhzad, O. C. Current Progress of Aptamer-Based Molecular Imaging. *Journal of Nuclear Medicine* **55**, 353–356 (2014).
136. Zhang, X. *et al.* A cell-based single-stranded DNA aptamer specifically targets gastric cancer. *The International Journal of Biochemistry & Cell Biology* **46**, 1–8 (2014).
137. Yu, B. *et al.* Receptor-targeted nanocarriers for therapeutic delivery to cancer. *Molecular Membrane Biology* **27**, 286–298 (2010).
138. Kurzrock, R. *et al.* Safety, Pharmacokinetics, and Activity of GRN1005, a Novel Conjugate of Angiopep-2, a Peptide Facilitating Brain Penetration, and Paclitaxel, in Patients with Advanced Solid Tumors. *Molecular Cancer Therapy* **11**, 308–316 (2012).
139. Zhang, X.-X. *et al.* Peptides in cancer nanomedicine: Drug carriers, targeting ligands and protease substrates. *Journal of Controlled Release* **159**, 2–13 (2012).
140. Rana, S. *et al.* Screening of a Novel Peptide Targeting the Proteoglycan-Like Region of Human Carbonic Anhydrase IX. *Molecular Imaging* **12**, 7290.2013.00066 (2013).
141. McGuire, M. J. *et al.* Identification and Characterization of a Suite of Tumor Targeting Peptides for Non-Small Cell Lung Cancer. *Scientific Reports* **4**, 4480 (2014).
142. Xia, W. *et al.* Folate-Targeted Therapies for Cancer. *Journal of Medical Chemistry* **53**, 6811–6824 (2010).
143. Varghese, B. *et al.* Folate Receptor- $\beta$  in Activated Macrophages: Ligand Binding and Receptor Recycling Kinetics. *Molecular Pharmaceutics* **11**, 3609–3616 (2014).
144. Thomas, M. *et al.* Ligand-Targeted Delivery of Small Interfering RNAs to Malignant Cells and Tissues. *Annals of the New York Academy of Sciences* **1175**, 32–39 (2009).
145. Shen, J. *et al.* Use of Folate-Conjugated Imaging Agents To Target Alternatively Activated Macrophages in a Murine Model of Asthma. *Molecular Pharmaceutics* **10**, 1918–1927 (2013).
146. Dennis, M. S. *et al.* Imaging tumors with an albumin-binding Fab, a novel tumor-targeting agent. *Cancer Research* **67**, 254–261 (2007).
147. Borsi, L. *et al.* Selective targeting of tumoral vasculature: comparison of different formats of an antibody (L19) to the ED-B domain of fibronectin. *International Journal of Cancer* **102**, 75–85 (2002).

148. Adem, Y. T. *et al.* Auristatin Antibody Drug Conjugate Physical Instability and the Role of Drug Payload. *Bioconjugate Chemistry* **25**, 656–664 (2014).
149. Liu, X. *et al.* Enhanced immune response induced by a potential influenza A vaccine based on branched M2e polypeptides linked to tuftsin. *Vaccine* **30**, 6527–6533 (2012).
150. Jeannin, P. *et al.* Immunogenicity and antigenicity of synthetic peptides derived from the mite allergen Der p I. *Molecular Immunology* **30**, 1511–1518 (1993).
151. Low, P. S. *et al.* Discovery and Development of Folic-Acid-Based Receptor Targeting for Imaging and Therapy of Cancer and Inflammatory Diseases. *Accounts of Chemical Research* **41**, 120–129 (2008).
152. Hillier, S. M. *et al.* <sup>99m</sup>Tc-labeled small-molecule inhibitors of prostate-specific membrane antigen for molecular imaging of prostate cancer. *Journal of Nuclear Medicine* **54**, 1369–1376 (2013).
153. Ginj, M. *et al.* Radiolabeled somatostatin receptor antagonists are preferable to agonists for in vivo peptide receptor targeting of tumors. *Proceedings of the National Academy of Sciences USA*. **103**, 16436–16441 (2006).
154. Krall, N. *et al.* A Small-Molecule Drug Conjugate for the Treatment of Carbonic Anhydrase IX Expressing Tumors. *Angewandte Chemie International Edition* **53**, 4231–4235 (2014).
155. Cazzamalli, S. *et al.* Chemically Defined Antibody– and Small Molecule–Drug Conjugates for in Vivo Tumor Targeting Applications: A Comparative Analysis. *Journal of the American Chemical Society* **140**, 1617–1621 (2018).
156. Cazzamalli, S. *et al.* Acetazolamide Serves as Selective Delivery Vehicle for Dipeptide-Linked Drugs to Renal Cell Carcinoma. *Molecular Cancer Therapeutics* **15**, 2926–2935 (2016).
157. Gasymov, O. K. & Glasgow, B. J. ANS Fluorescence: Potential to Augment the Identification of the External Binding Sites of Proteins. *Biochimica et Biophysica Acta* **1774**, 403–411 (2007).
158. Friess, S. D. & Zenobi, R. Protein structure information from mass spectrometry? Selective titration of arginine residues by sulfonates. *Journal of the American Society for Mass Spectrometry* **12**, 810–818 (2001).
159. Slavík, J. Anilinonaphthalene sulfonate as a probe of membrane composition and function. *Biochimica et Biophysica Acta* **694**, 1–25 (1982).
160. Almstedt, K. *et al.* Unfolding a folding disease: folding, misfolding and aggregation of the marble brain syndrome-associated mutant H107Y of human carbonic anhydrase II. *Journal of Molecular Biology* **342**, 619–633 (2004).
161. Motlagh, S. & Pawliszyn, J. On-line monitoring of flowing samples using solid phase microextraction-gas chromatography. *Analytica Chimica Acta* **284**, 265–273 (1993).

## References

---

162. Górecki, T. *et al.* Theory of analyte extraction by selected porous polymer SPME fibres†. *Analyst* **124**, 643–649 (1999).
163. Chapron, D. J. *et al.* Acetazolamide blood concentrations are excessive in the elderly: propensity for acidosis and relationship to renal function. *Journal of Clinical Pharmacology* **29**, 348–353 (1989).
164. Simpson, R. B. & Kauzmann, W. The Kinetics of Protein Denaturation. I. The Behavior of the Optical Rotation of Ovalbumin in Urea Solutions1. *Journal of the American Chemical Society* **75**, 5139–5152 (1953).
165. Schober, Y. *et al.* High-resolution matrix-assisted laser desorption/ionization imaging of tryptic peptides from tissue. *Rapid Communications in Mass Spectrometry* **26**, 1141–1146 (2012).
166. Brignole-Baudouin, F. *et al.* A new safety concern for glaucoma treatment demonstrated by mass spectrometry imaging of benzalkonium chloride distribution in the eye, an experimental study in rabbits. *PLOS ONE* **7**, e50180 (2012).
167. Brulet, M. *et al.* Lipid mapping of colonic mucosa by cluster TOF-SIMS imaging and multivariate analysis in cfr knockout mice. *Journal of Lipid Research*. **51**, 3034–3045 (2010).
168. Schober, Y. *et al.* Single cell matrix-assisted laser desorption/ionization mass spectrometry imaging. *Analytical Chemistry* **84**, 6293–6297 (2012).
169. Desbenoit, N. *et al.* Correlative mass spectrometry imaging, applying time-of-flight secondary ion mass spectrometry and atmospheric pressure matrix-assisted laser desorption/ionization to a single tissue section. *Rapid Communication in Mass Spectrometry* **32**, 159–166 (2018).
170. Kompauer, M. *et al.* Atmospheric pressure MALDI mass spectrometry imaging of tissues and cells at 1.4- $\mu\text{m}$  lateral resolution. *Nature Methods* **14**, 90–96 (2017).

This page intentionally left blank.

# Appendix A

## Standard Operating Procedure

The information of the following chapter has been gathered and written by the author of the thesis and other researchers and engineers (Volker Neu, Roger Steiner, Yin Zhu, Marcos Fabricio da Silva) who were previously involved in the development of the CGS.

## A.1 Introduction and Content

This picture-guided manual aims for the detailed description of the installation and usage of the CGS as a prototype. It is the basis for bringing the sampler to appropriate working conditions and should be seen as a “living document” which is steadily completed with appearing know-how.

## A.2 Materials

**Table A 1.** List of required tubing and spare parts.

Quantity	Description	Ordering information	
		Supplier	Part No.
variable	Tubing fused silica deactivated; 360 µm O.D. x 220 µm I.D. or	VWR	SGEA0624478
	Tubing fused silica; 360 µm O.D. × 200 µm I.D.	BGB	TSP-200350
variable	Tubing fused Silica; 360 µm O.D. × 50 µm I.D. or	IDEX	43024980
	Tubing fused Silica deactivated; 360 µm O.D. × 50 µm I.D.	VWR	SGEA06244503
variable	Tubing fused silica with thick-layer of Teflon coating. 360 µm O.D. × 50 µm I.D.	BGB	TSH-050375
variable	Tubing polyurethane 6 mm OD × 4 mm ID, black	SMC	TU-0604 (.L.AL2)
variable	Tubing polyurethane 6 mm OD × 4 mm ID, green	SMC	TU-0604 (GYP.3)
variable	Tubing polyurethane 4 mm OD × 2.5 mm ID, black	SMC	TU-0425 (.K.WE)
variable	Silicone Tubing; 4.65 mm O.D.; 3.35 mm I.D.	SEDAT	601335
variable	Teflon line TFE, 1.58 mm O.D., 0.5 mm	Supelco	58697-U
10 ft	Tubing PTFE, 10 ft × 1/16 in. × 0.031 in.	Sigma	58700-U SUPELCO
2	Dual connection nipple (4 mm O.D)	SMC	KQ2N04-99
2	Dual connection nipple (6 mm O.D)	SMC	KQ2N06-99

1	Reduction nipple (6 to 4 mm)	SMC	KQ2N04-06
2	Y-connection piece	SMC	KQ2U06-00
1	Vacuum generator	SMC	ZH 05B
5	Pressure line reduction units (6mm I.D to 1/4-28)	Roche Intern	
1	Compartments (each):	SMC	KQ2H06-M5
1	Hexagon socket head male connector	Ercatech AG	P-624
	Syringe adapter F Luer to 1/4-28 FB, M		
1	Pressure line reduction units (4mm I.D to 1/4-28)	Roche Intern	
1	Compartments:	SMC	KQ2H04-M5
1	Hexagon socket head male connector	Ercatech AG	P-624
	Syringe adapter F Luer to 1/4-28 FB, M		
2	Choke valve	SMC	A51211F-M3-04
1	3-Port bottlecap with hand valves	Bola	F-746-10
1	2-Port bottlecap	Bola	F-746-02
3	Duran Glass bottles 250 mL	Schott	
1	Duran Glass bottle 100 mL	Schott	
1	Duran Glass bottle 500 mL	Schott	
3	1/16" conic nut (incl. 1× special hexagon headed nut modified by Roche)	BGB	VV-ZN1FPK-10
3	Double grip ferrule, 1/16", PEEK	BGB	VV-ZGF1PK-10
2	PEEK Fingertight, natural, 10-32	BGB	200916
4	Sleeve FEP Green 1/16 × .0155 (395um I.D.)**	BGB	F-262X
1	F Luer to 10-32 C	Ercatech AG	P-659
2	Fingertight Fitting for 1/16" OD Tubing, long	Ercatech AG	F-130x



Appendix A

9	Flangeless Fitting for 1/16" tubing, PEEK natural, short	Ercatech AG	XP-235x
2	Flangeless Fitting for 1/16" tubing, PEEK natural, std.	Ercatech AG	XP-230x
2	Flangeless Fitting for 1/8" tubing, PEEK natural, std.	Ercatech AG	XP-330x
1	Flangeless Fitting for 1/16" tubing, PPS natural	Ercatech AG	XP-286x
1	VacuTight Fitting for 1/16" tubing, red	Ercatech AG	P-844x
12	Ferrule, ETFE, blue	Ercatech AG	P-200x
2	Ferrule, ETFE, yellow	Ercatech AG	P-300x
1	Ferrule, ETFE, red	Ercatech AG	P-840
1	PEEK Adapter, 10-32 C, F to 1/4-28 FB, F	Ercatech AG	P-627
1	PEEK Union for 1/16" OD Tubing	Ercatech AG	P-702
1	Y-PEEK Union for 1/16" OD Tubing	Ercatech AG	P-512
variable	Pin Tools	V&P Scientific	FP1 to FP9
variable	Metal Taper Tips, 320µm O.D. × 50 µm I.D. x 50 mm	MS Wil	MT320-50-3.5-5
variable	Hamilton gas tight 1 mL syringes, Model 1001 LTN SYR, Cemented NDL, 22 ga	Hamilton	HA-81316

**Table A 2.** List of required instruments.

Quantity	Description
3	SMC precision pressure regulator, IR2000-F02
1	SMC precision pressure regulator, AW20-F02BM
8	SMC Easy-plug connection with male screw; Part. No. KQ2S06-02S
1	SMC VK332 solenoid valve
1	Bronkhorst IQ <sup>+</sup> FLOW; IQP-600C-1KSG-ABD-00-V-200 mln/min N2
1	Vögtlin red-y compact gas flow meter; GCM-A9SA-FN00 incl.

	Pressure line reduction unit
2	neMESYS low pressure Syringe pump
1	IDS USB 2 UI-2230SE-M camera with L-IV-14-W illumination

**Table A 3.** List of required tools.

Quantity	Description
1	Hexagon 0.87 mm (pin fixation)
1	Hexagon 1.27 mm (pin fixation)
1	Hexagon 2.00 mm (rack fixation)
1	Hexagon 2.47 mm (gas blocking plate at ESI source)
1	Wrench 10 mm (rack fixation)
variable	Waterproof sand paper from SIA Abrasives Industries, 1913 siawat, 3100.3713.0600, 3100.3713.1000, 3100.3713.2000

### **A.3 Connection of Components and System Preparation**

It is recommended to install the entire system on a movable table with three levels:

Upper level: sampler, syringe pump, buffer dampening bottle, voltmeter

Middle level: mechanical and electrical pressure regulators, power supplies and controlling units

Lower level: Waste bottle for pin washing solvents.

### **A.4 Overview of Electric and Gas Connections**

Remark: removable lines for the power-supply of compartments as well as devices which are not controlled by the PC (e.g. gas flow meter and the volt meter) are not mentioned, but are considered later.

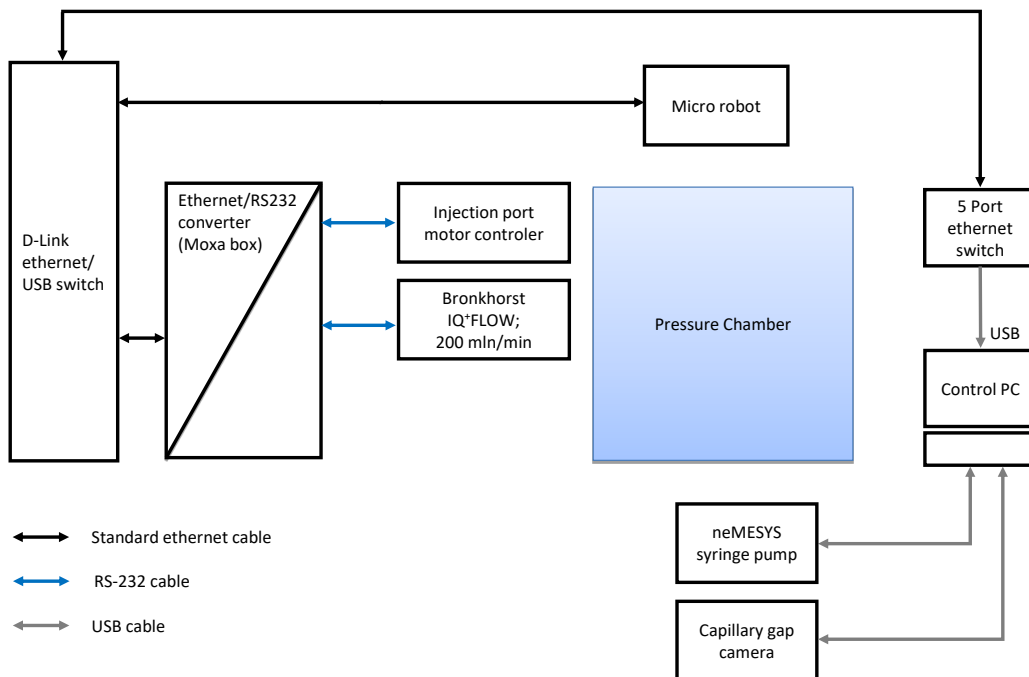


Figure A 1. Overview of electric connections.

Remark: The connection to the main gas supply (dashed line) depends on the present type of gas delivering (fixed lines, gas bottles, etc.)

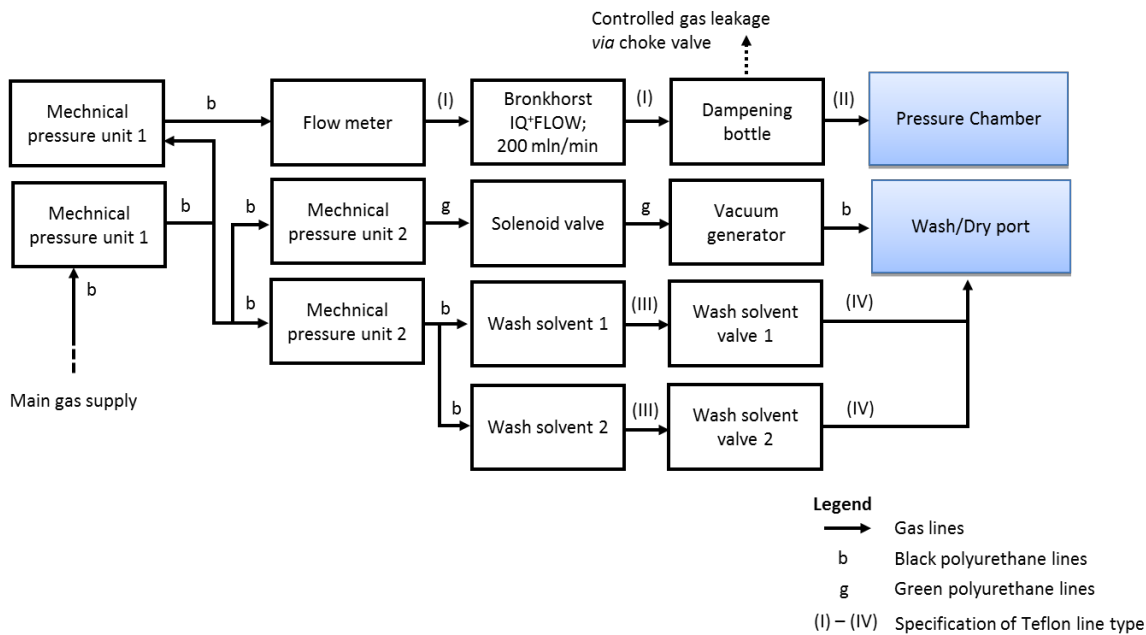


Figure A 2. Overview of gas connections.

## **A.5 Preparation of Gas Lines**

Prepare the following line types prior to the connection of sampler compartments using Teflon tubing. Following the block diagram above:



**Figure A 3.** Line type (I): 2 lines needed

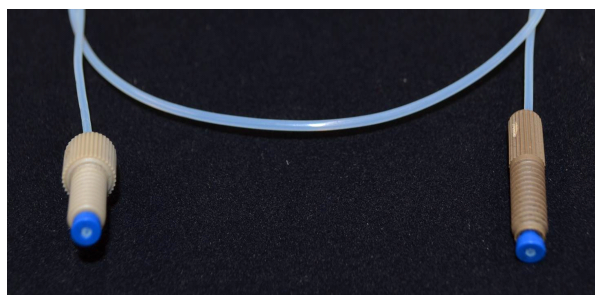


**Figure A 4.** Line type (II): 1 line needed



**Figure A 5.** Line type (III): 2 lines needed

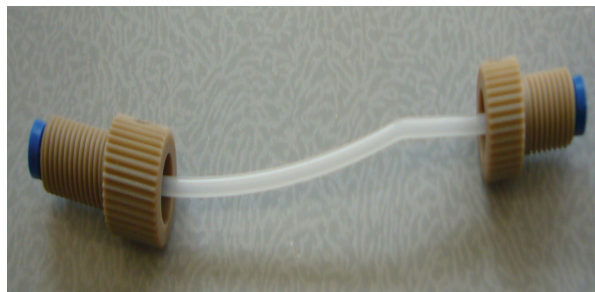


**Figure A 6.** Line type (IV): 2 lines needed

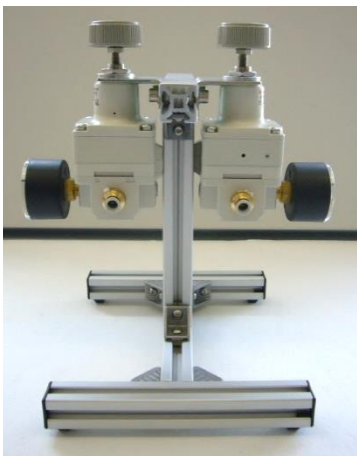
## A.6 Installation of Mechanical Pressure Regulators

### A.6.1 Station 1

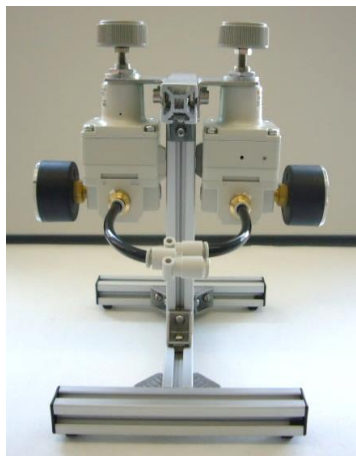
Figure A 7: Two IR2000-F02 mechanical pressure regulators are equipped with two KQ2S06-02S easy plug connectors each, and fixed on opposite side of a rack.

Figure A 8: Connect two short polyurethane lines (6 mm O.D.) with the pressure regulators and link the lines with a Y-connection piece.

Figure A 9: Connect the remaining port of the Y-connection with a longer polyurethane line.



**Figure A 7.** IR2000-F02 mechanical pressure regulators.



**Figure A 8.** IR2000-F02 connected to polyurethane lines.

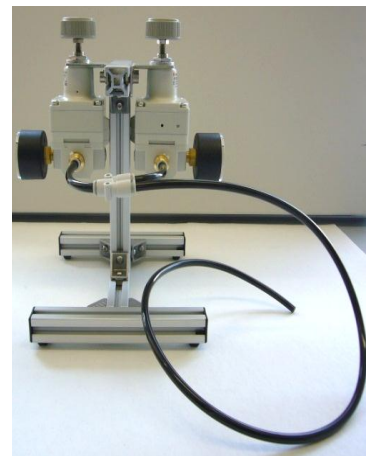


**Figure A 9.** IR2000-F02 connected to the gas exit line.

Figure A 10: Connect the inlet of the red-Y compact gas flow meter with the outlet of the mechanical pressure regulator by using a polyurethane line (6 mm O.D.). Connect the outlet of the pressure regulator with a reduction nipple (6 mm O.D. to 4 mm O.D.), a pressure line reduction unit (6 mm O.D. to 1/8"), and a PEEK Adapter 10-32 to 1/4-28, and a PEEK union for 1/8".

Figure A 11: Connect the PEEK union for 1/8" with line type I. The inlet of the other mechanical pressure regulator should be connected to the main gas supply.



**Figure A 10.** Gas flow meter.

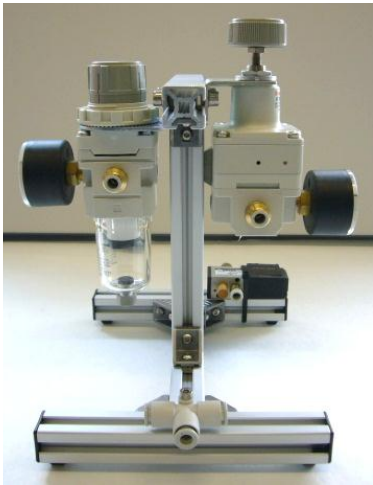


**Figure A 11.** Gas flow meter connected to the main gas supply.

### **A.6.2 Station 2**

Figure A 12: An IR2000-F02 and an AW20-F02BM pressure regulators are equipped with two KQ2S06-02S easy plug connectors each, and fixed on the opposite side of a rack. Moreover, a T-shaped easy plug connector is fixed on the rack as well as a VK332 solenoid valve on the opposite side of the rack.

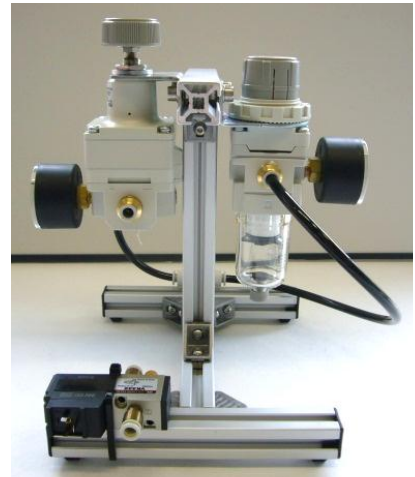
Figure A 13 and Figure A 14: Connect the inlets of both pressure regulators with the T-piece using short polyurethane lines (6 mm O.D.).



**Figure A 12.** Pressure regulator (step 1).



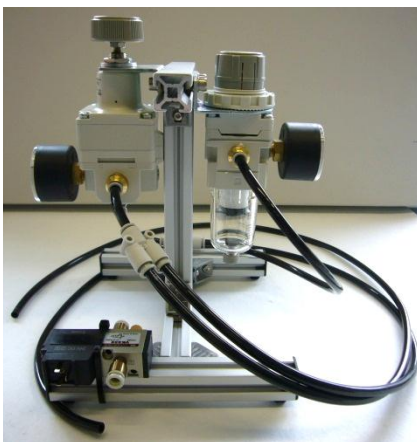
**Figure A 13.** Connected pressure regulator (front).



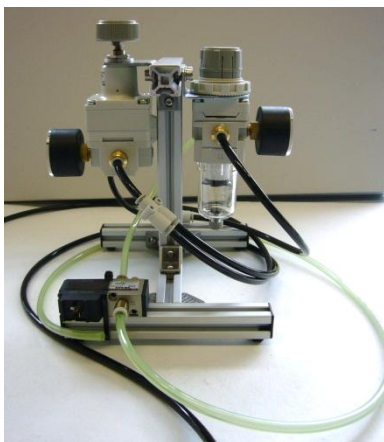
**Figure A 14.** Connected pressure regulator (back).

Figure A 15: Connect the outlet of the AW20-F02BM pressure regulator with a short piece of polyurethane line (6 mm O.D.), followed by a Y-piece. Connect two longer polyurethane lines (6 mm O.D.) with the Y-piece.

Figure A 16 and Figure A 17: Connect the outlet of the solenoid valve with a long green polyurethane line (6 mm O.D.). Connect the outlet of the AW20-F02BM pressure regulator with the inlet of the solenoid valve using a green polyurethane line (6 mm O.D.).



**Figure A 15.** AW20-F02BM pressure regulator (step 1).



**Figure A 16.** AW20-F02BM pressure regulator (step 2).



**Figure A 17.** AW20-F02BM pressure regulator (step 3).

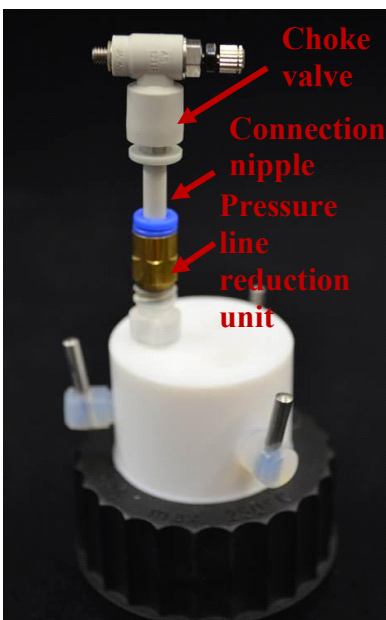
## **A.7 Installation of Pressurized Bottles and Valve Connectors**

### **A.7.1 Station 2**

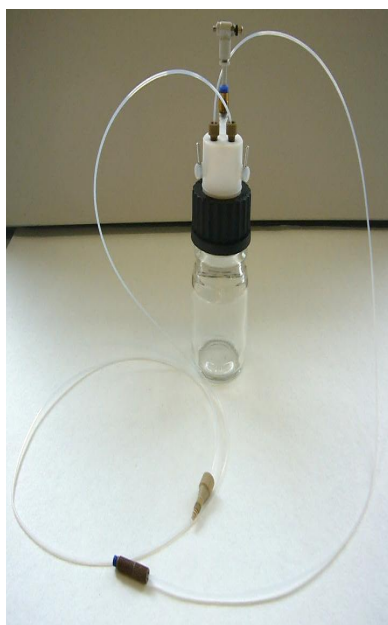
Figure A 18: Connect a 3-Port bottlecap with hand valves to a pressure line reduction unit (4 mm O.D. to 1/8"), followed by a dual connection nipple (4 mm I.D) and a choke valve.

Figure A 19: Put the bottle cap on a 100 mL buffer bottle and connect the remaining ports of the bottlecap with a shorter line type 1 and a longer line type 2.





**Figure A 18.** The buffer bottle cap components.



**Figure A 19.** The buffer bottle cap connections.

#### **A.7.1.1 Bottles for Wash Solvents**

Figure A 20: Connect the top side of a 2-port bottle cap with a pressure *line* reduction unit (6 mm O.D. to 1/8"), and the bottom side (opposite connection port with a FEP line by using a flangeless fitting P330x incl. yellow ferrule P-300x.

Figure A 21: Put the bottle cap on a 250 mL buffer bottle and connect the remaining port of the bottle cap with line type 3.

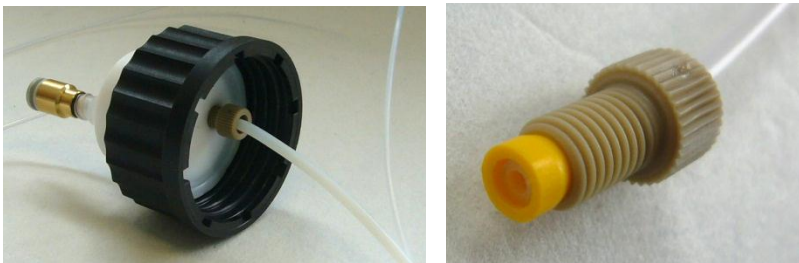


**Figure A 20.** The buffer bottle cap connections (line type 3).



**Figure A 21.** The buffer bottle connection to the pressure line.

#### **A.7.1.2 Waste Bottle for Pin Drying**

Figure A 22: Connect the top side of a 2-port bottle cap with two pressure line reduction units (6 mm O.D. to 1/8”). Connect one reduction unit with the vacuum generator *via* a dual connection nipple (6 mm O.D.) and the other reduction unit with a reduction nipple (6 mm O.D. to 4 mm O.D.).

Figure A 23: Put the bottle cap on a 250 mL glass bottle and connect the reduction nipple with a long polyurethane line (6 mm O.D.).

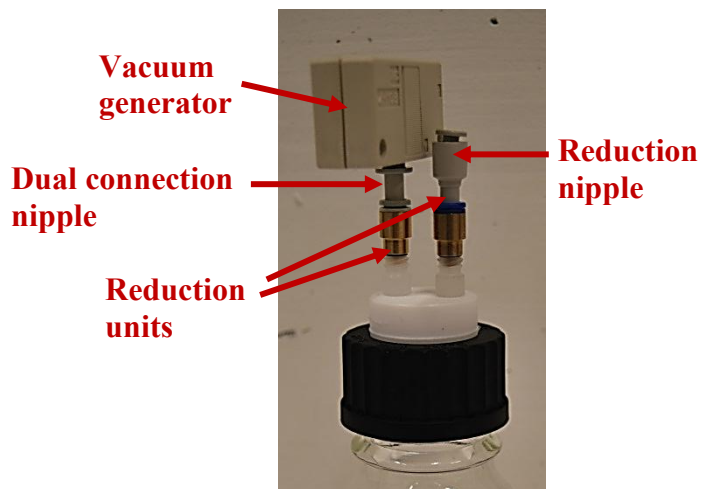


**Figure A 22.** Vacuum generator.



**Figure A 23.** Vacuum generator connected to a long polyurethane line.

#### A.7.1.3 Connector for Pin Washing Solvents

Connect a Y-PEEK union with two short lines of line type IV, and with a third line equipped with a red fitting P-840 including a red ferrule P-840.

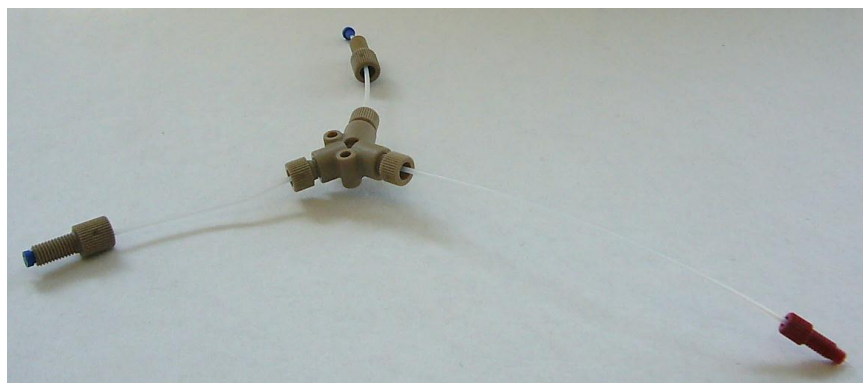


**Figure A 24.** A Y-PEEK union with two short lines of line type IV.

## **A.8 Zoomed Pictures of the System Setup**

### **A.8.1 Connections of Mechanical and Electrical Pressure Regulators**

*Remark:* Mechanical and electrical pressure regulators should be placed on the mid-level of the movable table of the entire sampler setup.

Figure A 25: Connection of the two mechanical pressure regulation stations (polyurethane line from pressure station 1 to T-piece of pressure station 2).

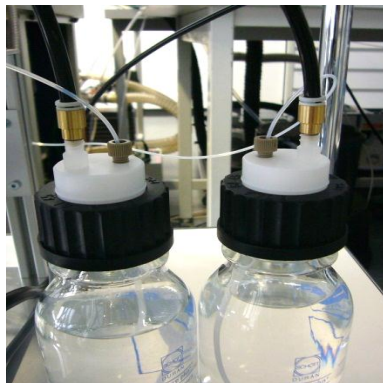
Figure A 26: Connection of the black polyurethane lines from mechanical pressure station 2 to the bottle for wash solvents.

Figure A 27: Connection of the green polyurethane line from mechanical pressure station 2 to the vacuum generator to the waste bottle for pin drying.

Figure A 28, A 29: Connection of Teflon lines (a) from mechanical pressure station 1 to the inlet of the Bronkhorst IQ flow gas regulator, and (b) from the Buffer dampening bottle to the outlet of the Bronkhorst IQ flow gas regulator:



**Figure A 25.** Connection of mechanical pressure station 2 to the bottle for wash solvents.



**Figure A 26.** Connection of mechanical pressure station 2 to the vacuum generator to the waste bottle.



**Figure A 27.** Connection of mechanical station 1 to the inlet of the Bronkhorst IQ flow gas regulator.

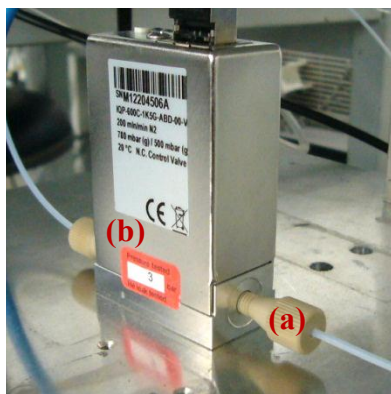
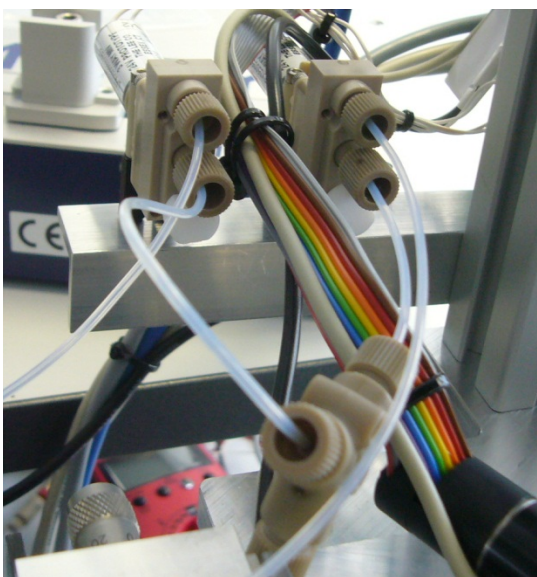


**Figure A 28.** Connection of buffer dampening bottle to the outlet of the Bronkhorst IQ flow gas regulator.

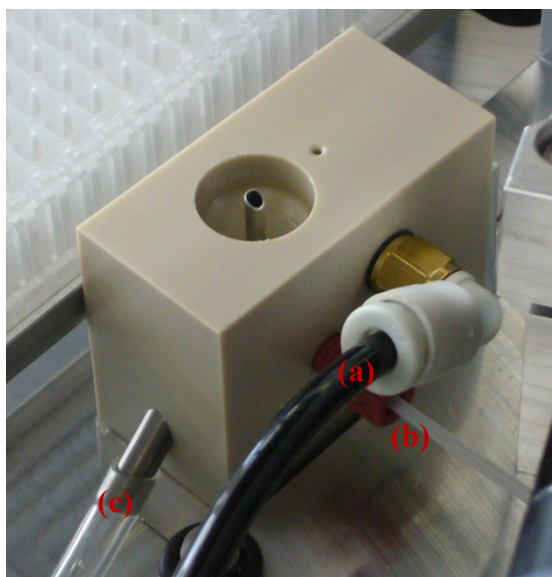
### **A.8.2 Connections to the Wash Solvent Valves and the Wash Port**

Figure A 29: Connections of Teflon lines from the washing solvent bottles to the wash solvent valves (upper ports) and the lines to the Y-connector

Figure A 30: Connection of (a) the black polyurethane line 4 mm I.D.) from the waste bottle for pin drying, (b) the Teflon line equipped with red fitting and red ferrule and (c) the waste line for pin flushing to the wash port:



**Figure A 29.** Connections of washing solvent bottles to the wash solvent valves



**Figure A 30.** Connections to the wash/dry station; (a) gas for pin drying, (b) solvent for pin washing, (c) solvent to the waste bottle.

### A.8.3 Connections to the Pressure Chamber

Figure A 31: Connection of the shorter line of the pressure dampening bottle (placed at the upper level of the moving sampler table) to the pressure chamber *via* a PPS fitting.

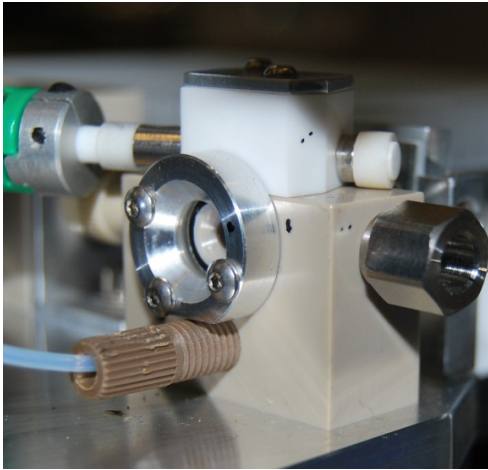


**Figure A 31.** Connection of pressure dampening bottle to the pressure chamber *via* a PPS fitting.

## A.9 Establishing Electrical Connections and Location of Control LEDs

### A.9.1 Removable Connections on the Upper Level of the Sampler Setup

USB-connections from laptop: Intermediate connections: Devices:

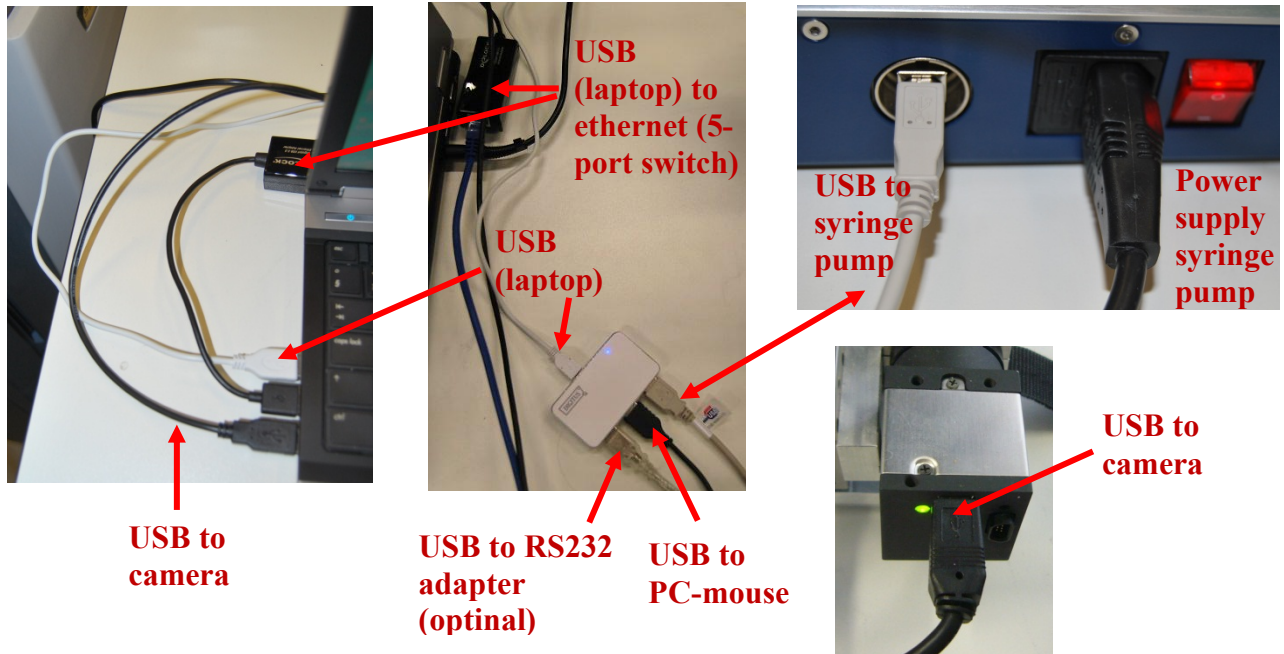
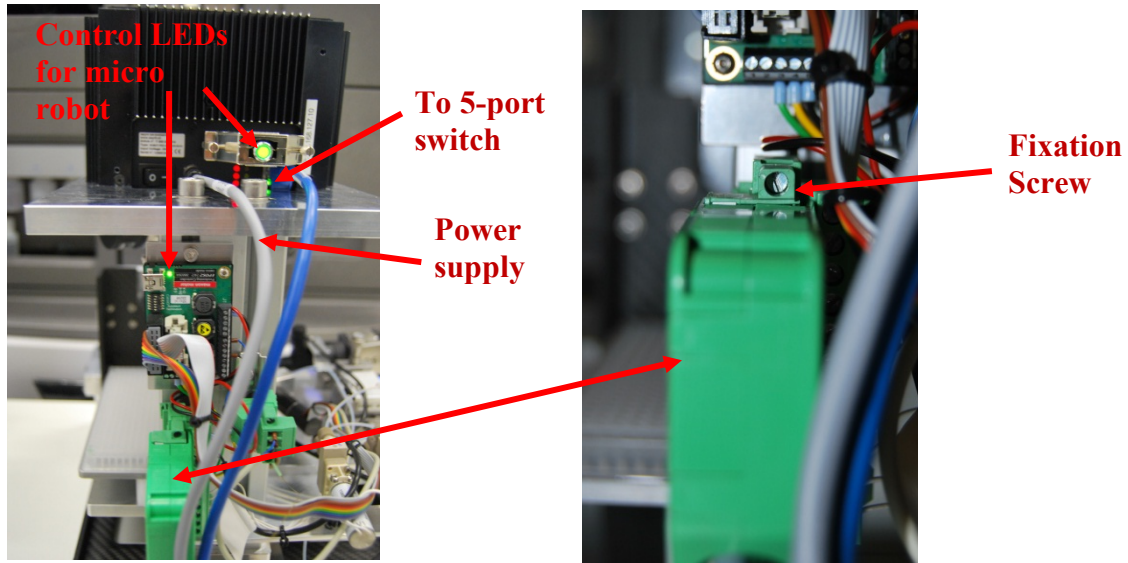


Figure A 32. Electrical Connections.



The multiple connection unit can be removed after loosening the fixation screws at the upper and lower side of the unit.



**Figure A 33.** Electrical connections and location of control LED.

### A.10 Connections on the Middle level of the Sampler Setup

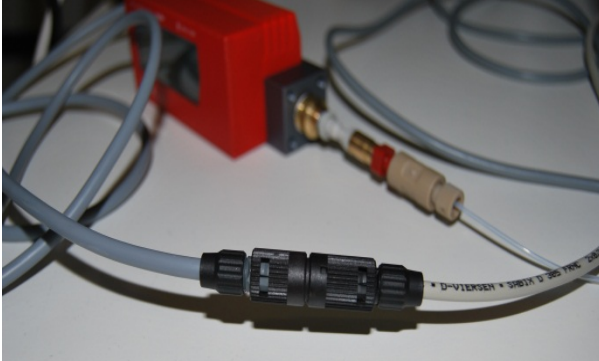


Figure A 34. Connection of power supply to the red-Y gas flow meter.

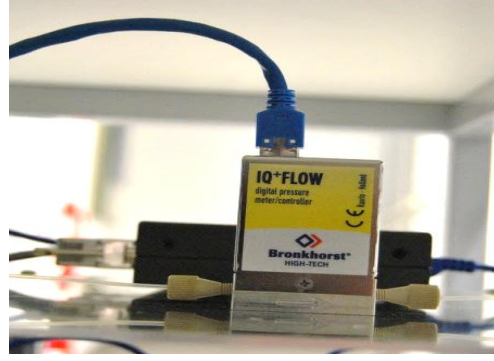


Figure A 35. Connection to electrical pressure regulator.

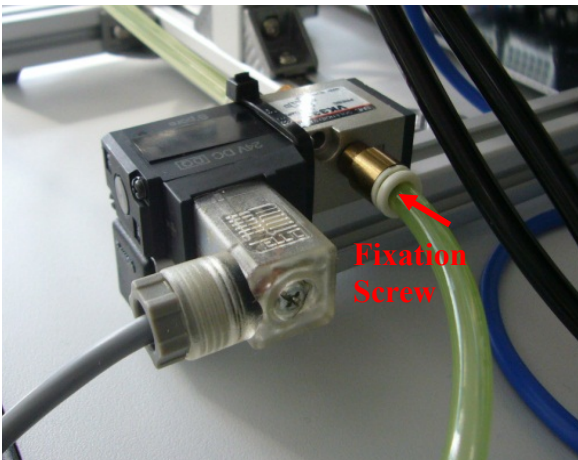


Figure A 36. Connection to solenoid valve at the mechanical pressure station 2:

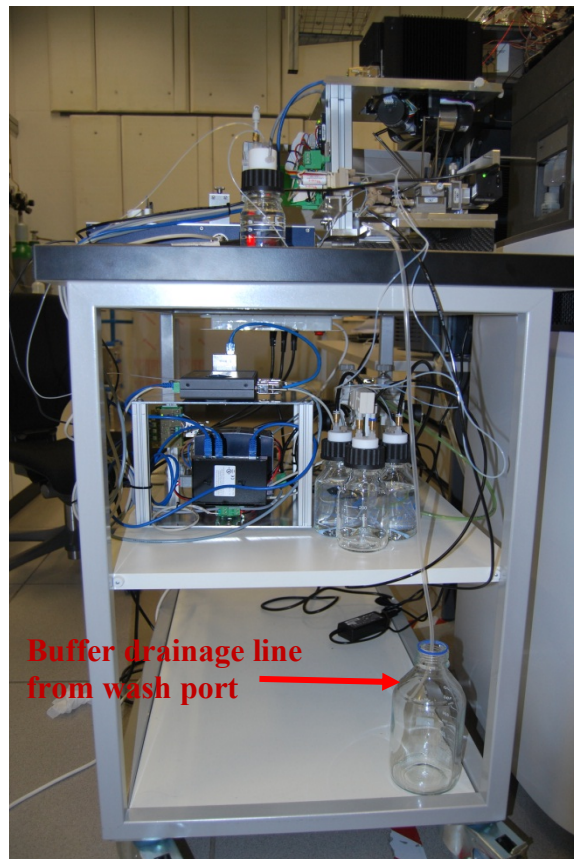
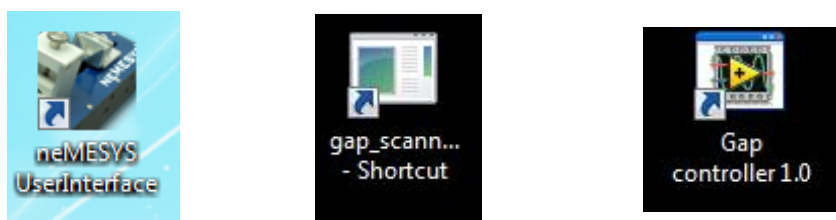


Figure A 37. Overview of the three levels of the sampler setup.

## A.11 Purging of the Buffer line Using neMESYS Syringe Pump

*Remarks:* the syringe pump should be placed on the top-level of the sampler setup; wearing gloves is recommended.

Start the neMESYS control or gap controller software (**before opening the gap controller, the gap scanner should be open first**):



**Figure A 38.** The neMESYS user interface, gap scanner and gap controller software.

Define the syringe parameters to be used according to the neMESYS pump manual if needed.

Calibrate the syringe pump by pressing the **calibration** button in the syringe pump setting page of gap controller. Then, press **refill** button to move the syringe mounting adapt to an appropriate level. Press **Stop**.

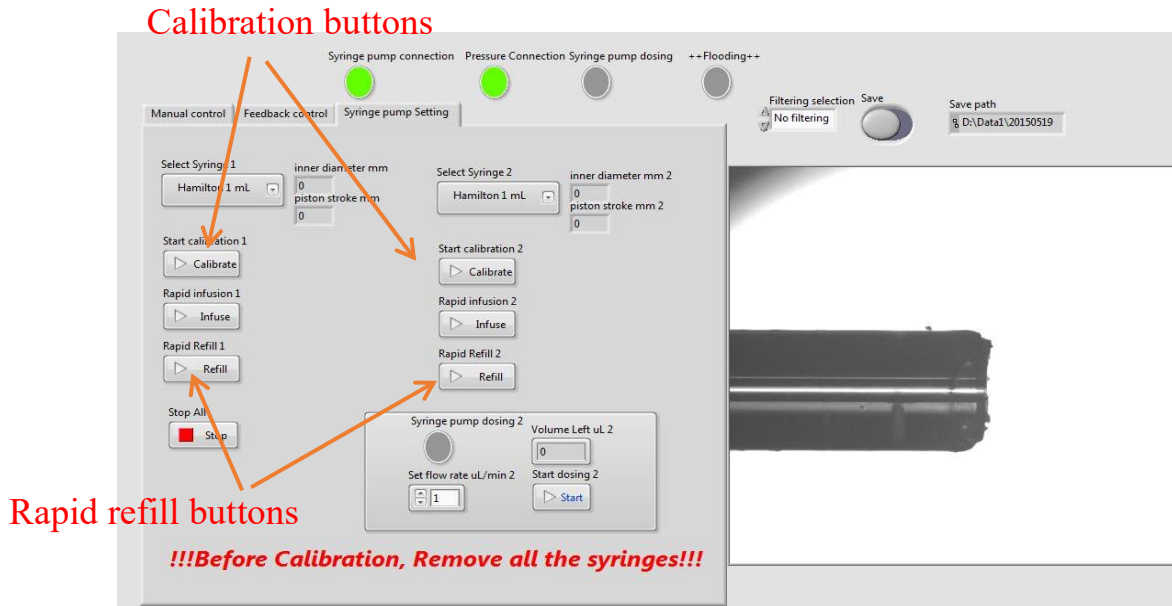


Figure A 39. Syringe pump setting on the gap controller software.

For installing the syringe, the following items are needed:

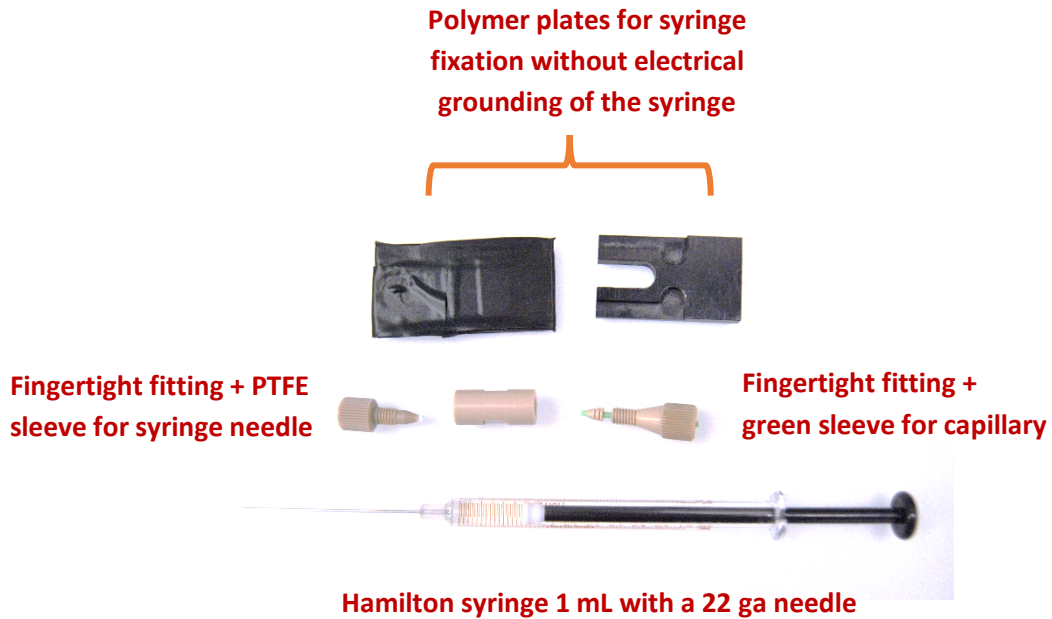


Figure A 40. Components for syringe fixation.

Fill the syringe with an appropriate solvent, e.g. using a 50 mL flacon tube; avoid bubbles during filling.

*Remark:* **Solvents should be sonicated before use for at least 10 min to remove the bubble.**

Solvents containing acids and bases can attack the black polymer layer covering the syringe plunger. Buffers as solvents which contain salts in high concentrations can lead to salt precipitations after some time. Thus, **the syringe should be flushed with water after use**, especially in case of storage for a couple of days.

Connect the bubble-free filled syringe to the connector and release a small amount of solvent through the connector by pressing the plunger cautiously.

Connect the syringe connector to a 360 x 50  $\mu\text{m}$  Teflon coated fused silica (50 cm) via the finger tight fitting + green sleeve. Release again a small amount of solvent by pressing the plunger and check for a leakage at the connection.

Connect the other tip of the Teflon-coated fused silica capillary buffer line with the special “hexagon-headed” PEEK finger tight + double grip ferrule + green sleeve:



**Figure A 41.** A hexagon-headed PEEK finger tight, double grip ferrule and a green sleeve.

Fix the syringe in the syringe holder by using the PEEK spacers:

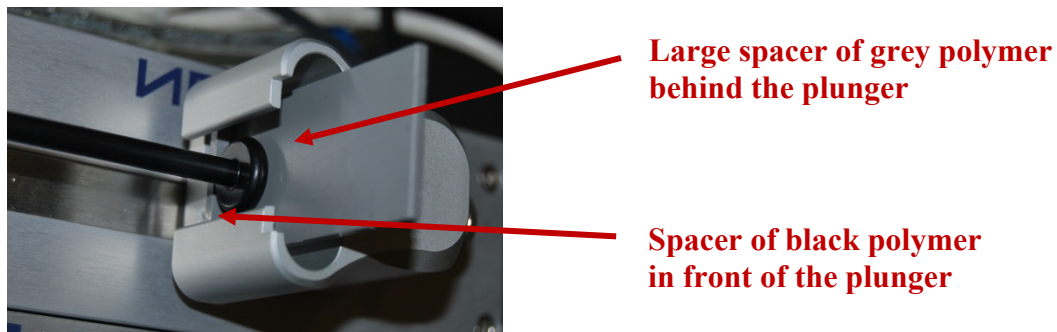


**Figure A 42.** Syringe fixation in the syringe holder (step 1).

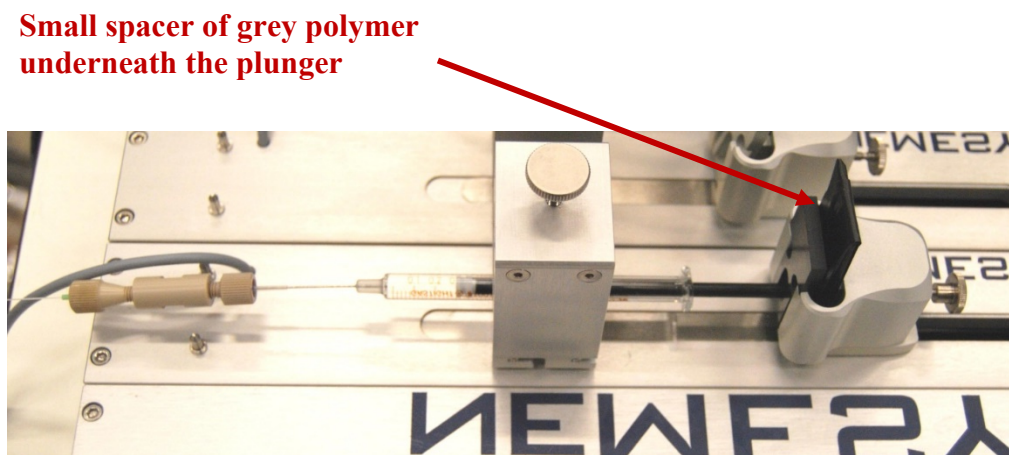


**Figure A 43.** Syringe fixation in the syringe holder (step 2).

Start the buffer flow in the neMESYS pump application (typically  $F=1 \mu\text{L}/\text{min}$ ) and purge the buffer lines for at least 15 minutes. Before stopping the purging process, check for the presence of leakages at the connections and for drops appearing at the open end of the  $360 \times 50 \mu\text{m}$  buffer line by using a magnifying glass. **The buffer flow should be bubble-free before installing the sampler.** If no drops appear, stop the buffer flow and wait for 5 min.

## A.12 Adjustment of the Pin Tool

*Remark:* wearing gloves is recommended.

A bunch of five full metal Pin Tools of different diameter can be chosen for adjustment:

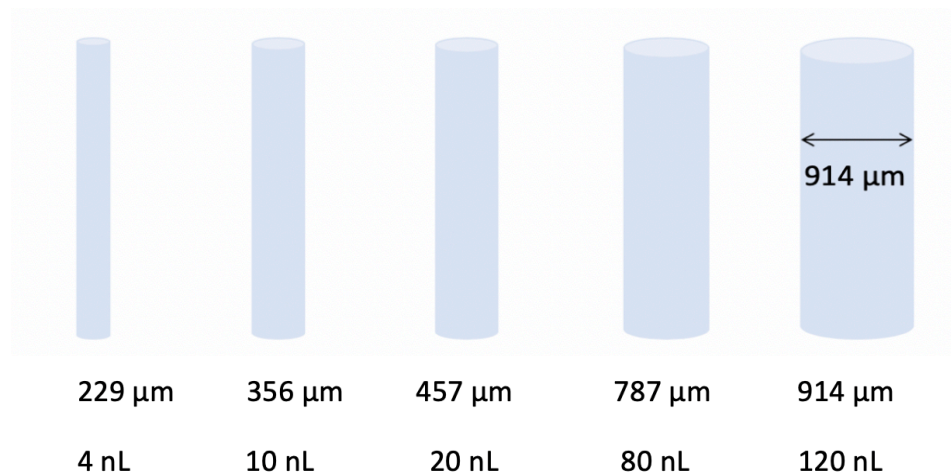


**Figure A 44.** Metal pin tools.

*Remarks:* There are also slotted pins available for higher volume sample transfer without increasing Pin-Ø, as well as hydrophobically coated pin (see homepage of V&P Scientific).

***Reduce the diameter of the pin sleeve with precise polishing steps.*** The pin sleeve can be slightly polished to make it more robust. The original diameter of the pin sleeve is 1.58 mm, which can be reduced to 1.5–1.55 mm. Lathes in the machine shop, combined with sandpaper (mesh size of 100) can be used to do such polishing. Safety glasses should be worn and special training of the lathes should be taken before do such job. ***Measuring the diameter every two minute to avoid over reduction.***

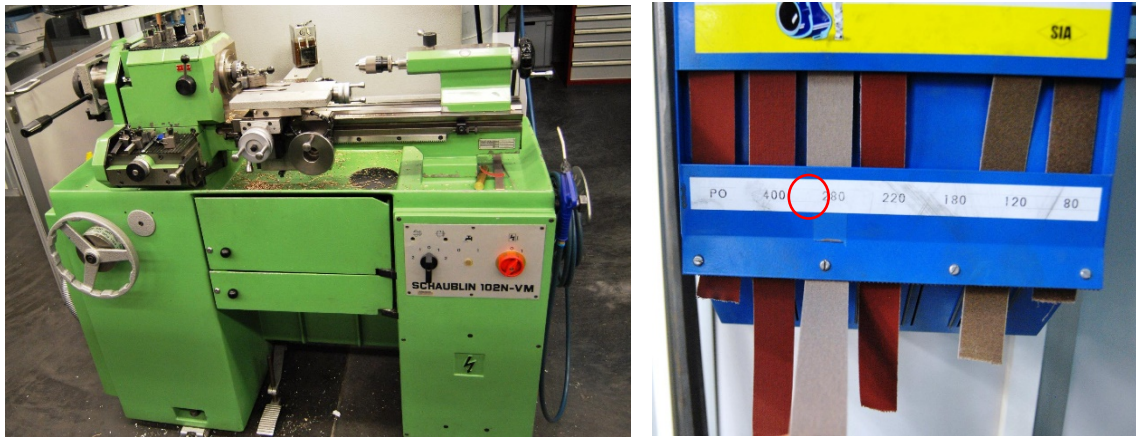


**Figure A 45.** Pin tool diameter fixation.

Pin Tools originally delivered from V&P Scientific have a length of the exposed pin of about 17 mm. In order to be useful as sampling device for the CGS, the exposed pin has to be reduced to a length of about 5 mm by cutting of pin at the back end (not at the exposed end!) and subsequent crimping of the pin sleeve at the back end for fixation of the shortened pin. Moreover, the back end of the pin has to be locked by a drop of glue in order to ensure gas tightness of the pin. This procedure has been done manually by R. Rietmann at Roche, and explains the observed differences in exposed pin lengths. Christian Marro from HCI workshop performs the pin cutting.

Use the following items to fix the pin tool:





**Figure A 46.** Pin tool fixation components.

Cautiously fix the appropriate pin within the holder by using the 0.89 mm hexagon. Usually, the pin sleeve is plugged into the pin holder as deep as possible (see also remarks)

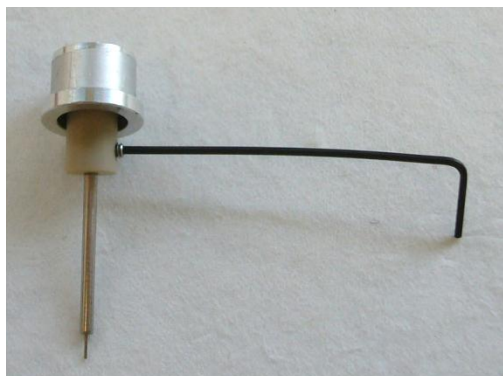


**Figure A 47.** Pin tool fixation (step 1).

*Remarks:*

Be cautious when fixing the pin; the pin holder consists of sensitive mechanic compartments!  
If the length of pin is too short for touching the capillaries forming the gap (limit in robot movement for the z-coordinate is reached), the pin can also be plugged in a way that it does not penetrate the pin holder as deep as possible. But be aware that the pin is hanging straight into the holder.

Put the small weight on the pin holder and guide the pin holder from downwards through the fixation unit of the delta robot.

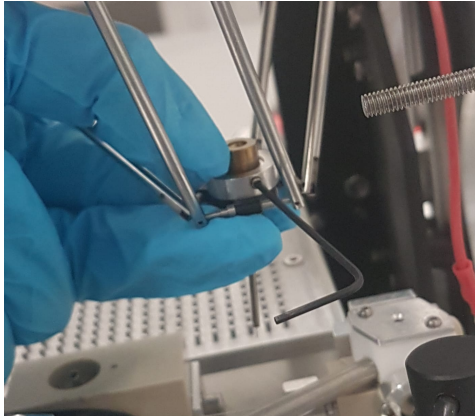


**Figure A 48.** Pin tool fixation (step 2).

While holding the position with one hand, carefully slip the fixation ring of the pin holder over the pin holder from upwards. Press the fixation ring and the pin holder against each other and fix the fixation ring carefully using the 1.27 mm hexagon.

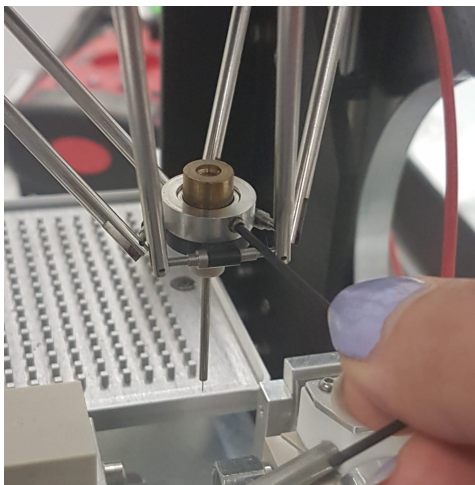


**Figure A 49.** Pin tool fixation (step 3).

After fixation, the pin should still be flexible within the holder and center again after manual deflection.

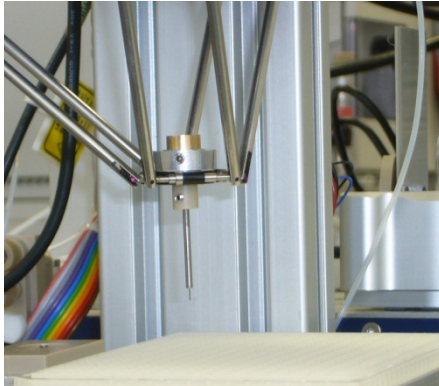


**Figure A 50.** Fixed pin tool.

### **A.13 Gap Formation**

*Remark:* wearing gloves is recommended.

Start “CGS application.exe” the working platform should appear including the camera field of view.

- (a) Be sure that the main pressure valve is turned off during gap formation; the current chamber pressure should show [mbar g]=0
- (b) Initialize the injection port motor via “Init”; after few seconds, the motor is running idle and the injection port should be open.
- (c) Toggle the box “show lines”; the orientation lines should appear.
- (d) Turn off the micro robot by clicking "Robot Control Off". Hold the robot arms and loose the brakes of the micro robot by clicking "Brakes off".

*Remark:* The robot always has to be held manually when brakes are turned off. Moving the robot when brakes are active can cause damage of the brakes.

Guide the robot arm carrying the pin tool manually into the injection port, such that it appears within the camera field of view. Align the green orientation lines with the pin for defining the gap diameter (here: Pin O.D. is 356  $\mu\text{m}$  gap size is about 250  $\mu\text{m}$ ).

*Remark:* A fluctuating green circle in the right upper corner of the field of view indicates that the camera monitoring the capillary gap is still active. If the circle stops fluctuation, you should restart the Sampler application.

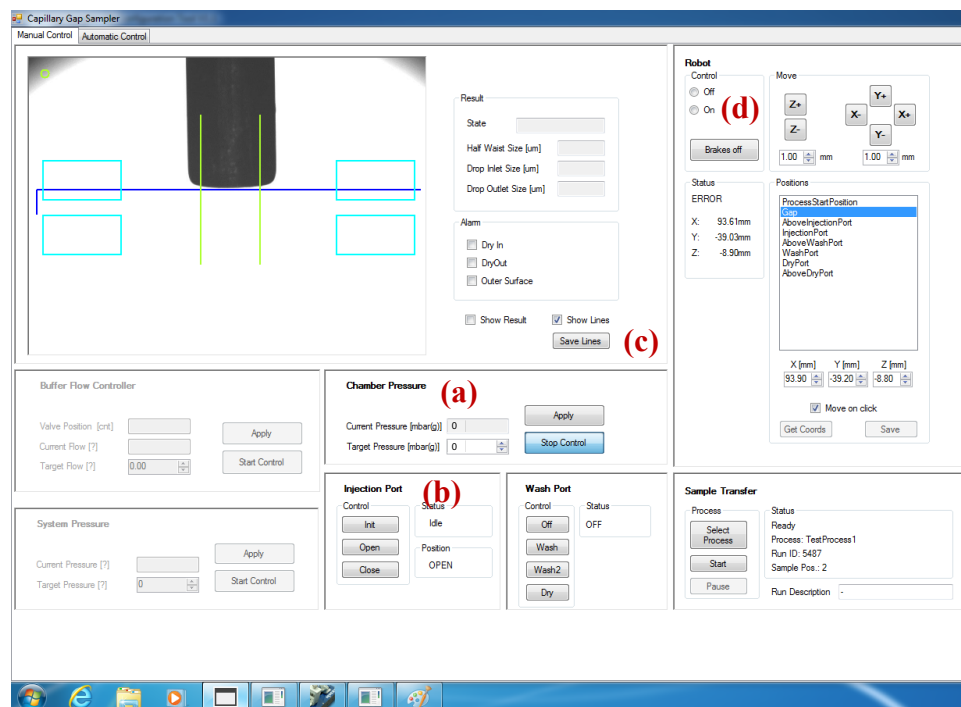


**Figure A 51.** Original gap controller software, (a) chamber pressure, (b) injection port, (c) online monitoring, and (d) robot control.

Guide the 360 x 50  $\mu\text{m}$  fused silica tube equipped with the special “hexagon-headed” PEEK fingertight + green sleeve into the pressure chamber, until it appears in the camera field of view. Fix the fused silica tube according to the green orientation line by using a 7-inch wrench.

*Remark:* Avoid any contact of the fused silica line with the pressure chamber and the tube fittings. Use lint-free paper if the capillaries butt-face appears to be dirty.

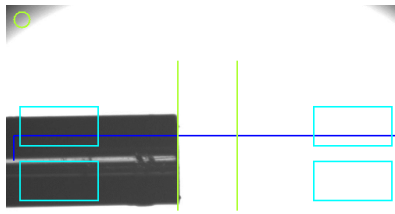


**Figure A 52.** Capillary adjustment (step 1).

Guide the metal tip through the metal nut including the conductive ferrule, such that the capillary blunt-end appears by about 1 mm. Guide the nut including the capillary cautiously through the chamber bore without touching it. Fix the blunt-end of the metal tip hand-tight according to the green orientation line.

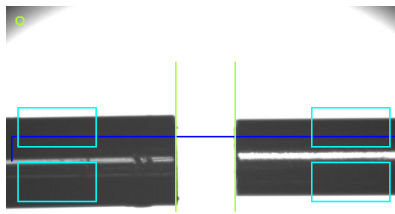


**Figure A 53.** Capillary adjustment (step 2).

Connections to pressure chamber after gap mounting:

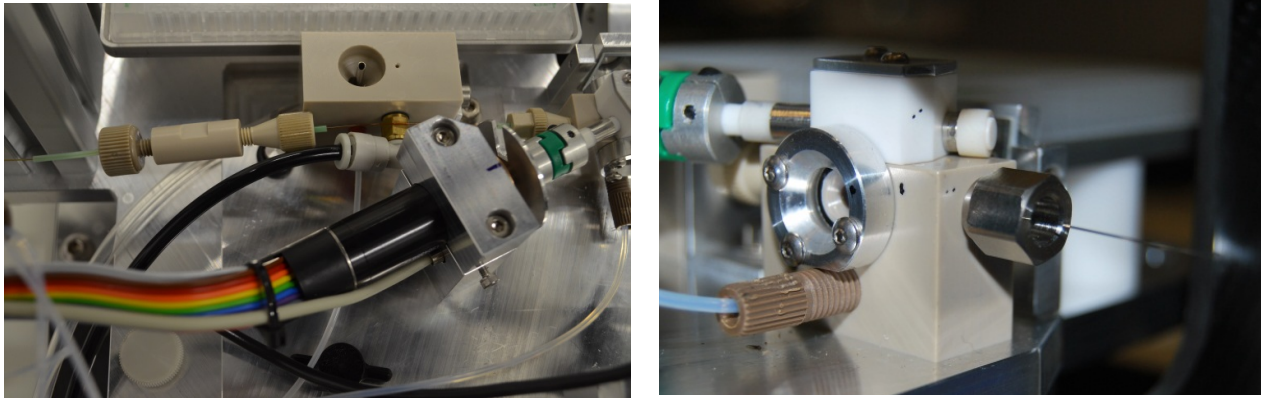


Figure A 54. Capillary adjustment inside the chamber (step 3).

## A.14 Teaching the Microrobot

*Remark:* wearing gloves is recommended.

### A.14.1 Robot Positions

In the robot section of the sampler application tool you find robot positions typically used in a sampling method:

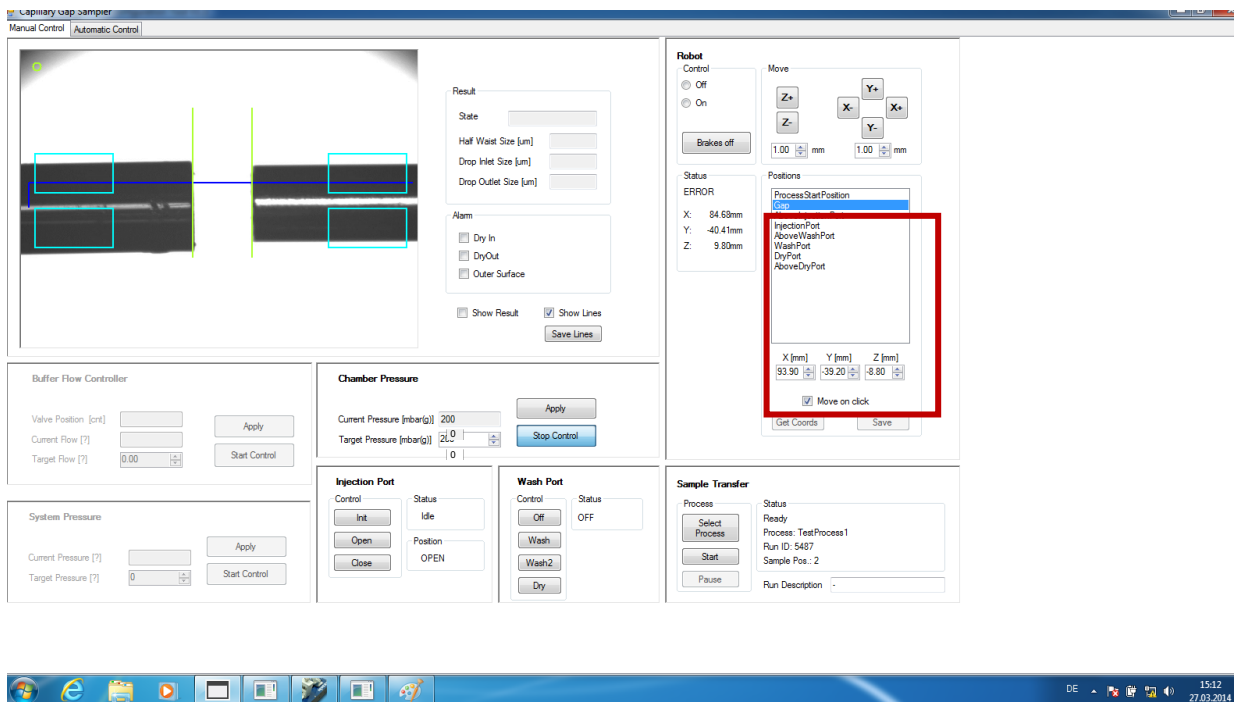


Figure A 55. Robot position training.

Remark: More positions can be generated in the Sampler Configuration tool in the section Robot positions (see section 11.1).

Start the micro robot by clicking "Robot Control On". The robot will automatically move to a centered position. The shown x, y, z-positions should be identical to the coordinates saved under "**Process Start Position**".

Turn off the micro robot by clicking "Robot Control Off". Open the injection port. Hold the robot arms and loose the brakes of the micro robot by clicking "Brakes off".

*Remark:* During teaching, the robot always has to be held manually when brakes are turned off. Moving the robot when brakes are active can cause damage of the brakes.

Guide the pin carefully through the port until it appears within the camera field of view and hangs centrally about 100  $\mu\text{m}$  above the gap (the buffer capillary O.D. of 360  $\mu\text{m}$  can be used as orientation length). "Record" these coordinates for the position "**Gap**" and confirm with "Save".

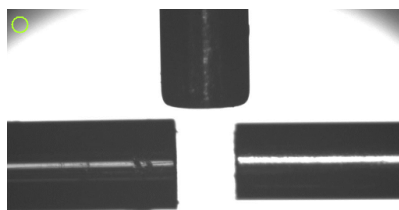


**Figure A 56.** Gap position.

Move the pin carefully out of the chamber and close the injection port. Push the metal sleeve gently back into the port such that touches the injection port axis. Note the x and y-coordinates for the position "**Injection port**". They should be identical to the x and y-coordinates of the former position "Gap". As z-coordinate note the given vale minus 1 mm. This prevents touching of the metal pin with the injection port axis in a later experiment when the sampling pin carries a hanging droplet of sample. Confirm with "Save".

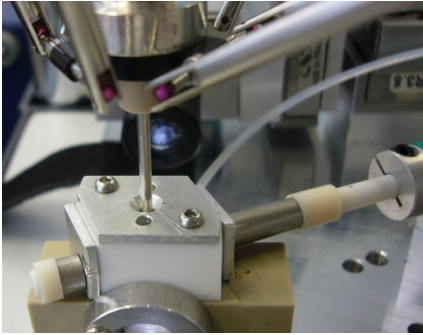


**Figure A 57.** Above gap position.

Note the x and y coordinates from the positions “Injection port” and “Capillary Gap” also for the position “**Above injection port**”. The z-coordinate is equal to the z-coordinate of the position “**Process Start Position**”. Confirm with “Save”.

Guide the pin to the metal sleeve of the wash port such that the end of the pin is about 1 mm below the edge of the metal sleeve. Note the coordinates as “**Wash Port**”. Confirm with “Save”.

Transfer the x and y coordinates from the position “Wash port” also for the position “**Above Wash Port**”. The z-coordinate is equal to the z-coordinate of the position “Process Start Position”.

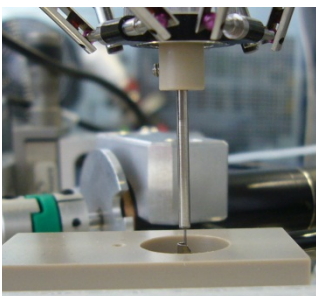


**Figure A 58.** Washing position.

Guide the pin to the dry port such that metal sleeve of the pin is about 1 mm above the edge of the port (pin should enter the dry port as deep as possible). Note the coordinates for the position “**Dry port**”. Confirm with “Save”.



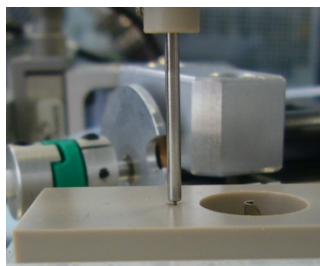


**Figure A 59.** Drying position.

Define the position “**Above Dry Port**” by using the x and y coordinates from the positions “Dry port”. The z-coordinate is equal to the z-coordinate of the position "Process Start Position". Confirm with “Save”.

It is highly recommended to check every position of an injection cycle by manual position activation. *Be sure that the injection port is open during manual position check.* Generally, manual position check is done in a two-step approach:

1) Toggle the box "Move on click" and select the position "Above injection port". Use the button "-Z" in the "Move" field of the robot section to move the robot stepwise down in -Z direction. If the robot does not enter the pressure chamber properly, fine-tune x- and y-coordinates by using the corresponding buttons (-X, +X, -Z, +Z). Change x- and y- coordinates for all relevant positions (“Above Injection Port”, “Injection Port”, “Gap”), and confirm with “Save” separately.

The same procedure is valid for the position pairs “Above Wash Port” / “Wash Port” and “Above Dry Port” / “Dry Port”.

*Concluding remarks:*

***Be sure that the following positions only differ in the z-coordinate:***

“Above Injection Port”, “Injection Port”, “Gap”

“Above Wash Port”, “Wash Port”

“Above Dry Port”, “Dry Port”

2) Re-check the positions taught by toggling "Move on click" and stepwise activation of positions taught. It is recommended to follow a typical scheme of an automated injection cycle:

- Process Start Position
- Above injection port
- Injection port
- Gap
- Injection port
- Above injection port
- Above wash port
- Wash port
- Above wash port
- Above dry port
- Dry port
- Above dry port
- Process Start Position

*Remark:* If the robot crashes during manual check, loose the brakes, guide pin manually back towards the process start position and re-activate the robot by clicking "off" and subsequently "on".

### A.14.2 Sample Plate Configuration

Open the Sampler Configuration Tool and go to section "Plate Config".

Process	Sample Sequence	Method	Method Steps	Plate Config	Robot Position							
	Name	FirstPosX	FirstPosY	FirstPosZ	FirstRowLastColPosX	FirstRowLastColPosY	FirstRowLastColPosZ	FirstColLastRowPosX	FirstColLastRowPosY	FirstColLastRowPosZ	NbrCols	NbrRow
	via_pin	27.100	-0.800	-14.300	-13.500	-0.800	-14.300	27.100	40.900	-14.500	10	10
	384Well_193Pos	9.410	0.500	-11.000	-26.500	-31.000	-11.000	26.500	31.000	-11.000	12	16
	via_capillary	26.000	0.000	-16.000	-14.200	0.000	-16.000	26.000	41.900	-16.000	10	10
*												

**Figure A 60.** Sample plate configuration.

Set a proper name for the plate configuration (e.g. by specifying the desired plate type) and give for each coordinate a value of 0. Define the number of columns as "Nbr Cols" as well as "Nbr.

Rows". The product of both the column and the row number is equal to the final number of positions.

Place a well plate (e.g. 384 format) on the sample rack. Fill the microwell #A1 with 40  $\mu$ L of water.

Turn off the micro robot in the Sampler Application by clicking Robot Control "Off". Hold the robot arms and loose the brakes of the micro robot by clicking "Brakes off".

Guide the pin centrally above the microwell # A1, such that the exposed pin slightly enters the water surface by about 1 mm. Transfer the x, y, z-coordinates given in the sampler application to the field "FirstPosX", "FirstPosY" and "FirstPosZ", respectively. Alternatively, you can also define only the x and y positions, and use manual position.

Repeat the process for 2 further microwells: the last microwell of the first row (coordinates named "FirstRowLastCol") and for the first microwell of the first column (coordinates named "FirstColLastRow"), both without water filling.

*Remark:* Plate configuration works via 3-Point calibration and the given number of columns and rows. The software automatically calculates all positions out of the 3 master points by parallel translation.

Consequently, identical coordinates for a plate configuration are

"FirstPosX" and "FirstColLastRowPosX"

"FirstPosY" and "FirstRowLastColPosY"

"FirstPosZ" and "FirstColLastRowPosZ" and "FirstRowLastColPosZ"

## **A.15 Defining and Testing a Custom Automated Process**

### **A.15.1 Additional Robot Positions**

Go to the section "Robot Position" in the Sampler Configuration Tool.

All robot positions formerly taught (section 10.1) were automatically transferred from the Sampler Application and should appear in the Sampler Configuration tool. Additional positions needed for an automated injection cycle are:

Sample Plate

Above Sample plate

No movement

These positions are not needed to be taught in the Sampler Application and are therefore not toggled as "Is teachable position" (first column in section robot position).

For defining the pseudo position "**Sample Plate**", set all coordinates to 0. The sample positions will be taken automatically from the sample plate configuration.

The position "**Above Sample Plate**" is only defined in the z-coordinate. Thus, set the x and y coordinates to 0. The z-coordinate should be set as the sum of the absolute values of the z-coordinates of "Process Start Position" and the z-coordinate in the sample plate configuration. In this context, it stands for the absolute difference in z-level between the process start position and the z-position for sample uptake.

For defining the pseudo position "**No Movement**", set all coordinates to 0.

### **A.15.2 Method**

Go to the section "Method" in the Sampler Configuration Tool.

Name the method you want to define (here "Test Method 1"). Confirm by pressing enter.

### **A.15.3 Method Steps**

Go to the section "Method Steps" in the Sampler Configuration Tool.

Select the Method you want to edit under "Method Name".

Add method steps by clicking on the field "Add Step...". The following window pops up:

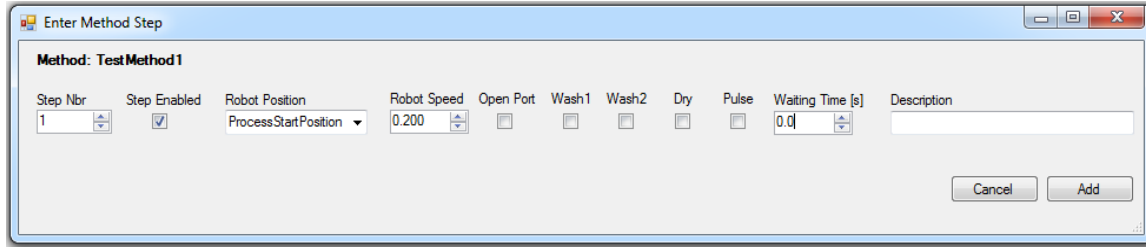


**Figure A 61.** Defining method steps (step 1).

Define the step number, the Robot Position, the Robot Speed (standard speed 0.2) as well as the corresponding waiting time (usually 0.0 seconds). The options "Open Port", "Wash 1 & 2", "Dry" and "Pulse" trigger external devices. Click "Add" to save the method step.

Define method steps according to the robot movements within an injection cycle by an increasing step number. A typical method for automated sample infusion includes 19 steps:

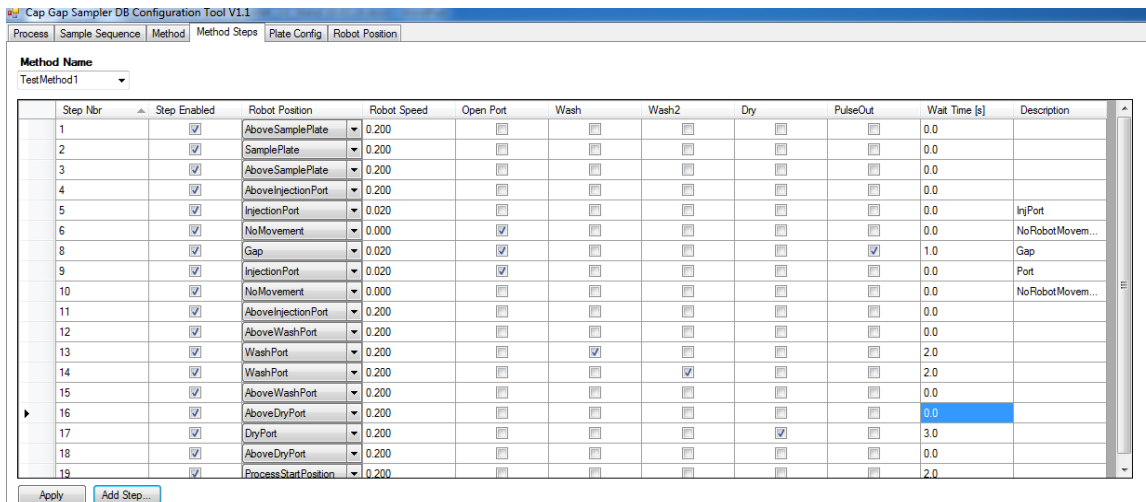


**Figure A 62.** Defining method steps (step 2).

*Remarks:* All method steps concerning robot movements where the pressure chamber is involved ("Above Injection Port", "Injection Port", "Gap") should be performed at a lower robot speed of 0.02.

Be aware of proper controlling external devices such as the port axis, the wash port and the dry port by checking the corresponding boxes.

Define proper waiting times where needed.

Confirm the method by clicking "Apply".

#### **A.15.4 Process**

Go to the section "Process" in the Sampler Configuration Tool.

Name the process you want to define (here "Test Process 1") or add new process. Select the sample plate configuration. Confirm by pressing enter.

### A.15.5 Sample Sequence

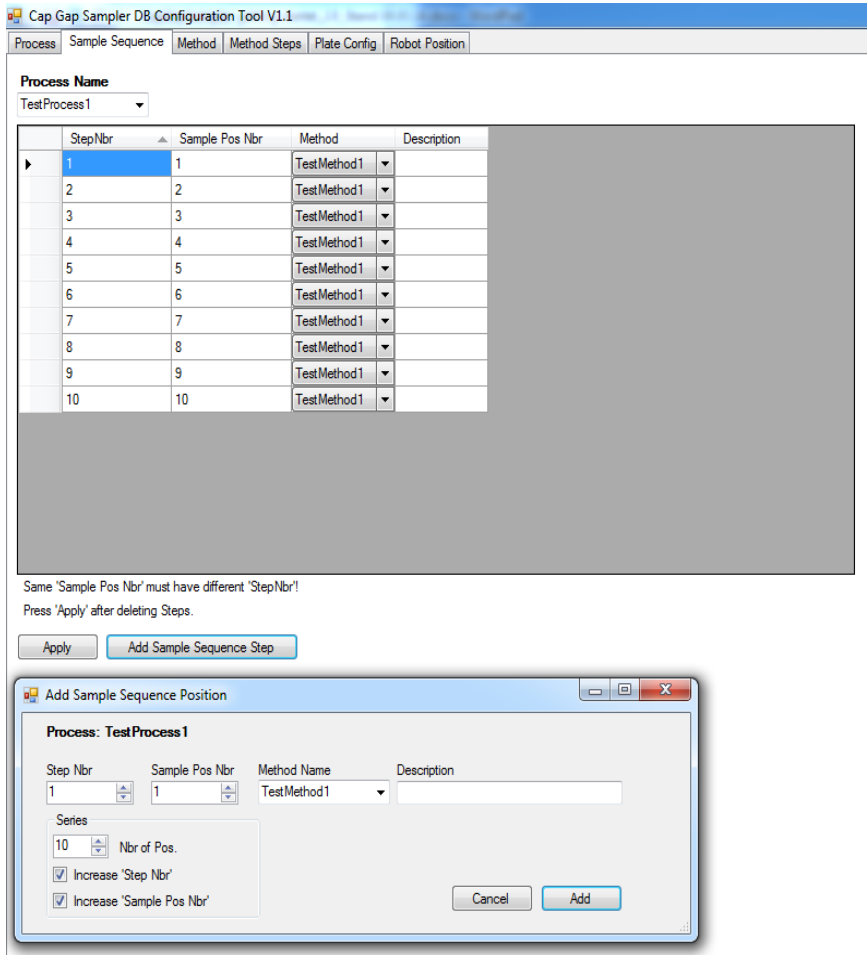


**Figure A 63.** Defining sampling sequence.

Select the Process you want to edit under "Process Name". Click on " Add Sample Sequence Position". Select the Method name you want to use. Set the number of Sample positions included in the sequence. Toggle "Increase Step Nbr". Non-checking of "Increase Position Nbr" will give multiple analysis of the sample sample, while checking will give single analysis of multiple samples.

### A.15.6 Process Testing

Connect the sampler to the main gas supply at mechanical pressure station 1. Open the main pressure valve and set the target pressure values for pressure station 1 to 2.0 bar (main pressure

line) and 1.5 bar, respectively, and for pressure station 2 to 0.1 bar (wash liquids) and 2.0 bar (to solenoid valve).

Go to the Sampler application tool and perform testing of the sampler workflow by choosing the programmed sample process and clicking on “Start”. A fully automated injection cycle should include sample pickup from the microwell plate, interference free pin guidance into the pressure chamber combined with automated injection port opening and closing, and defined pin washing and drying.

### **A.16 Operation of New Process Automation Software**

Apart from the manually defined, step-by-step movement sequences that can be created by the user, the CGS control software contains functionality to take inputs in a graphical interface to set every parameter of the two main experimental processes that are to be executed using the existing prototype the SPME) and the standard infusion process. The graphical interface allows the user to set parameters for a fully automated process execution functionality. The processes can be repeated arbitrarily in several different coordinates within a sample plate in order to achieve maximum sample throughput and to create reproducible, standardized experiments.

The current version of the graphical user interface is illustrated in Figure A 64..



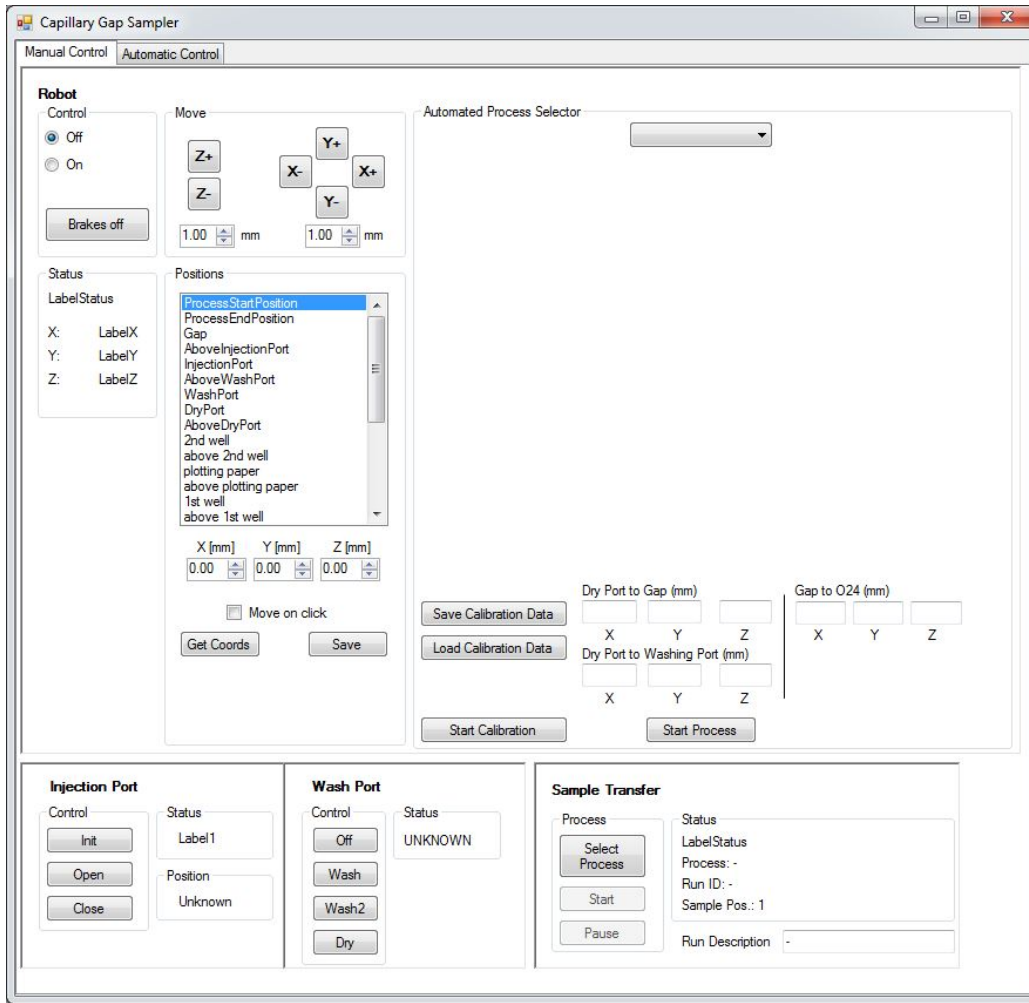
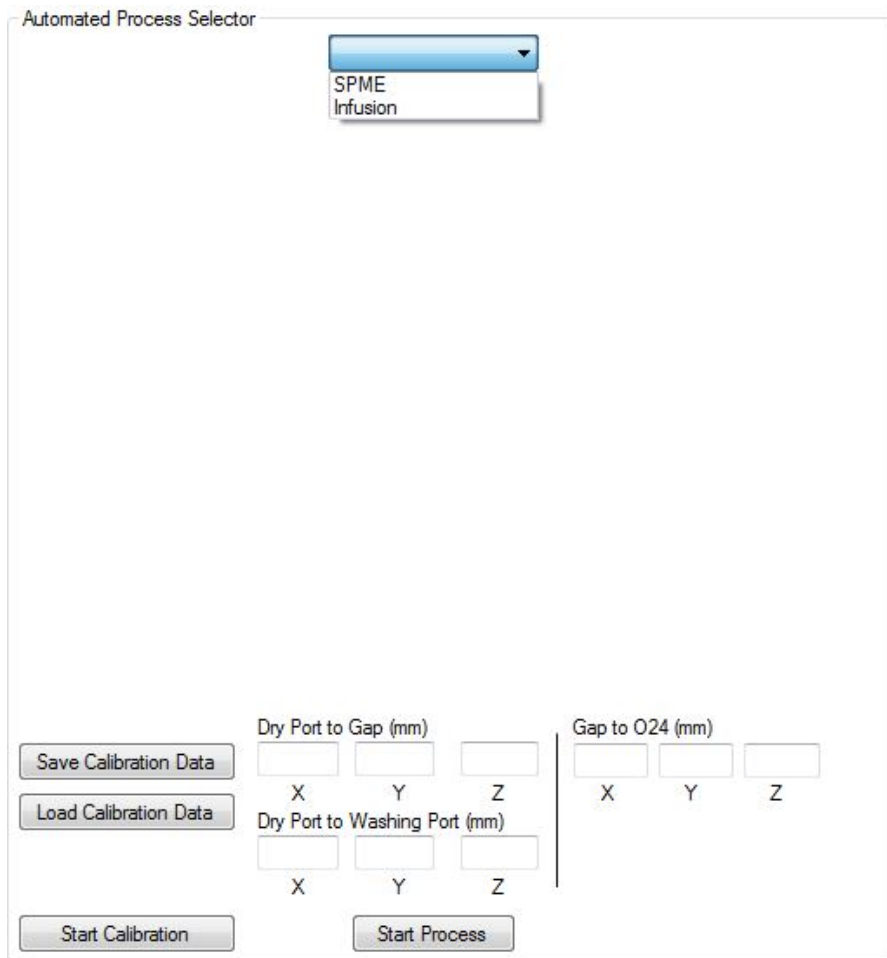


Figure A 64. Robot control GUI.

To the upper right side of the window, in the panel denoted by “Automated Process Selector”, a drop-down list can be used to select one of the two processes that were fully automated within the robot control software of the CGS. Selecting one of the processes in the list will update the blank field directly below it by revealing the corresponding parameters and user controls for the given process. These will be clarified in the coming subsections. Figure A 65 shows the list-box with both fully automated procedures available for selection.



**Figure A 65.** Process Selection Interface.

The operation manual for this software is contained within this section. The first subsection will clarify the calibration procedure that is necessary to correct for slight offsets in the absolute position coordinates that result from device power-off. Following is one subsection for each of the processes. A closing subsection summarizes the most important notes and requirements for correct operation of the software.

### **A.16.1 Calibration Procedure**

Due to the presence of a slight offset in the absolute measurement of the robot workspace coordinates that can occur at every power-off of the robot, a calibration procedure is necessary to ensure precision and safety at every power-on.

The user interface for the calibration procedure is already shown in the bottom part of the Automated Process Selector area. Since the delta-robot possesses a binary encoder to measure distances, the offset does not affect the measurement precision between two points that lie at a fixed distance to each other. The repeatability of the delta-robot is given by the Asyril datasheet to be within a few micrometers, which means the measurements provide enough precision to correct for this offset by using the robot itself and two or more predefined points with a known distance between each other.

The chosen points are the dry port, the gap, the O<sub>24</sub>-well and the washing port. The distances between these points can be calculated by positioning the delta robot end-effector at these points and by comparing the coordinates output by the robot control system on the left side of the interface (“Status” field on the left side of the window). These distances in the X, Y and Z axes need then to be input into the correct fields in the calibration interface and saved to the database service that runs in the background of the software by clicking the “Save Calibration Data” button. Note that the values to be input in the user interface are not the absolute coordinates, but rather relative distances between two points, i.e. the difference in X, Y and Z coordinates between the drying port and the gap, then the same between the gap and the O<sub>24</sub> well, then the same between the drying port and the washing port.

The latest calibrated distances can be loaded from the database by using the “Load Calibration Data” button and either changed or applied at any given time by clicking the button “Start Calibration” to trigger the user-assisted calibration sequence.

A series of message boxes will appear to guide the user through the process. Basically, the end-effector of the robot needs to be placed in the dry port hole, taking care not to generate any deviations of the end-effector pin from the vertical axis. When this is done, a click by the user will cause the current absolute coordinates of the robot to be saved as the new drying port coordinates into the database, and update not only the washing port, gap and O<sub>24</sub> coordinates but also other auxiliary positions such as the M<sub>24</sub> and A<sub>1</sub> wells.

Next figure shows the beginning of the procedure. The user should hold the robot arms before release of the brakes in order to prevent the end-effector from falling.

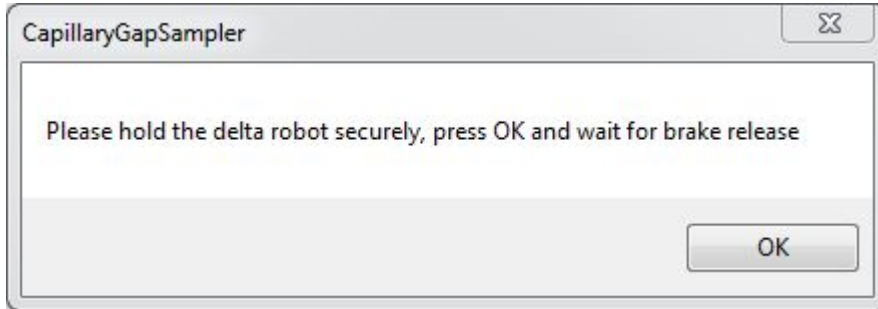


**Figure A 66.** Delta Robot Break Message.

Following brake release, the user is required to place the robot above the initial reference point that's defined for calibrating distances to the other relevant points in the calibration scheme. Currently, the drying port is used as the reference position. A calibration piece with a deeper hole is being designed to increase precision by additionally providing a vertically stabilizing mechanism for the end-effector pin and will be integrated as the reference point in the future. This is shown in the figure bellow.

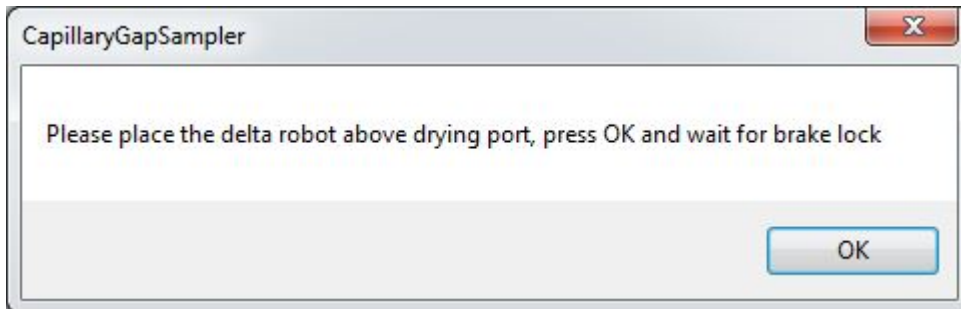


**Figure A 67.** Reference Point Placement.

Finally, after the brakes lock again, the closing message indicates that the procedure was successfully completed. It is recommended to manually release the brakes using the functionality at the upper left corner of the interface.

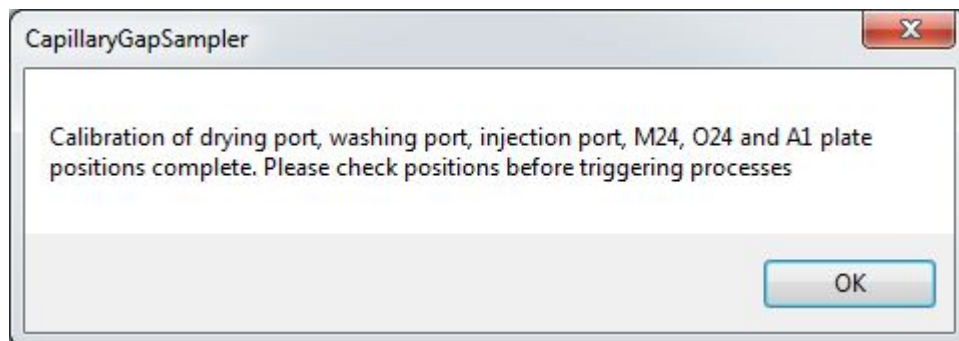


**Figure A 68.** Final Calibration Message.

The calibration process can be executed as long as no other processes are running with the robot and preventing the interface from being operated. The values go into effect immediately and it is highly recommended to test the positions with the “Positions” part of the robot control interface before triggering any processes.

### **A.16.2 Solid-phase Microextraction**

The SPME process consists of 5 distinct stages, requiring a total of 5 sets of position coordinates in the robot’s workspace: one for each of 4 sample wells and the position coordinate of the injection port where the capillary solvent gap is located. Upon selecting the SPME process. The SPME user controls will be revealed in the Automated Process Selector field.

First off, the user defines a starting position, i.e. the well position for the first SPME step. The positions for the 3 subsequent wells will be automatically updated according to the user’s input of the increment sign in the letter coordinate, given by the list-box under the label “Incr”.

The rest of the inputs will define the waiting times of the end-effector inside each of the 4 wells as well as in the capillary gap inside the injection port chamber. The checkboxes for stirring positions define in which wells the end-effector will execute a circular stirring movement to enhance extraction. The stirring speed and radius of this movement are also input by the user.

Furthermore, the grid scaling, i.e. the distance between two wells, is set by the user. Finally, the software allows for repetitions of the SPME process for different quadruples of wells, and the user

can choose how many repetitions in what direction in the numbered axis are to be executed. The software checks the boundaries of the desired process repetitions against the plate coordinates and warns the user if the desired number of repetitions would drive the robot outside of the sample plate.

All process data can be saved to and loaded from the database running in the background of the software. Clicking the “Start Process” button will check if all the critical process data is present and trigger the start of the process if everything checks.

Automated Process Selector

SPME

Pos1 Pos2 Pos3 Pos4 Chamber

Waiting Time (s)

Volume (uL)

Stir Position

Stiring Speed (mm/s)

Stiring Radius (um)

Process repetitions

Grid Scale (mm)

Save Load Last

Save Calibration Data Load Calibration Data

Dry Port to Gap (mm) Gap to O24 (mm)

X Y Z X Y Z

Dry Port to Washing Port (mm)

X Y Z

Start Calibration Start Process

Figure A 69. SPME control panel.

The screenshot shows a software interface for SPME position input. At the top, a dropdown menu is set to 'SPME'. Below it, there are several input fields and controls:

- Pos1:** A dropdown menu with 'M', a numeric input field with '24', and an 'Incr' dropdown menu with '+'. Below this is a 'Waiting Time (s)' input field with '1'.
- Pos2:** A dropdown menu with 'N24'. Below it is a numeric input field with '2'.
- Pos3:** A dropdown menu with 'O24'. Below it is a numeric input field with '2'.
- Pos4:** A dropdown menu with 'P24'. Below it is a numeric input field with '1'.
- Volume (uL):** A numeric input field with '1'.
- Chamber:** A numeric input field with '5'.
- Stir Position:** A row of four checkboxes. The first is unchecked. The second is unchecked. The third and fourth are checked.
- Clear:** A button located at the bottom right of the interface.

**Figure A 70.** SPME position input.

### A.16.3 Infusion

The infusion process, contrary to the SPME, relies on direct liquid dissolution of the sample-carrying pin into the solution present in the 4 wells. This means that one well may need to be serviced several times before repeating the process for another well.

Apart from the starting well of the process, not only the injection port but also the washing and drying port and blotting paper coordinates are needed as positions for this process. They will, however, not be checked against all the process coordinates in case of planned repetitions. Assuring that the robot does not dip too deep into the blotting paper well and pierces it, causing accidents, material damage and interruption of the experiment, lies with the user.

The well repetitions can be defined by the user and the process repetitions can be incremented in one of two axes – either the numbered or the letter axis. The software checks the boundaries of the sample plate against the desired number of repetitions, analogously to the SPME process.

Waiting times and well volumes can be input as in the SPME process. Furthermore, the blotting paper is assumed to be placed on one of the sample plate wells and its coordinates are input in the letter-number scheme of the well positions.

Automated Process Selector

Infusion

Position 1

Well repetitions  Incr Num Incr Letter

Process repetitions

Well Time (s)  Gap Time (s)  Drying Time (s)

Well Volume (uL)

---

Washing Solutions

1  2

Washing times (s)

Grid Scale (mm)

Blotting Paper Position

Blotting paper dips

Save Load Last

Save Calibration Data Load Calibration Data

Dry Port to Gap (mm)

X Y Z

Gap to O24 (mm)

X Y Z

Dry Port to Washing Port (mm)

X Y Z

Start Calibration Start Process

Figure A 71. Infusion Control Panel.

#### A.16.4 Important Considerations

The sample plate models that are used in all the experiments executed with the prototype are mapped in a 2D scheme where one axis goes from the letter A to the letter P, and the other axis is numbered from 1 to 24, giving a total of 384 wells. Deviations from this model are not foreseen. Nevertheless, in case of change, the boundary checks need to be changed in the software to adapt to the new dimensions. The class *RobotGUI* coded in the file “RobotGUI.vb” in the Visual Basic language contains the boundary checks for process repetitions in the event handler “startProcess\_Click()”. In the SPME\_control.vb class, the auxiliary function “updatePosition()” contains checks that need to be updated if changes in the plate configuration occur.



One of the main parameters for both processes is the grid scaling of the sample plate. The most important consideration in this sense is that the distance between two wells is assumed to be constant throughout the entire plate and to be the same in both directions.

The increment signs that can be set by the user in the SPME and Infusion processes will increase or decrease the plate coordinates in its own frame of reference, that is, they will increase or decrease the letter or number of the respective axis. These directions do not necessarily correspond to the robot coordinate directions, i.e. increasing the letter coordinate from D to G might incur in decreasing the X coordinate of the robot frame of reference.

Problems maintaining reliable functionality of the injection port motor can lead to accidents and end-effector pin damage, interrupting experiments and causing time-consuming breaks for maintenance. The functionality of the injection port needs to be checked thoroughly before triggering long processes and, should the motor not respond correctly for more than a certain period of time, different repetitions of a given process should be triggered one by one instead of all in a row.

The coordinates of the blotting paper are not checked against the process coordinates, should these include many repetitions. The user is responsible for ensuring that the blotting paper coordinates don't conflict with process coordinates in order to avoid damage and interruption of experiments. Finally, it is important to note that the well volume inputs, although intended to automatically adjust the depth of sample pin insertion by using the well shape and calculating the depth that would represent the same amount of volume above and below the sampling pin, are not being used for any purpose at the moment due to lack of technical data from the manufacturers. A rough estimate of a cubic well of side size 3.5mm would yield a total volume of roughly 45 microliters, which corresponds approximately to the real, empirically measured well volume. This cubic approximation does not, nonetheless, help in providing a more precise calculation of an insertion depth, since a cubic well's half-volume is simply halfway down the well, which does not correspond to an accurate calculation considering the complex, irregular real well shape.

## **A.17 Sampler Connection to the Mass Spectrometer**

Set the ESI standard source into standby. Unplug all electric and fluidic connections of the standard ESI-source to the mass spectrometer (sliding door above the source block of the mass spectrometer).



**Figure A 72.** Tools for fixing the sampler at the ESI source basis plate.

Fix the rods and the source gas line blocking tool (socket screw on top of the tool) at the source basis plate of the mass spectrometer. The rod without thread at one side should be fixed to the left lower position of the mass spectrometer basis plate.

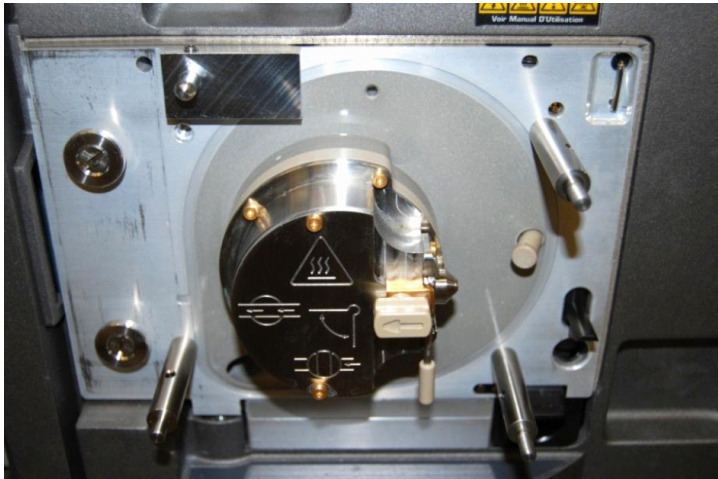


**Figure A 73.** Fixation screws for Synapt G2-S source.

Connect the dongle to the blue framed electrical connection plug, located behind the sliding door above the mass spectrometer source plate. Close the sliding door afterwards.

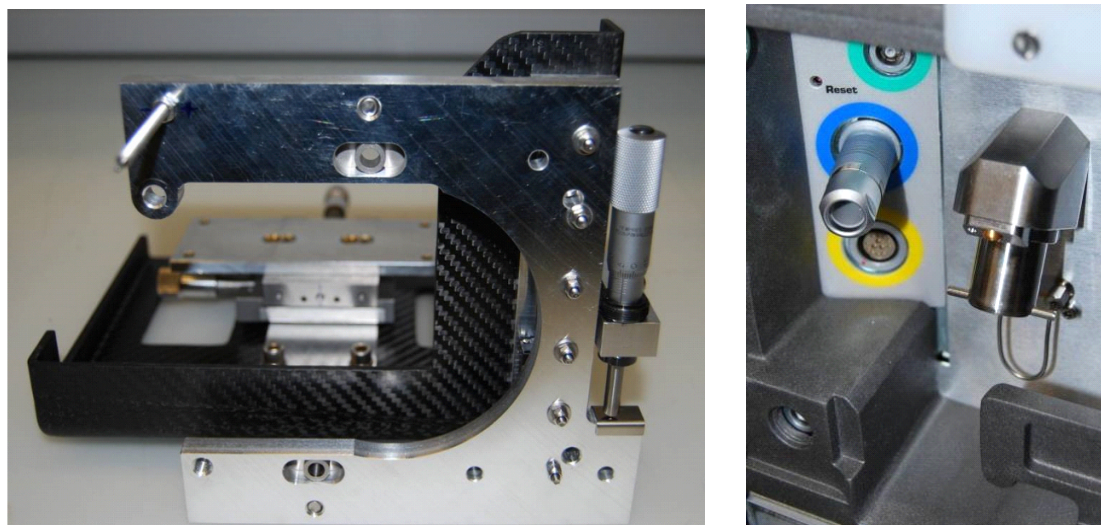


**Figure A 74.** X, Y and Z fixation platform (left), (right), dongle connection to the blue frame at the electrical connection plug.

The sampler rack should be equipped with a pin for electrical contact closure.

- (a) Fix the rack at the exposed rods with thread by using the screw nuts and washers.

(b) The rod without thread can be fixed optionally by the corresponding socket screw, using a 2 mm hexagon.

(c) Verify that the pin for electrical contact closure pushes the metal contact sheet at the source.

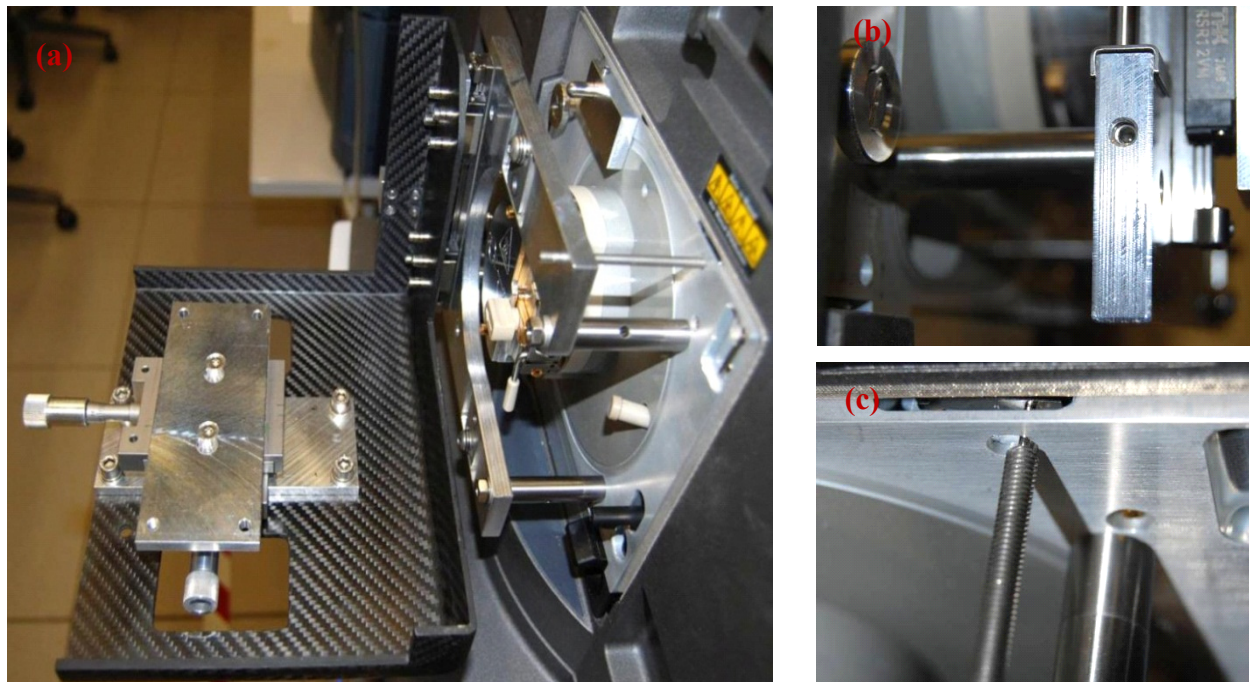


**Figure A 75.** CGS fixation to the MS. (a) screw the X, Y and Z stand, (b) socket screw, (c) pin for electrical contact closure.

Adjust the x, y-table of the rack at a position with maximum distance from the MS orifice, in order to prevent touching or bowing of the spray capillary to the MS orifice during sampler positioning on the rack (screwing directions are indicated by dashed arrows)!

Shift the movable table close to the mass spectrometer. Use the indicated bores of the rack basis plate to place the sampler on the rack (the sampler basis plate provides corresponding pins).

Fix the two basis plates by using the corresponding fixation screw including washer.



**Figure A 76.** The plate fixation screw.

Connect the Voltmeter (a) for measuring the spray current to the high-voltage plug at the mass spectrometer (b), and to the conductive nut holding the spray capillary using a metal clip (c). Set the measurement range of the voltmeter to 0-200 mV.

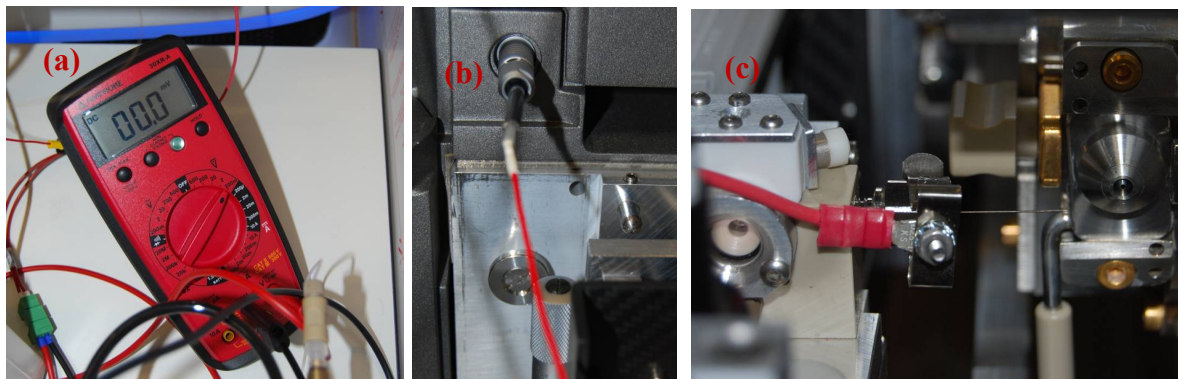


**Figure A 77.** Connection of the Voltmeter in three steps.

## A.18 Sampler Operation

### A.18.1 Establishing a Stable Liquid Bride and ESI Plume

Move the spray capillary by using x, y and z screws to a position where that the nozzle is about 2 mm off axis to the source in z-dimension, about 2 mm in x-dimension, and 5 mm in y-dimension.

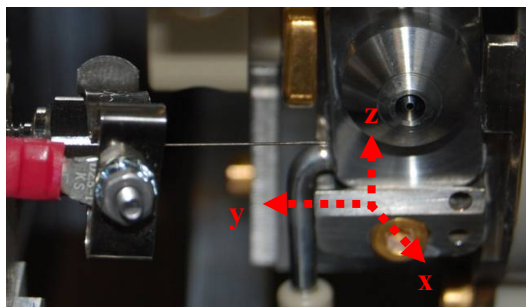


**Figure A 78.** Optimized spray position.

Close the pressure chamber and set the chamber pressure to 150 mbar.

Start the MassLynx application.

Choose “Nanoflow source” as source type within the MassLynx software. Load a suitable tuning file for the CGS and turn the mass spectrometer into operate. An ESI plume should be formed which can be recognized by jumping but measurable voltmeter potentials in the range of several mV. Avoid high potential values of  $> 20$  mV or even corona discharge, which is also indicated by a voltmeter overload (“OL”). If potential values are too high, increase the distance of the spray capillary to the MS orifice by using the x, y-moving table of the sampler rack.

Start the buffer flow in the neMESYS pump application; the standard flow rate is  $F=1\mu\text{L}/\text{min}$ .

Wait until the buffer liquid appears at the blunt end of the buffer line. At 150 mbar chamber pressure, appearing buffer droplets should be immediately transferred trough the spray capillary resulting in a condition of fast periodic breakdown of the liquid bridge.

Set the spray voltage to a value between 2.5 – 2.8 kV. The surface buffer of the buffer liquid should indicate an increased tendency to move towards the spray capillary. Moreover, the Voltmeter should show jumps in the spray current, indicating periodic formation of an ESI plume.

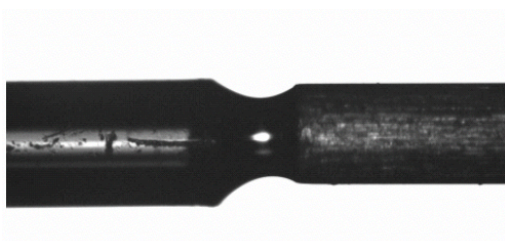


**Figure A 79.** A stable liquid bridges.

Reduce the chamber pressure to stepwise until a stable liquid bridge is formed to about (usually 30 - 60 mbar). During this process, also the gas flow through the choke valve will be reduced, which is indicated by the red-y gas flow meter (usually 15 - 30 mL/min).

### **A.18.2 Analysis**

Verify a proper filling of the sample plate (sufficient sample volume for the set depth of immersion of the sampling pin, no gas bubbles at the micro-well bottom).

Select a previously defined process in the sample transfer section of the sampler application including proper sample sequence, sampling method(s), and sample plate configuration. Standard parameters for method steps including time specification are a gap waiting time of 1 sec, washing times of 2 seconds per solvent, and a drying time of 4 sec.

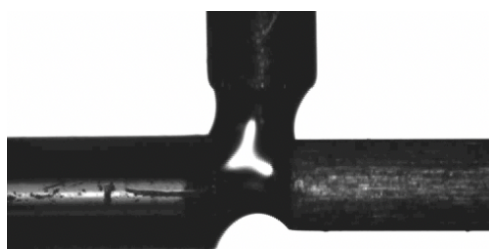


**Figure A 80.** Contactless injection into the liquid bridge.

Choose an appropriate detection mode, acquisition time and mass range of the mass spectrometer, and start MS-acquisition.

Click on “Start” within the sample transfer section to start the sampling process. Snapshot of a typical injection:

*Remark:* At standard conditions of  $F=1 \mu\text{L}/\text{min}$  at gap sizes of 200-300  $\mu\text{m}$ , the sample peak width for small molecules is about 10-12 seconds. It is recommended to adapt the sampling speed (=total time of the sampling method) in a way that the next injection cycle starts at the peak top of the previous sample. Higher frequencies of injection cycles can lead to overlapping peaks and broader peak widths.

## A.19 Troubleshooting

**Table A 4.** Troubleshooting of common errors.

Error in injection port initialization or in initialization of wash/dry ports	Check for green LEDs of control units, which are located at the metal pillar carrying the delta robot. If LEDs appear red, shut down the computer and unplug der main power supply for sampler compartments; restart the system.
No buffer appears during buffer line conditioning	Check the buffer line connections for tightness. Check for the fixation of the syringe (glass body + plunger). Cut a few mm of the capillary outlet.
Buffer bubbles appear even after 15 min of line flushing, or during bridge formation	Check the buffer line connections for tightness and for the quality of cut (no broken capillary edges!).
No stable bridge can be established	Check the electrical current for its stability and for its absolute value; for a standard buffer system without high salt concentrations, the electrical current measured by the voltmeter should be in a range of 8-20 mV at a spray voltage of 2.5–3 kV. If values are out of this range, check for leakage currents (isolation of the syringe plunger, incomplete isolation at the high-voltage cable). If no leakage is detectable, replace the spray tip.  Moreover, voltage at the voltmeter should not jump by more than 1 mV. If it does so, check for interfering, external air streams close to the source and shield the source if necessary.



	<p>Check for dryness of the pressure chamber:</p> <ul style="list-style-type: none"><li>- in case of a small liquid accumulation, open the chamber, set the chamber pressure to maximum, and wait for at least 20 min;</li><li>- in case of a large liquid accumulation or even chamber flooding, first use a syringe to remove most of the liquid within the chamber, then let the chamber dry at maximum chamber pressure (injection port open!)</li></ul>
--	--

## A.20 Coating Single Layer Beads on the Tip of Pin Tool for SPME

A key point for successful executing the SPME procedure is the coating of pin with single or two layers of extraction beads. Single layer bead can facilitate the rapid elution and release the sample into ESI buffer, and thus to avoid excess dilution the sample.

The coating method was adapted from the work by Pawliszyn group, making the coating with HPLC beads and PAN glue. We improved this method to generate single to two layers of bead on the tip end of the pin.

- Preparation of PAN (Polyacrylonitrile) glue  
Weigh 0.5 g PAN particle and mix with 4.5 g DMF in a glass vial. Put the vial into a 90°C for about 1 h, until a yellowish clear solution was obtained. The vial should be sealed tightly to avoid the evaporation of DMF. Cool the solution to room temperature.
- Cleaning of the pin tool  
The stainless-steel pin should be well cleaned before coating.
  1. sonicate in 2-propanol for 10 min
  2. sonicate in methanol for 10 min
  3. dry with high pressure nitrogen gas
  4. 2 minutes O<sub>2</sub>-Plasma
- Coating the pin with HPLC beads  
HPLC beads can be bought from phenomenex, USA. Usually, Fully Porous Silica beads with C<sub>8</sub> or C<sub>18</sub> stationary phase can be used for most of application.

1. Make a spacer using microscope slide, coverslip, and magic tapes.

Formation of very thin layer of glue is a key to coat single layer beads on the pin. A self-made spacer is a good choice. The Scotch Magic tape has an excellent uniform thickness, so it can be used to make a spacer between slide and coverslip. The thickness of the tape is 50  $\mu\text{m}$ . Two layers of tape (100  $\mu\text{m}$ ) is suggested to be used for forming glue layer.

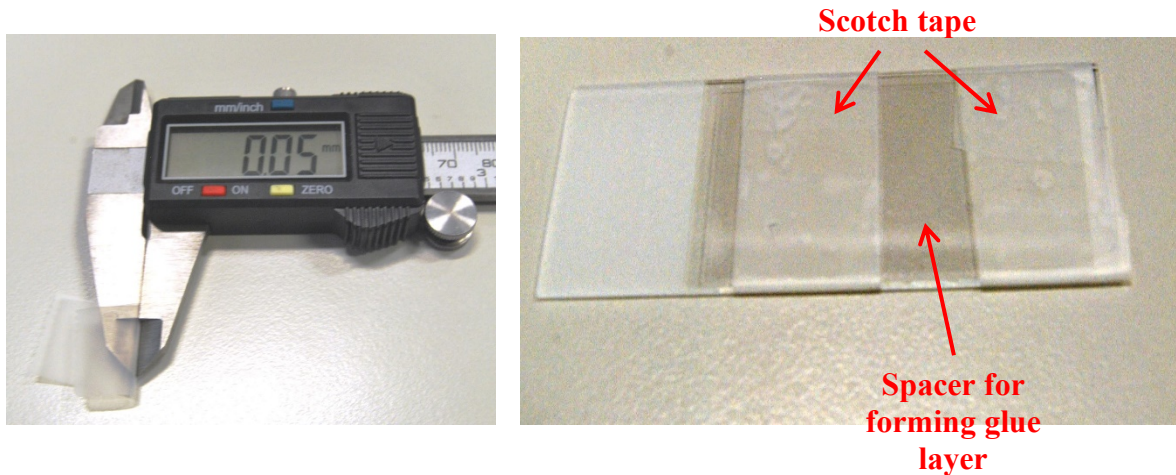


**Figure A 81.** Preparation of a thin layer of beads for SPME extraction tool.

- Put a drop of glue into the spacer, and quickly cover it with coverslip. Press the coverslip to form the glue layer.
2. Form a layer of beads (50  $\mu\text{m}$  or 100  $\mu\text{m}$ ) on microscope slide using similar method as described above.
  3. Dip the tip of the pin into the glue layer vertically to the slide surface for 1–2 times.
  4. Dip the pin into bead layer for one time to absorb the bead on the tip. Since DMF evaporate very fast, step 4 should follow step 3 rapidly.

- Put the pin in a metal supporter, keeping the tip upward.

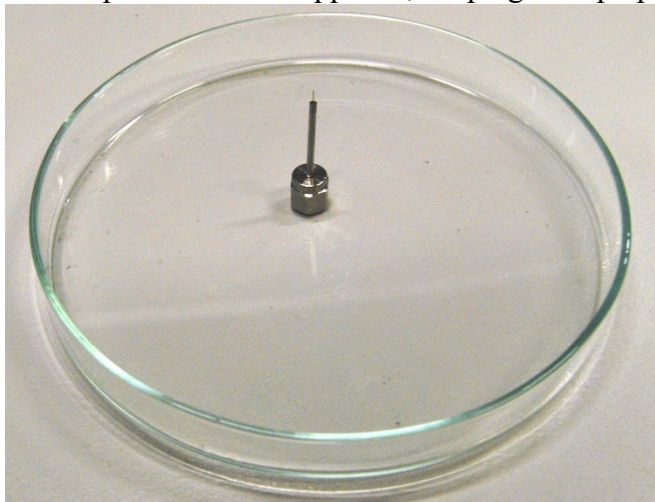


**Figure A 82.** Fresh coated metal pin.

- Cure the glue in the oven at 180°C for about 2 min.
- Examine the tip with microscope and SEM

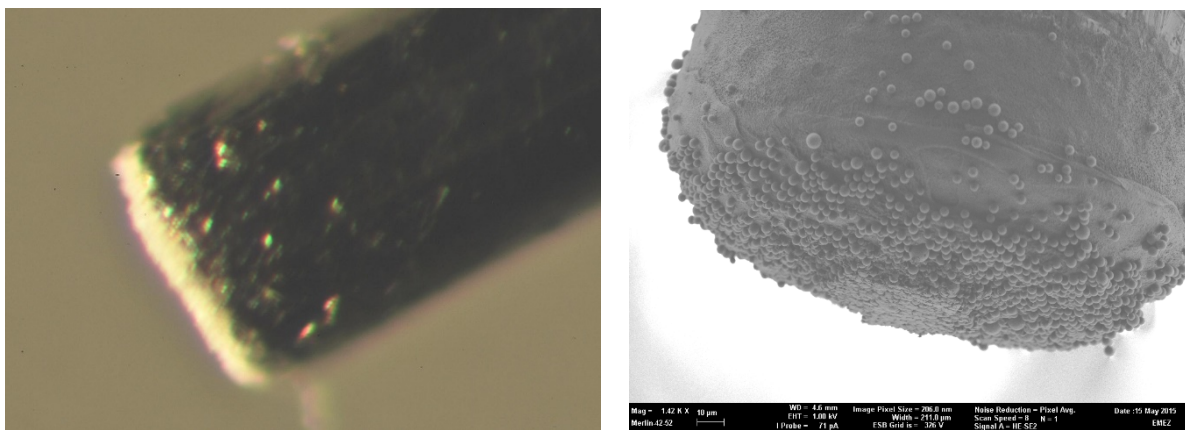


**Figure A 83.** Microscope (left) and SEM (right) images of a single layer coated C<sub>18</sub> beads.

This page intentionally left blank.

# **Appendix B**

## Curriculum Vitae

This section contains the Curriculum Vitae of the author, Sahar Ghiasikhou.

# SAHAR GHIASIKHOV

---

 Ghyiasikhoo@gmail.com  
 Gattikerstrasse 5, 8032, Zurich, Switzerland  
 +41 78 679 58 93  
 Date of Birth 23.06.1989



## WORK EXPERIENCE

---

- 04.2019-Present Business Development Manager, SuSoS, Dübendorf.**
- 09.2014- 03.2019 Research Assistant in Chemistry and Applied Biosciences, ETH Zurich, Roche Basel.**  
Topic: Development of an auto-sampler coupled to ESI Mass Spectrometry.  
 - Successfully accomplished the design of a novel sampling microfluidic platform, implementing different sample cleanup methods prior to ESI-MS.  
 - Independent Project Management, guiding a Master project student (Grade 6/6).  
 - Presentation at 6 National and International Conferences (2014-2018).  
 - Teaching Liquid Chromatography and Polarography for 3 semesters (2015-2018).  
 - Q-TOF MS Lab Chief. Mentoring and disciplining lab staff. (2014-2018).
- 11.2016- 02.2017 Lecturer and Organizing Committee for Iranian Inventions Grand Prize Festival, Tehran, Iran (More than 2000 Participants).**  
Lecture topic: Preparation of business plan and fundraising for startups.
- 09.2013- 03.2014 Internship. Logitech SA, Scientific Park, EPFL, Lausanne.**  
Topic: Physical property of material with powders in Thermal Management applications.  
 -A successful (Material/ Mechanical) design of the Logitech Gaming Mouse with an advanced heat dissipation/cooling approach.
- 02.2013- 07.2013 Internship. Mat-search, Pully, Lausanne.**  
Topic: Study of critical rare-earth elements.
- 09.2012- 05.2013 Research Assistant. Powder Technology Laboratory, EPFL, Lausanne.**  
Topic: 1. Controlled new synthesis of iron oxide nanoparticles for hyperthymic cancer treatment. 2. Synthesis and characterization of environmentally friendly cement.
- 10.2007- 07.2012 Director and Teacher of Scientific Olympiads. National Organization for Development of Exceptional Talents (nine provinces), Iran.**  
 Preparing students for national and international Olympiads.  
 Organizing workshops, seminars and teaching courses.  
 Wrote "Key to solution" for 3 International Chemistry Olympiad books.  
 Achievements: More than 20 gold, silver and bronze medals among a few millions of participants in 5 years.

## EDUCATION

---

- 09.2014- 03.2019**    **PhD candidate in Chemistry and Applied Biosciences.**  
**ETH, Zurich, Switzerland.**  
*Thesis:* Capillary gap sampler, a device for high throughput screening of low sample amounts by ESI mass spectrometry.
- 09.2012- 08.2014**    **Master of Sciences in Material Science & Engineering.**  
**EPFL, Lausanne, Switzerland.**  
*Thesis:* Fast determination of resection margins in breast cancer tissue with lab-on-chip.
- 01.2008- 07.2012**    **Bachelor of Science in Chemistry.**  
**Sharif University of Technology, Tehran, Iran.**  
*Thesis:* Synthesis and characterization of salpe/celite superabsorbent composites.
- 10.2001- 09.2007**    **Mathematics and Physics Diploma.**  
**National Organization for Development of Exceptional Talents (Top 2%), Iran.**

## HONORS AND AWARDS

---

- 04.2018**                **Travel Award from Swiss Group in Mass Spectrometry.**
- 05.2016**                **Selected Entrepreneur by Commission for Technology and Innovation, Switzerland.**
- 09.2006**                **Silver Medal in Iranian National Chemistry Olympiad held by the Young Scholars Club.**
- 01.2008- 09.2012**    **Undergraduate Studies Grant from National Foundation of Elites, Iran.**
- 08.2003**                **Gold Medal in Basketball (High School Iranian National Olympics).**

## COMPUTER/LANGUAGE SKILLS

---

Languages known	Pascal, Delphi
Packages	MS Office, Gaussian, GaussView, Spartan, Chem 3D, Origin, Image J
Operating Systems	Solid knowledge of Windows, Linux, OS

English	Professional
German / French / Arabic	Basic
Persian / Azeri / Turkish	Mother tongue

## HOBBIES

---

Travelling, Hiking, Basketball, Swimming, Dancing  
Painting (Oils, Watercolor)  
Reading (Psychology)